International Doctorate in Atomic and Molecular Photonics

XXXI PhD cycle - FIS/03

Emilia Conti

In vivo optical imaging of cortical plasticity induced by rehabilitation after stroke

PhD Dissertation

Supervisor: Dr. Anna Letizia Allegra Mascaro.

PhD school Coordinator: Prof. Francesco S. Cataliotti.

External referees:

Prof. Maurizio Corbetta, Padova Neuroscience center, University of Padova.

Prof. David A. Boas, Boston University, Department of Biomedical Engineering.

Contents

Contents

Summary

In my PhD thesis I have studied the changes in functional and structural plasticity induced by a photothrombotic stroke in mouse primary motor cortex. In order to dissect the multiple aspects consequent to the damage we exploit fluorescent imaging techniques that allow to investigate the functional and structural rearrangement of the cortex at different scale, from the entire hemisphere, with wide-field calcium imaging, up to the single synapse with two-photon microscopy.

To promote a functional recovery of the mouse forelimb we applied different rehabilitative strategies in order to both foster the stabilization of regions of the cortex linked to the stroke core, and stimulate the remodelling of peri-infarct areas. We took advantage of a robotic platform (M-Platform), developed by our collaborator in Pisa, to perform the rehabilitation of mouse forelimb through a repetitive motor training. Together with this approach we applied different strategies to mould cortical activity. We temporary inhibited the healthy primary motor cortex, with an intracortical injection of Botulin Neuro Toxin E, in order to counterbalance the iper-excitability of the healthy hemisphere and to promote the structural and functional remodelling of the peri-infarct cortex. This combined rehabilitative protocol promotes the recovery of cortical maps of activation during motor training and the rewiring of interhemispheric connectivity, both from functional and structural level. Then we applied an optogenetic approach as a pro-plasticizing treatment by stimulating with light the region of the cortex surrounding the damage. By coupling this treatment with an intense motor training on the M-Platform we observed a generalized recovery of forelimb functionality in terms of manual dexterity and cortical profiles of activation. In this study, we have shown that different rehabilitative protocols that combines repetitive motor training and neuronal modulation of specific cortical regions induce a synergic effect on neuronal plasticity that promotes the recovery of structural features of healthy neuronal networks.

Introduction

1.1 Metabolic alterations in acute stroke

Interruption in the blood supply to the brain leads to a debilitating neurological state termed stroke [1]. During a stroke, neuronal cells that are deprived of their normal metabolic substrates, such as oxygen and glucose, cease to function in seconds and show signs of structural damage after only 2 minutes [2]. As energy-dependent processes fail, neurons are unable to maintain their normal transmembrane ionic gradients, resulting in an ions and water imbalance that leads to apoptotic and necrotic cell death cascades [1-3] and, ultimately, to the impairment of sensory and motor function [1-4]. As a consequence of blood supply loss, cellular derangements such as metabolic failure, exocitotoxicity, mitochondrial breakdown, oxidative stress and neuroinflammation take place resulting in an irreversible tissue damage. The area of the tissue that borders the stroke core typically experiences reduced blood flow and is termed *penumbra*. This area is a brain region that suffers from ischemia, but in which the ischemic damage is potentially reversible. The penumbra is also defined as the region of perfusion-diffusion mismatch by MRI imaging, in which blood flow might be reduced but infarct-related diffusion signals have yet to be found. Neuronal survival in the penumbra is a time limited process and cells will die within hours or few days without intervention such as reperfusion. Surviving neurons in the peri-infarct cortex, which is situated at the border of an infarct but has sufficient blood perfusion, undergo active structural and functional remodelling after stroke.

A focal lesion can cause damage that also disrupts the structural and functional connectivity of other areas of the brain distal from the lesion. Neuronal metabolism and cerebral blood flow's depression caused by a damage in an anatomically separated but functionally related neuronal region is termed *diaschisis*. The main mechanism of diaschisis is functional deafferentation [5], consisting in the loss of the input of information from the damaged brain region. The decrease in

information and neural firing to distal brain area lead to the impairment of synaptic connections and to structural and functional modification of neural connectivity around that area.

1.2 Stroke classification

A stroke can occur in three different ways: ischemic, haemorrhagic and transient.

Ischemic strokes accounts for about 87% of stroke cases. They occur as a result of an obstruction within vessel supplying blood to the brain. The underlying condition for this type of obstruction is the development of fatty deposits lining the vessel walls (atherosclerosis). These deposits can cause two types of obstruction such as cerebral thrombosis and cerebral embolism. In the first case a blood clot called thrombus clogs a vessel. In case of a cerebral embolism a blood clot, formed at another location in the circulatory system, breaks loose enters the bloodstream and travels through the brain's blood vessels until it reaches vessels too small to let it pass. An irregular heartbeat, known as atrial fibrillation, is a second important cause of embolism as it creates a condition where clots can form in the heart, move and travel to the brain.

Haemorrhagic stroke accounts for about 12% of stroke cases. It results from chronic alterations of the intima and media of the endothelium, caused by hypertension. A weakened vessel breaks and bleeds into the surrounding brain. The blood accumulates and compresses the surrounding brain tissue. In addition to hypertension, two types of weakened blood vessels usually cause haemorrhagic stroke: aneurysms and arteriovenous malformations (AVMs). An aneurysm is an expansion of a weakened region of a blood vessel. If left untreated, the aneurysm continues to weaken until it ruptures and bleeds into the brain. An arteriovenous malformation (AVM) is a cluster of abnormally formed blood vessels that can rupture causing bleeding into the brain.

A transient ischemic attack (TIA) is a temporary blockage of blood flow to the brain. The clot may dissolve on it its own or get dislodged so that it stops causing the symptoms.

During a stroke, a prompt and early intervention can be crucial.

In case of ischemic stroke, the use of thrombolytic treatments during the acute phase helps restoring blood flow perfusion, but due to the short treatment window (up to 24 hours) and the high risk of haemorrhage only few stroke patients receive them [6, 7]. Another approach consists in the physical removal of the blood clot through an endovascular procedure or a mechanical thrombectomy. These procedures should be done within six hours of onset of acute stroke symptoms. In case of haemorrhagic stroke an endovascular catheter that reaches the source of the bleeding, deposits a mechanical agent, such as coil, to prevent further rupture.

About 75% of patients will show complete or strong recovery; while approximatively 30% will not recover much. In addition, the overall recovery is about 70% of max.

Thus, as it stands now, the options for minimizing stroke-induced brain damage are limited, and the need to better understand and treat the functional consequences of this damage continues.

1.3 Brain plasticity after stroke

The majority of people that survive a stroke will experience some form of sensory, motor, or cognitive impairment. Although stroke damage can be devastating, many patients undergo some spontaneous recovery. Two general mechanisms connected to each other are thought to contribute to the spontaneous improvement in function after stroke (*Figure 1*).

In a first time, the restoration of blood flow, metabolism, and the resolution of temporary disruptions in neural activity in regions connected to and surrounding the injured tissue act together in order to restore the pre-stroke conditions.
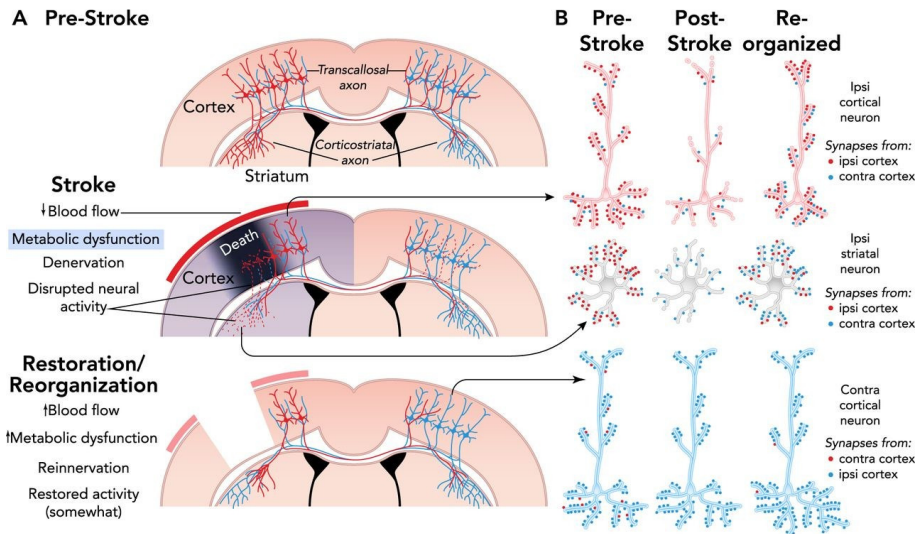
*Figure 1: **Mechanisms of spontaneous functional improvement after stroke.** (A) Schematic illustration of a coronal section in which are represented axonal projections of cortical pyramidal neurons. The death of the tissue in the ischemic core lead to the denervation of peri-infarct region and more distal areas correlated to the affected one. The peri-infarct cortex is characterized by a gradient of blood flow reductions, denervation of intra-cortical connections (not shown), and various degree of dendritic retraction I surrounding neurons. When the blood flow perfusion and metabolic activity were restored, spontaneous processes of sprouting and synaptogenesis occur in order to re-establish the reorganized connectivity. Processes of restoration and reorganization are interrelated depending on some degree of blood flow perfusion. (B) Schematic representation of potential changes in structural connectivity after stroke in the acute phase and during the reinnervation in the ipsi-lesioned cortex and in the contra-lesioned one. Modified from Jones and Adkins 2015 [8].*

Then, surviving neurons reorganize their connectivity patterns in order to supports partial restoration of, or compensatory substitution for, the lost functions. In previous studies it has been observed that cortical damage increments the expression of molecules that promote survival and proliferation of cells and structural remodelling of dendrites, axons and synapses [9, 10]. Furthermore, the expression of growth inhibitory molecules, known to inhibit axonal plasticity in the adult brain, is reduced [11, 12] thus fostering axonal sprouting of surviving neurons in

the peri-infarct regions [13, 14]. The growth of new synapses is followed by selective pruning and maturation [15].

In contrast with healthy condition, after a stroke the reduction of inter-hemispheric homotopic integration and the reduction of intra-hemispheric segregation between different brain regions occur [16]. Both of these changes are consistent with a reduction in network modularity, observed in stroke patients [17, 18].

Stroke recovery mechanisms are based on both structural and functional changes in brain circuits that have a close functional relationship to those affected by stroke (*Figure 1*), following rules similar to those of the nervous system development and experience-dependent plasticity.

At a structural level, axonal sprouting and synaptogenesis are coordinated with dendritic remodelling in both post and presynaptic neurons [19-23]. The whole process, that involves also glial cells, vasculature and extracellular matrix remodelling, leads to the formation of new connectivity patterns [24, 25]. It's now well established that the more abundant and the more active remaining afferents, the most tend to contribute to reinnervation [26-31]. This makes neural activity a promising therapeutic target.

Although many are the hypotheses on how the adult brain adapt in response to injury, the neuro-biological mechanisms of this process are still widely unknown. It was previously observed that the reorganization of areas of the brain, adjacent to the damaged one, is fundamental to the functional recovery after stroke. The set of regions that are directly damaged or indirectly affected is in turn embedded within a larger functional system that is in a dynamic balance with other systems in the brain [32]. Peri-infarct regions appear to undergo large-scale functionally changes in neuronal response properties. Electrophysiological and imaging studies have shown that peri-infarct regions become more active or responsive to stimulation of somatic regions that they are not typically associated with, suggesting that peri-infarct cortex may take over the function of brain regions lost to stroke [33-36]. Previous studies have demonstrated that the peri-injured region

is an exceptionally fertile area for plasticity, because there are robust changes in the expression of growth promoting or inhibiting proteins involved in neuronal rewiring [37-39]. As recovery from stroke depends on the ability of surviving neural circuitry to reorganize and compensate for the loss of damaged tissue [40, 41], cortical regions that are in close proximity to the damaged one or are functionally related (e.g. the contralesional homotopic area) to it are well positioned for vicarious function [42, 43]. Motor and sensory cortices are loosely organized into somatotopic functional maps that exhibit high levels of use-dependent plasticity [33]. After stroke, cortical remapping is both activity dependent and based on competition: peri-infarct regions, in which brain circuitry is compromised, rival with adjacent tissue of different functional areas.

1.4 Animal models of stroke

Rodent models offer a unique opportunity to dissect mechanisms of plasticity and circuit reorganization of the motor system after stroke [44]. Experimental stroke models are widely used to investigate the events associated with both the cellular response within the ischemic or healthy cortical area, and the mechanisms of recovery in the peri-infarct regions. Very common animal models of focal ischaemic stroke include i) intraluminal suture of the middle cerebral artery (MCA), ii) the middle cerebral artery occlusion (MCAO), iii) endothelin and iv) photothrombosis.

 i) In the first technique a coated suture is advanced into the carotid artery until it lodges at the junction of the MCA. The damage that results from the interruption of blood flow is mainly in the striatum and cortex [45]. The suture is withdrawn after 30-120 min, which results in the reperfusion of ischaemic tissue. Occlusion durations of 90-120 min are required to achieve reproducible tissue damage and result in very large infarcts that occupy much of the hemisphere. These often include hypothalamic injury,

which can complicate the interpretation of histological and behavioural outcomes owing to impaired motivation and temperature regulation. Such extensive damage is akin to a malignant infarct in humans, which is frequently fatal or untreatable [46]. Furthermore, this technique produces a considerable volume of potentially salvageable penumbra [47-49]. This makes it a useful model for studies investigating the impact of therapeutic approaches on either the volume or lifespan of the penumbra or tissue salvage following the reperfusion [50, 51].

ii)   In the MCAO model, the MCA is transiently occluded using microvascular clips, or permanently occluded by cauterization. Damage is restricted to the cortex if blood flow is interrupted distal to the striatal branches of the MCA, whereas occlusion proximal to these small arteries results in both striatal and cortical injury. This process produces a region of penumbra which gradually becomes incorporated into the infarct over the first 3-4 hours after MCAO [52].

iii)   Endothelin (ET-1) vasoconstriction produces ischaemia by constricting blood vessels. ET-1 is stereotaxically injected into parenchymal regions of interest, to constrict local arterioles, or near the MCA [53, 54]. Reperfusion occurs, but at a much slower rate than with the intraluminal suture model. Lesion size can be adjusted by varying the concentration or volume of ET-1 or achieve reproducible injury. It is unclear how much penumbral tissue this model produces. However, there are a number of studies that have used the model and demonstrated reductions in infarct volume with therapeutic approaches suggesting the potential for tissue salvage [55-57].

iv)   In the photothrombotic model a photosensitive dye, usually Rose Bengal, is injected systemically. The light source can be applied on the intact skull with no need of craniotomy,

which allows targeting of any area of interest, within the dorsal cortex, in a reproducible and non-invasive way. As a consequence of illumination the dye is activated, producing singlet oxygen; these oxygen intermediates induce endothelial cell membrane peroxidation, leading to platelet adhesion and aggregation, and eventually to the formation of thrombi which determine local cerebral flow interruption [58]. This procedure generates a sizeable volume of penumbra when assessed acutely with MRI [59].

The first two techniques require complex surgical procedures and produce an extensive damage that affect much of one hemisphere and striatal and cortical regions respectively. On the other hand, the photothrombotic approach aims to induce a cortical infarction through the photo-activation of a light-sensitive dye which results in local vessel thrombosis in the areas exposed to the light. In particular, animal models of focal cerebral ischemia allowed to identify the critical cerebral blood flow thresholds responsible for irreversible cell death, electrical failure, inhibition of protein synthesis, energy depletion and thereby the lifespan of the potentially salvageable penumbra. In detail, they allowed to understand the intricate biochemical and molecular mechanisms within the 'ischaemic cascade' that initiate cell death in the first minutes, hours and days following stroke [60]. Photothrombosis is a non-canonical ischemic model that does not occlude or break only one artery as it usually happens in human stroke, but induces lesions in more superficial vessels. In spite of this, the photothrombotic damage shares essential mechanisms occurring in brain stroke. Similarly to artery occlusion in human stroke, platelet aggregation and clot formation determine interruption of blood flow in the irradiated area [58]. Likewise, this model also shares essential inflammatory responses as in middle cerebral artery occlusion [61].

1.5 Spontaneous rewiring of brain circuits of stroke
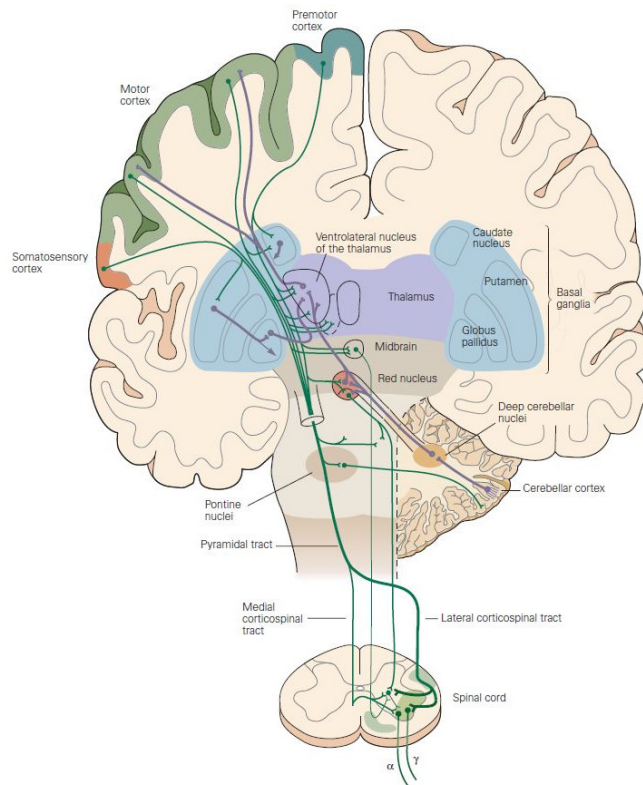
*Figure 2: **Corticospinal tract.** The principal components are the motor cortex, basal ganglia, thalamus, midbrain, cerebellum, and spinal cord. The principal descending projections are shown in green; feedback projections and local connections are shown in purple. All of this processing is incorporated in the inputs to the motor neurons of the ventral horn of the spinal cord, the so-called "final common pathway" that innervates muscle and elicits movements. Modified from Kandel et al., 2013 [62] .*

A brief digression on description of motor circuit will allow a better understanding of the possible targets to promote optimal rewiring and recovery after stroke.

Most pathways in the central nervous system are bilaterally symmetrical and cross over to the opposite (contralateral) side of the

brain or spinal cord. As a result, sensory and motor activities on one side of the body are mediated by the cerebral hemisphere on the opposite side. Thus, movement on the left side of the body is largely controlled by neurons in the right motor cortex and vice versa. The pathways of different systems cross at different anatomical levels within the brain. In detail, the axons of layer V of the primary motor cortex project through the corticospinal tract to the ventral horn of the spinal cord. These axons descend through the subcortical white matter, the internal capsule, and the cerebral peduncle in the midbrain. The descending corticospinal tract crosses to the opposite side of the spinal cord. Most of the corticospinal fibers cross the midline in the medulla (pyramidal decussation). However, approximately 10% of the fibers do not cross until they reach the level of the spinal cord at which they will terminate (*Figure 2*) [62].

Persistent motor deficits generally occur after stroke damaged the motor-associated cortices. In their work Siegel et al. [18], showed that despite severe disruption, post-stroke brain is capable of returning to a state of modular organization in the course of recovery.

The spontaneous recovery of motor deficits is often partial, owing to the limited degree of intrinsic brain repair [64].

In this framework, ipsilateral pathway could provide a means to recovery after brain injury [63] (*Figure 3*).

It has been already observed, both in animals and in patients, that healthy hemisphere is involved in radical changes in neuronal connectivity pattern after stroke [28, 65]. This leads to the alteration of neural circuitry within the intact contralesional hemisphere that is associated with a less lateralized activation [63].

Previous studies have shown that after a cortical stroke the unaffected hemisphere shows an increment of excitability, which may overly constrain cortical activity in the injured hemisphere [25, 66-69].
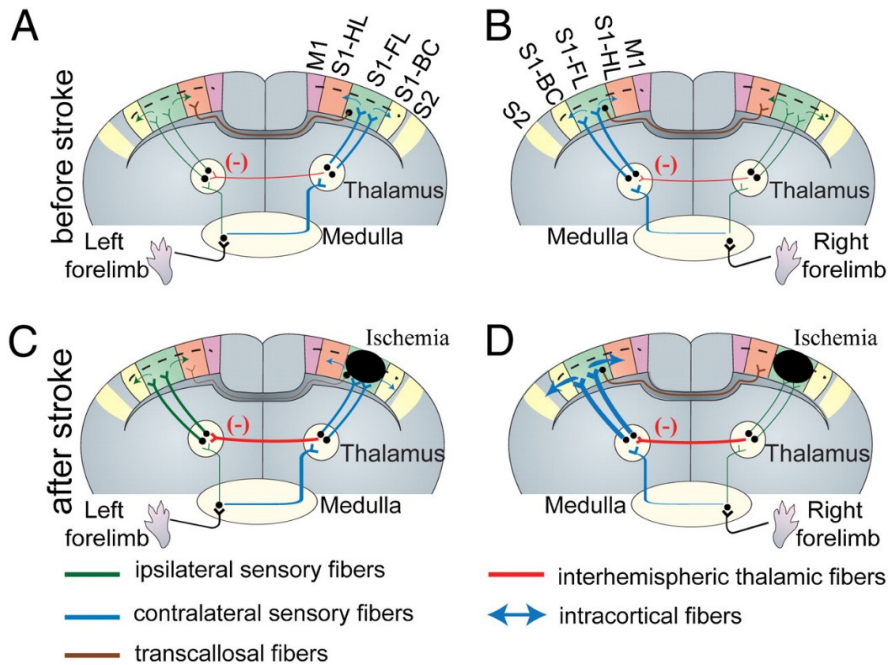
*Figure 3: **Mechanisms of interhemispheric rewiring after stroke on sensory cortex.** (A) and (B) Schematic representation of healthy condition: sensory axons coming from the left (A) or right (B) forepaw communicate through the indirect pathway (blue) or direct pathway (green), that is weak compared to contra-lateral ones. Interhemispheric reticuloreticularis connections between thalami in either hemisphere are shown in red. (C) After stroke in right forelimb area contralateral thalamocortical inputs are disrupted with the consequent block of activity spread through the corpus callosum (brown). At the same time the damage may increase the interhemispheric inhibition (red) revealing the ipis-lateral pathways (green, from left forepaw) through disinhibition of thalamic relay neurons (inhibition of inhibitory neurons) within contralesional hemisphere. (D) The downregulation of interhemispheric thalamic inhibition (red) may increase the excitability of thalamocortical pathways (blue). Modified from Mohajerani et al., 2011 [63].*

1.6 Rehabilitation

Strategies that promote brain plasticity, like motor rehabilitation, pharmacological treatments and brain stimulation techniques, can enhance neural rewiring and dramatically improve functional motor outcomes.

1.6.1 Motor rehabilitation via conventional physiotherapy and robotic devices

As it is well known, motor practice with the paretic limb improves functional recovery and behaviourally-relevant neural restructuring both in humans [35, 70-73] and in animal models [33, 74, 75]. For example, after a subtotal damage of the forelimb area of the primary motor cortex (M1) in a rat model, without rehabilitative training, forelimb movement representations in the peri-infarct area are lost [33, 76, 77]. Otherwise, training of the affected forelimb in skilled reaching tasks restores movement representation in the remaining forelimb region of the M1 [8]. Furthermore, the size of movement representation of the non-paretic forelimb in the contralesional (opposite to stroke) M1 is reduced by rehabilitative motor training [78].

As it has been observed in previous animal studies, beginning motor rehabilitation during the first weeks after stroke leads to a better functional improvement and neural rearrangement than does later training [79-81]. The underneath idea is that sudden interventions can act during a more dynamic phase of neuronal remodelling, thus promoting a better reorganization. Clinical studies confirmed that earlier interventions are more effective [82, 83].

In the last years neurorehabilitation protocols based on the use of robotic devices have shown to provide promising clinical results. In particular, mechatronic devices have key advantages over conventional physiotherapy as they provide an intensive and highly repeatable

practice and offer a quantitative and objective evaluation of the outcome for each patient, exploiting the built-in sensors that measure different parameters such as forces exerted by the subject and the smoothness of movement [84]. Furthermore, the use of robotic devices in murine models and human patients gives an unbiased evaluation of recovery of motor performances providing an accurate description of kinetic and kinematic aspects on motor performance during rehabilitation after stroke.

1.6.2 Pharmacological treatments

A promising approach to increase recovery after brain injury is the administration of pharmacological agents [85]. Growth factors may be ideal candidates because they control differentiation and growth in developmental processes and recovery and regeneration after traumatic brain lesions. There is a growing consensus that brain-derived neurotrophic factor (BDNF) might be particularly well suited because exogenous administration of BDNF exhibits potent protective effects after various types of ischemic lesions [86-89]. For the first time Schäbitz et al. showed in its work of 2004 [85] the role of BDNF as a strong inducer of recovery after stroke, and not only as a neuroprotective agent. They demonstrated that the intravenous infusion of BDNF clearly improved functional outcome preventing the disinhibition due to the downregulation of the GABAergic system [90]. Furthermore, BDNF treatment was shown to increase long-term potentiation and cognitive function after transient forebrain ischemia [89]. Similar to other drugs (amphetamines, basic fibrinogen growth factor), BDNF treatment may increase expression of markers for axonal sprouting and synaptogenesis such as MAP1/2 or synaptophysin [91, 92].

Other studies focused their attention on chondroitin sulfate proteoglycans (CSPGs) that condense in lattice-like structure which enwrap specific sub-population of neurons, including fast spiking inhibitory interneurons [93]. The CSPG side chains, responsible for the

growth-inhibiting activity can be digested via local delivery of the bacterial enzyme chondroitinase ABC, thus promoting axonal sprouting. It was shown chondroitinase ABC injected into the cervical spinal cord enhanced plasticity following a cortical stroke [94].

Furthermore, in order to promote neural growth after brain injury another strategy consists in the pharmacological blockade of ephrin-A5, a potent inhibitor of neurite outgrowth, normally induced in the membrane of reactive astrocytes in the peri-lesional cortex [95]. The inhibition of ephrin-A5 led to a robust axonal sprouting in the areas adjacent to the infarct, producing a significant improvement in behavioural recovery of the forelimb function.

Finally, another strategy to modulate neuronal activity requires the use of the clostridial enzyme botulinum neurotoxin E (BoNT/E). This protein is a metalloprotease that enters the cytosol of nerve terminals close to the site of delivery and specifically cleaves the synaptic protein SNAP-25 (synaptosomal-associated protein of 25 kDa), causing a prolonged blockade of transmitter release [96, 97]. Costantin and colleagues [98] in a work on rat hippocampus observed that the inhibitory effect of BoNT/E lasted for at least two weeks. Several studies took advantage of this properties in studies of the development of nervous system [99]. In a recent study of Spalletti et al. [100], BoNT/E was exploited as a plasticizing treatment after stroke to counterbalance the augmented excitability of the contralesional hemisphere. By combining the transiently silencing of the contralesional homotopic cortex with motor training, they observed a recovery of pre-lesioned motor pattern in behavioural tests.

1.6.3 Modulation of brain functionality by manipulation of neuronal activity

Stimulation techniques such as transcranial magnetic stimulation (TMS) and transcranial direct current stimulation (tDCS) represent non-

invasive approaches to improve cortical remapping after stroke by modulating neural excitability.

Transcranial magnetic stimulation (TMS) is a non-invasive procedure that uses magnetic fields to stimulate nerve cells in the brain. An electromagnetic coil is placed against the scalp and the electromagnet painlessly delivers a magnetic pulse. The magnetic pulses easily pass through the skull, and causes small electrical currents that stimulate nerve cells in the targeted brain region. In particular, it has been observed that repetitive high-frequency TMS (5-20 Hz pulse trains) induces neural activation while low-frequency TMS (0.2-1 Hz pulse trains) inhibits neurons activation. Because this type of pulse generally does not reach further than two inches into the brain, scientists can select which parts of the brain will be affected and which will not be. The magnetic field is about the same strength as that of a magnetic resonance imaging (MRI) scan.

Transcranial direct current stimulation (tDCS) is non-invasive neuromodulatory technique that delivers a low electric current to the scalp. A fixed current between 1 and 2 mA is typically applied. tDCS works by applying a positive (anodal) or negative (cathodal) current via electrodes to an area, facilitating the depolarization or hyperpolarization of neurons, respectively. The positioning of the anode and cathode electrodes is used to influence how current flows, and where in the brain it does. The current delivered by tDCS is not considered strong enough to trigger an action potential in a neuron; its sub-threshold effect works by bringing the neurons closer to, or farther from firing. tDCS augments the resting voltage of the neuronal membrane to prod a neuron's activity in a desired direction. By intervening on ion channel activation, tDCS modulates neural activity using relatively weak electric currents (~1-2 mA) [101-103]. In this way, tDCS may work by strengthening or weakening synaptic transmission between neurons by augmenting synaptic plasticity. It has been already demonstrated that excitatory tDCS (anodal) improves motor learning by reinforcing synaptic connections [104-106].

In the context of stroke treatment, plasticity in the injured hemisphere plays a major role in post-stroke motor recovery and is a primary target for rehabilitation therapy. Indeed, tDCS of the ipsilesional motor cortex, especially when paired with motor training, facilitates plasticity and functional restoration[107] [108]. In addition, previous studies have shown that repeated optogenetic neuronal stimulation of the ipsilesional hemisphere induces a significant improvement in cerebral blood flow and neurovascular coupling response[109]. Furthermore, it has been demonstrated that chronic optogenetic stimulation of ipsilesional brain regions promotes remodelling both at a structural level, fostering the formation of new and stable thalamocortical synaptic boutons, and at a functional level, inducing the rewiring of thalamocortical circuitry [110].

On the other hand, the role of the contralesional hemisphere remains highly controversial[111-113]. Attempts to promote stroke recovery by inhibiting the contralesional hemisphere are based on the interhemispheric competition model, which posits an enhanced transcallosal inhibition exerted by the healthy side over the spared perilesional tissue[111, 114-117]. Previous studies demonstrated that repetitive TMS applied after a stroke in acute, increases motor evoked potential amplitudes [118]. Furthermore, after stroke both the tDCS excitation of the damaged motor cortex or the contralesional inhibition enhances motor performances on standardized tests for motor functionality [119-122].

Nevertheless the inactivation of the healthy hemisphere via either low-frequency, repetitive transcranial magnetic stimulation (rTMS) or cathodal (inhibitory) tDCS has yielded some positive yet variable effects in clinical trials [122-125].

This variability in outcome may depend on the extent of damage: interhemispheric competition dominates in patients with limited damage in the affected hemisphere, while after large lesions the contralesional side appears to vicariate the lost functions[58, 125, 126].

1.6.4 Combined rehabilitative treatments

It is also increasingly recognized that the combination of physical rehabilitation with 'plasticity-stimulating' or neuromodulatory interventions synergistically resulting in a more susceptible to experience-dependent modifications spared CNS networks [127-129].

Here we describe two exemplary studies on the synergic effect of combined treatments on functional rehabilitation after stroke.

Wahl et al. [130] demonstrated in a rats model of photothrombotic stroke that anti-Nogo-A immunotherapy, realized in a specific time window during which the brain is most responsive to plasticizing treatments, combined with a specific motor training, affects the recovery of lost motor function and the pattern of fiber sprouting. In detail, they observed that the combination of the pharmacological treatment with the rehabilitative training provided a better recovery compared to the single treatment.

Furthermore, Kilgard and colleagues [131] have shown that vagus nerve stimulation delivered during motor rehabilitation is effective in improving functional restoration of forelimb function. The authors trained rats to pull a handle and generate a threshold force in order to obtain a reward. Ischemic lesions acutely impaired task success and forelimb strength, but these parameters returned to pre-lesion values when training in the device was paired with vagus nerve stimulation. Neither intensive training alone, nor delivery of stimulation after motor rehabilitation was effective in yielding such improvements, indicating the importance of timing for the induction of plasticity and recovery.

1.7 Optogenetics

Optogenetics is a branch of science that exploit the expression of genes encoding for light-activated ion-conductance regulators or biochemical signalling proteins into targeted cells. In particular, optogenetics take advantage on the use of microbial rhodopsin proteins that acts as

unitary activated ion pumps or channels which can be activated by specific wave lengths. In neuroscience, the expression of light sensitive protein within neurons allow inducing either activation or inhibition depending on the *nature* of the channel (cationic or anionic respectively).
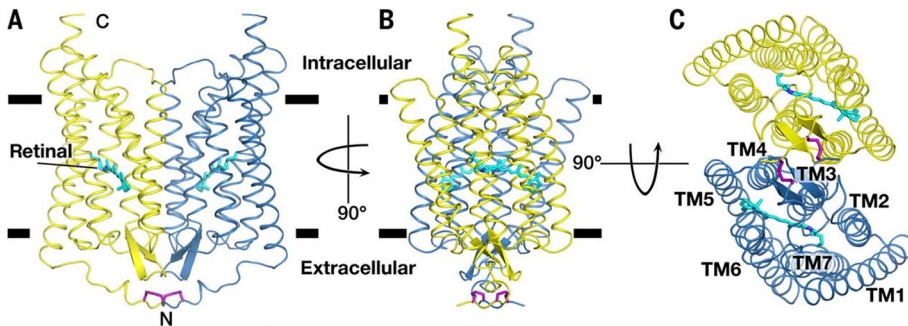
*Figure 4: **Structural models of Channelrhodopsine 2.** Overall structure presentation of the ChR2 dimer. In cyan the retinal residue. Cysteine bridges are shown in purple. Modified from [144].*

The first two channelrhodopsins identified were two isoforms from the single-cell green alga *Chlamydomonas reinhardti*, named ChR1 and ChR2 [132-135]. In their native form, ChRs are photoreceptors allowing the unicellular algae to move towards or away from light (phototaxis) in order to optimise photosynthetic growth [136]. Subsequently, further ChRs were found in related algae including *Volvox cateri* (VChR1 and VChR2), *Dunaliella salina* (DChR1) and *Mesostigma viride* (MChR1) [137-141]. Although these opsins differ among each other in cation selectivity, kinetics and light wavelength sensitivity and intensity, all ChRs share a common architecture comprising an N-terminal membrane-spanning domain and a C-terminal cytosolic domain (*Figure 4*). ChRs are characterized by a seven transmembrane helices structure constituting the ion channel and a long C-terminal extension of unknown function. The light-absorbing chromophore retinal, a vitamin A derivative, is embedded within the hydrophobic centre of the seven helices. Upon activation with blue or green light channelrhodopsins undergo a typical

photocycle that can be analysed by time-resolved absorption and vibrational spectroscopy [142, 143].

Light absorption leads to isomerization of the retinal from the all-trans configuration to the 13-cis form, followed by a protein conformational change and opening of the 6°A ion pore. Upon stimulation with blue light, ChR2 opening allows the entry of cations into the cell, causing depolarization and neuronal firing.
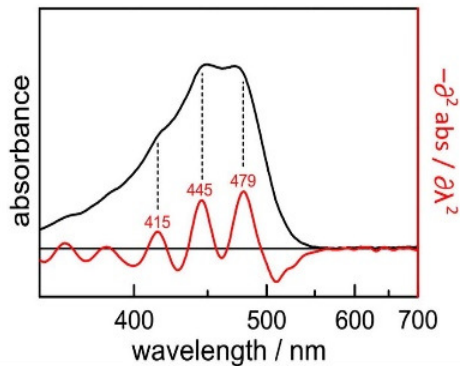
*Figure 5: **Absorption spectrum of the retinal in ChR2.**It's possible to observe its fine structure (dashed vertical lines), resolved in the second derivative spectrum (red trace). Modified from [145] .*

In the light-activated ion pumps, bacteriorhodopsin and halorhodopsin undergo similar conformational changes, which lead to active proton export and Cl⁻ import, respectively. Interestingly, internal and external pHs strongly influence ChR2 channel closure and recovery from desensitization [134].

The structural changes are reversed during closure of the conducting pore and reversion to the dark state via several non-conducting late photocycle intermediates.

The spectral characteristics of retinal absorption of ChR2 depend on the retinal chromophore. In ChR2, the absorption spectrum of the retinal shows a global maximum at roughly 470 nm (*Figure 5*).

In the last decades the huge development of optogenetics allowed neuroscientists to investigate the elicited physiology and behaviour by controlling neural activity of specific cell populations.

The key advantage of optogenetics over conventional microelectrode stimulation/recording is its ability to control cell-and circuit-specific behaviour with temporal precision. Melchior et al. [146] compared optogenetic activation versus electrical stimulation of dopamine release and demonstrated that selective optogenetic stimulation increase dopamine release with respect to electrical stimulation. Furthermore, they observed that the multi-synaptic modulation caused by electrical stimulation was absent in the selective optogenetic stimulation.

Up to now, many transgenic mouse lines expressing ChR2 has been developed [147]. The transfection methods are broadly classified into three groups: biological, chemical and physical. These methods have advanced to make it possible to deliver nucleic acids to specific subcellular regions of cells by use of a precisely controlled laser-microscope system [148]. The most commonly used method in clinical research is virus-mediated transfection [149]. Virus-mediated transfection is highly efficient and it is easy to achieve sustainable transgene expression in vivo owing to the viral nature of integration into the host genome. Chemical transfection methods, exploit the electrical properties of cationic polymers, calcium phosphates, cationic lipids, to introduce foreign genes into mammalian cells [150]. Positively charged chemicals make nucleic acid/chemical complexes with negatively charged nucleic acids. These positively charged nucleic acid/chemical complexes are attracted to the negatively charged cell membrane. Depending on factor such as nucleic acid/chemical ratio, solution pH, and cell membrane conditions, the process results in low transfection efficiency, especially in vivo, compared with virus-mediated methods [148].

The physical transfection methods use diverse physical tools to deliver nucleic acids. The methods include direct micro injection, biolistic particle delivery, electroporation, and laser-based transfection [151]. As

electroporation is an easy and rapid way, able to transfect a large number of cell in a short time, is the most widely used physical method. A short electrical pulse disturbs cell membranes and makes holes in the membrane through which nucleic acids can pass [152].

Optogenetic reporters are either inserted downstream of a variety of neuronal promoters, such as the neuronal marker Thy1 [153], or cell-specificity is introduced by crossing Cre driver lines with lines containing optogenetic probes down-stream of a floxed STOP cassette [154]. Another way to achieve cell-specific expression of opsins is to use viral vectors that confine the expression within specific neuron types. For example, by using a viral vector expressing ChR2 under a promoter such as CamKII, the protein will be present only in excitatory neurons.

1.8 Genetically Encoded Calcium Indicators (GECIs)

In the context of evaluating brain remapping and neuronal rewiring, a novel approach that can be used is the monitoring of brain activity via genetically encoded calcium indicators (GECIs).

In neurons, action potentials (APs) trigger large and rapid calcium influx through voltage-gated channels. Similarly, activation of neurotransmitter receptors during synaptic transmission causes calcium transient in dendritic spines. More in details, in neurons cytoplasmic-free calcium is maintained extremely low concentration, at 50-100 nM at rest. Neuronal activity induces influx via multiple routes [155]: when stimulated, calcium flows into the cytoplasm through calcium channels (voltage-gated cation channels or calcium-permeable, receptor-operated channels) or is released from calcium-loaded organelles, rapidly raising the local concentration of calcium. Ionotropic receptors for excitatory neurotransmitters pass calcium , for example NMDA-type glutamate receptors mediate a calcium rise in spines up to 1 µM [156]. Dendritic voltage-gated calcium channels allow calcium entry during local dendritic spiking [157]. Finally, voltage-gated calcium channels allow calcium entry throughout the neuron during AP

propagation. In cortical neurons, this results in an intracellular calcium rise of ~150 nM within 10 ms that then persists with a half decay time of 50–70 ms [158, 159]. Calcium levels then return to baseline through extrusion from the cell and reloading of intracellular buffers and stores. The spatiotemporal dynamic of calcium transients is shaped by the localization, mobility, affinity and kinetics of these processes, including buffering by endogenous proteins and exogenous GECI [160].

With appropriate indicators, imaging intracellular calcium dynamics can be used to measure neuronal spiking and synaptic activity across populations of neurons in vitro and in vivo.

Calcium ions are universal second messengers for neurotransmitter reception and membrane depolarization regulating essential cellular signalling events in a wide range of tissues and organisms. Although there are many fluorescence synthetic calcium indicators widely used for investigating calcium dynamics [161-164] both in living cells and animals they suffer from many drawbacks that prevent their broadly applicability in neuroscience. First of all these calcium dyes cannot be easily targeted to specific cell types, population or subcellular location [165], then the loading is highly invasive and can damage the tissue and finally, they are incompatible with repeated, longitudinal in vivo studies. Many of these limitations are overcome using GECIs based on chimeric fluorescent proteins. The great advantage of GECIs is the possibility to target specific cell types, populations, or subcellular compartments, allowing to detect calcium signalling at different scales: from subcellular resolution [166] to the entire cortical surface.

Thanks to the features of neuronal physiology characterized by a fast calcium dynamics and low peak calcium accumulation [167], these indicators are ideal for any application in neurons [168-171].

In general, the structure of calcium indicators consists of a calcium-binding domain (e.g. calmodulin, CaM, or troponin C), fused to one or two fluorescent proteins (FPs).

The development of genetically encoded optical indicators of neuronal activity has enabled progress toward this aim to an extent that was unimagined two decades ago. GECIs, based on fluorescent proteins,

provide many advantages deriving from both optical reporting and genetic encoding; thanks for their sensibility and high signal to noise ratio GECIs allow to monitor calcium transients in living cells and organism.
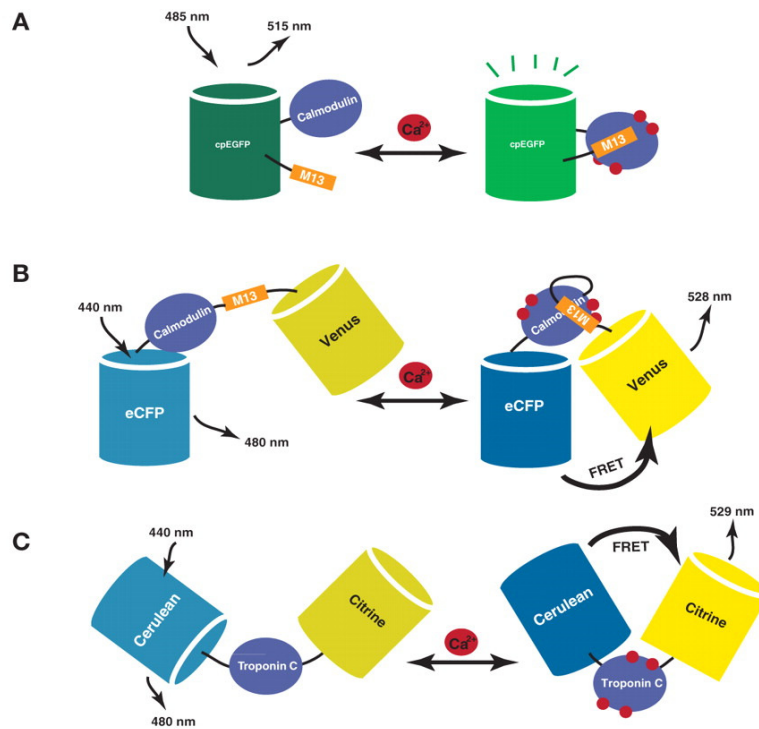
*Figure 6: **Schematic representation of the three major GECI classes.** (A) Schematic representation of the G-CaMP-type calcium indicator based on florescence intensity changes of split or circularly permuted single FPs. The conformational changes in the calmodulin–M13 complex induce fluorescence changes in the circularly permuted enhanced GFP (cpEGFP). (B) Schematic representation of cameleon family of FRET-based GECIs. A calcium-dependent increase in FRET between a CFP and YFP FRET pair is coupled to the binding of calmodulin to the M13 peptide. (C) Schematic representation Troponin C–based FRET GECIs. Binding of calcium to troponin C induces conformational changes and an increase in FRET between CFP and YFP. Modified from Tian et al., 2012 [172].*

Principle advantages and limitations of calcium imaging depends on calcium kinetic. Through biochemical changes induced by calcium indicators, the transient membrane-localized events of neurotransmitter receptor opening or AP generation are as a more prolonged event. This amplification, combined with the fluorescent signal of the indicators, makes GECIs responses larger in terms of photonic output and thus easier to detect.

Many efforts have been made to design different calcium indicators with improved sensibility and speed.

Based on the structures we can distinguish two classes of GECIs: single fluorescent proteins (single FP, Figure 6 A) and two fluorescent proteins (two FP, Figure 6 B and C).

In the first category, the fluorescence intensity is modulated by calcium binding-dependent changes in the chromophore environment [173], while in two FP GECIs, calcium binding allosterically modulates the relative donor-acceptor emission spectra through a distance and orientation dependent change in fluorescence resonance energy transfer (FRET) [174]. In many cases the protein is fused to a conformational actuator (e.g. M13 peptide) in order to enhance the conformational change and fluorescence modulation (*Figure 6*).

The first GECI, Cameleon, was composed of calmodulin and M13 domains between ECFP and EYFP and reported calcium with increased FRET [176]. Single fluorophore GECIs have achieved larger responses than FRET-based GECIs such as Cameleon. The first single-fluorophore GECI was Canmgaroo, constituted by a YFP bearing a CaM domain near the chromophore [173]. This was the first indicator in which conformational changes in a domain attached near the chromophore modulate its brightness [173]. The subsequent evolution of this idea leads to the development of GCaMP family indicators. GCaMP consists of circularly permuted green fluorescent protein (cpGFP), the calcium binding protein calmodulin and CaM-interacting M13 peptide (*Figure 7*).
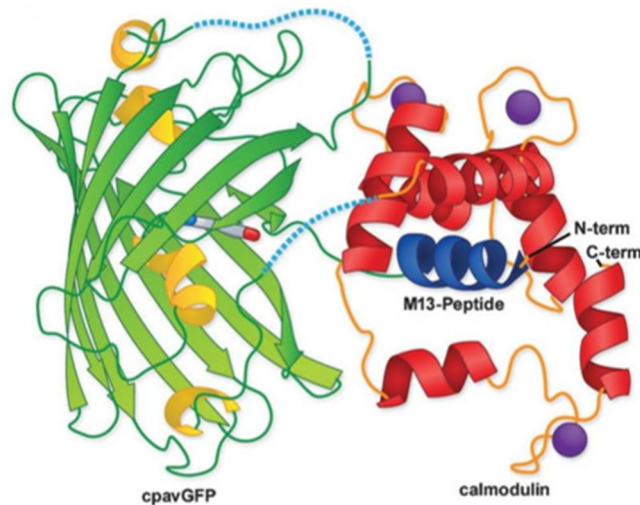
*Figure 7: **Schematic representation of GCaMP structure**. The beta barrel (in red) of GFP carries the chromophore and it is linked to the CaM-M13 complex (CaM in blue, M13 domain in green). The calcium binding protein is able to interact with 4 calcium ions (in purple). Modified from Frommer et al., 2009 [175].*

The CaM-M13 complex is located in proximity to the chromophore, inside the β barrel of GFP. The binding of four calcium ions to the CaM-M13 domain induces a conformational changes of the protein that causes an increase of brightness.

Many GCaMP variants has been produced in order to improve the sensitivity via mutagenesis. For example, three GCaMP6 sensors has been developed GCaMP6s, 6m, 6f, characterized by slow, medium and fast kinetics respectively. In particular, GCaMP6f shows variation in fluorescence signal of 2,8% across a calcium concentration of 0 to ~1 μM; furthermore, GCaMP6f is capable to report single APs in mouse cortex with ~20% $\Delta F/F$, superior to that of organics dyes, and a 142-ms half-decay time [177]. Other calcium indicator such as GCaMP6s, GCaMP6m and GCaMP7 are able to produce even larger responses to single APs, with the important drawback of increment of decays that are 93-190% longer than with GCaMP6f [177, 178]. To conclude, GCaMP6 sensors are more sensitive and faster than commonly used synthetic

calcium dyes or other variants of GCAMP. Furthermore, these indicators are suitable for different kind of studies as they allow imaging large groups of neurons as well as tiny synaptic compartments, such as dendritic spines, over multiple imaging sessions separated by months. For this reason, GCaMP6 sensor find widespread applications for different studies in brain research and calcium signalling.

1.9 Fluorescence microscopy

Fluorescence is the emission of light that occurs within nanoseconds after the absorption of light with a shorter wavelength. This phenomenon has been described for the first time in 1852 by the British scientist George G. Stokes who observed that emitted fluorescent light has a longer wavelength and lower energy than the excitation light.

Due to the fact that part of the energy is lost during this process, the emitted photon is characterized by less energy than the absorbed photon. Therefore, light emitted from an indicator usually has longer wavelength than the excitation light. The difference between the exciting and emitted wavelength is called Stokes shift. The fundamental property allows separating the excitation light from the emitted fluorescent signal. To better understand the details of excitation and emission processes is possible to take advantage of the Jablonski diagram (*Figure 8*). Electrons are normally at the lowest energy state, indicated by S_0. When a photon with appropriate energy interacts with a molecule the photon may be absorbed, causing an electron to jump to one of the levels of an excited state (S_1 or S_2 in the diagram). This process is very fast, on the order of 10^{-15} seconds (a millionth of a billionth of a second). An excited-state electron rapidly (on the order of 10^{-12} seconds) loses its energy to vibration (heat), a process called internal conversion, and falls to the lowest level of the first (S_1) excited state. From there the electron may fall to one of the sub-levels of the ground (S_0) state, emitting a photon with energy

equivalent to the energy difference of the transition. This happens on a time scale of nanoseconds ($10^{-9} - 10^{-8}$ seconds) after the initial photon was absorbed. Since the emitted photon has less energy than the absorbed photon it is at a longer wavelength. This explains the magical process of fluorescence that converts light of one wavelength (colour) to another, and leads to the phenomenal display of highly saturated colours in corals and so many other marine organisms.
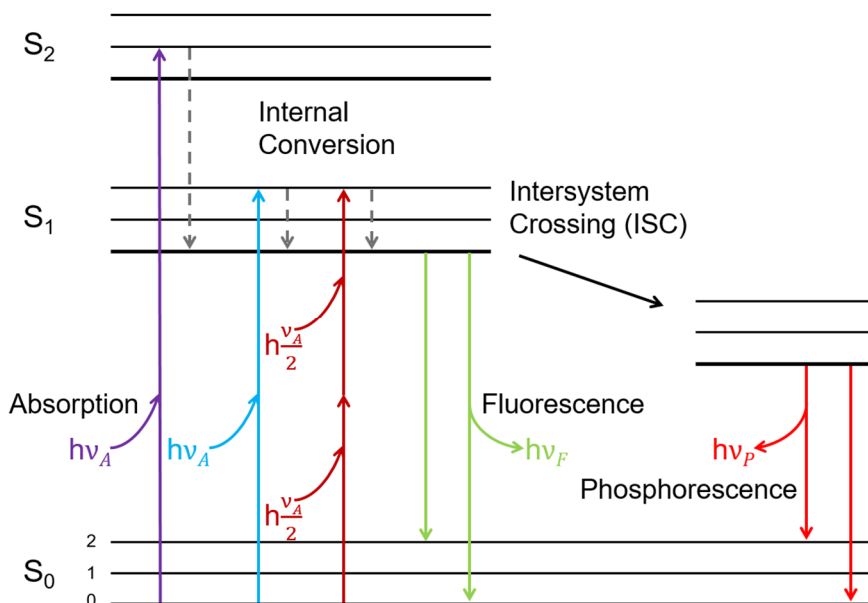
*Figure 8: **Jablonski diagram and spectra**. The image shows the typical temporal behaviour and fundamental photophysical processes in organic molecules such as absorption of a photon (S0>S1, S2), internal conversion (S2>S1, non-radiative), fluorescence (S1>S0), intersystem crossing and phosphorescence. Adapted from Lakowicz [179].*

This loss of energy may involve non radiative transitions, such as internal conversion, intersystem crossing or vibrational relaxation, or radiative transitions, such as fluorescence and phosphorescence.

Vibrational relaxation and fluorescence emission are the principal ways for the fluorophore to come back to its ground state.

When a fluorophore absorbs light, all the energy of a photon is transferred to the molecule. The energy of the photon is inversely related to the photon's wavelength according to the following equation:

$$E = h \times \frac{c}{\lambda}$$

where h is Plank's constant and c and λ are the speed and the wavelength of light in vacuum respectively.

1.9.1 Wide-field Microscopy

One of the simplest techniques for fluorescence imaging is the wide-field configuration microscopy.

Here, a collimated beam of light simultaneously illuminates the whole sample thus exciting the fluorophore. Traditionally, the excitation light is provided by a mercury or xenon high-pressure bulb and the required wavelengths are selected with appropriate filters. An excitation filter is used to select the proper wavelengths, in order to excite fluorophores around the maximum of their absorption spectrum. A new approach that is rapidly spreading for excitation light, is the use of light emitting diode (LEDs) characterized by long life, fast switching and tight wavelength control. In a fluorescence microscope the sample is irradiated by an appropriate light source through an objective and then, the emitted fluorescence is separated from the exciting light.

Appropriate filters select specific bands to separate the absorption and the emission spectra. In the majority of fluorescence microscope, especially those used in life science, the fluorescence signal, emitted from the sample in all the directions, is collected by the same objective used for the excitation (epifluorescence), deflexed by a dichroic mirror

to separate excitation and emission path, filtered and then collected by a detector. Since most of the excitation light is transmitted through the specimen, only reflected excitatory light reaches the objective together with the emitted light and the epifluorescence method therefore gives a high signal-to-noise ratio.

One of the most significant advancements has been the development of electron multiplied (EMCCD) and very low-noise, cooled CCD cameras for fast detection of low-light fluorescence (EMCCD) or gradual accumulation of fluorescence signal integrated with little noise (cooled CCD) still maintaining high resolution. These improvements consent faster imaging increasing contrast at low signal levels, allowing to minimize the excitation light to prevent photo-bleaching and phototoxicity.

Wide-field microscopy provides good XY dimension resolution, a very fast temporal resolution (particularly with the new EMCCD cameras). Furthermore, it is one of the least expensive microscopy technique.

XY resolution (Rxy) is a function of the numeric aperture (NA) of the objective and the wavelength (λ) of the excitation light according to Ernst Abbe's diffraction limit expression:

$$R_{xy} \approx 0.61\lambda/NA$$

Thus, for example an excitation of wavelength of 505 nm combined with an objective with a numerical aperture of 0,075 provide a lateral resolution of 4,1 µm.

The main disadvantage of this technique is that all the emission light is integrated through the sample in the Z dimension. Therefore, it is difficult to tell where the fluorescence from a point in the sample originated in the Z dimension. For samples that are thin or where Z-discrimination is not critical this may not be a limiting factor. Nevertheless, the possibility to achieve a large field of view represents a great advantage for mesoscale studies in which single cell resolution is not necessary.

1.9.2 Two-Photon Microscopy

An alternative technique to achieve subcellular resolution but at the expense of a small field of view is represented by two-photon fluorescence microscopy.

In 1931 Maria Göppert-Mayer first understood that an atom or a molecule could adsorb two photons simultaneously generating an excitation produced by the absorption of a single photon of higher energy in a process called multiphoton excitation (MP). Two-photon microscopy, represents the simplest version of her theoretical prediction: two photons of about equal energy (from the same laser) interact nearly simultaneously ($\sim 10^{-16}$ s) with a molecule, producing an excitation equivalent to the absorption of a single photon possessing twice the energy. If the excited molecule is fluorescent, it can emit a single photon of fluorescence as if it were excited by a single higher energy photon (*Figure 9A*).

Multiphoton processes such as two photon excitation (TPE) are often termed 'nonlinear' because the rate at which they occur depends nonlinearly on the intensity. The transition probability (P) through two-photon absorption is proportional to the square of the intensity (I) of the excitation light:

$$P \propto I^2$$

The intensity squared dependence of the transition probability is the basis of the localized nature of two-photon excitation: doubling the intensity produces four times the fluorescence. Since the intensity of a focused laser decay quadratically with distance, fluorescence is generated only in the proximity of the focal volume.
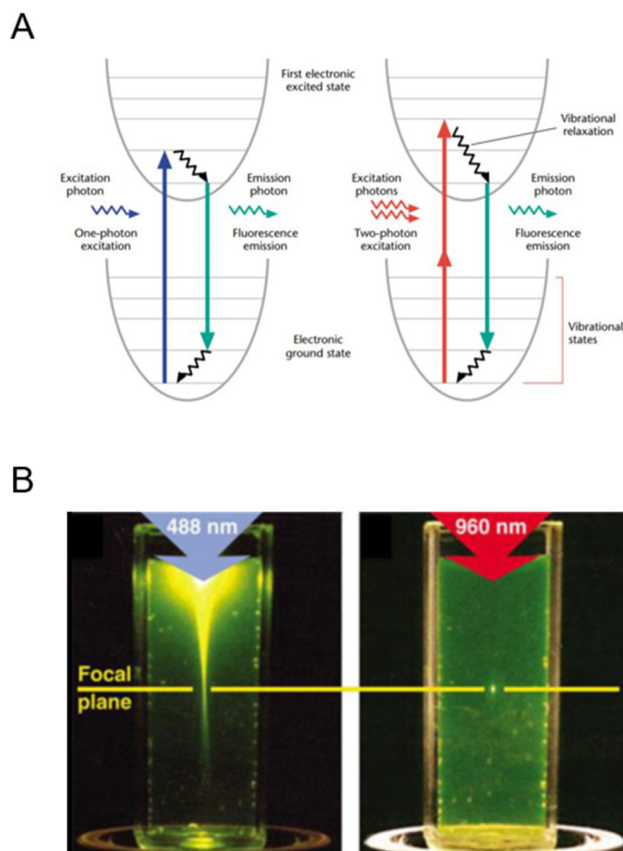
*Figure 9: **Two-photon excitation**. (A) Jablonski's diagram of one-photon (left) and two-photon (right) excitation, which occurs as fluorophores are excited from the ground state to the first electronic states. One-photon excitation occurs through the absorption of a single photon. Two-photon excitation occurs through the absorption of two lower-energy photons via a virtual state. After either excitation process, the fluorophore relaxes to the lowest energy level of the first excited electronic states via vibrational processes. The subsequent fluorescence emission process for both relaxation modes is the same. Modified from Zipfel et al. 2003 [180]. (B) Localization of excitation by two-photon excitation. On the left, single-photon excitation of fluorescein by focused 488 nm light (0.16 NA). On the right, two-photon excitation using focused (0.16 NA) femtosecond pulses of 960 nm light. Excitation volume is localized by the two-photon transition. Modified from Zipfel et al., 2003 [180].*

In MP microscopy, as in conventional laser-scanning confocal microscopy, a laser is focused and raster-scanned across the sample. To generate an image, the laser is scanned over the sample; since the excitation occurs only in the focal volume, all fluorescence photons captured by the objective constitute useful signal.

Since TPE probabilities are extremely small, focusing the excitation beam with high objective number aperture increases the local intensity at the focal point and thus the probability of emission.
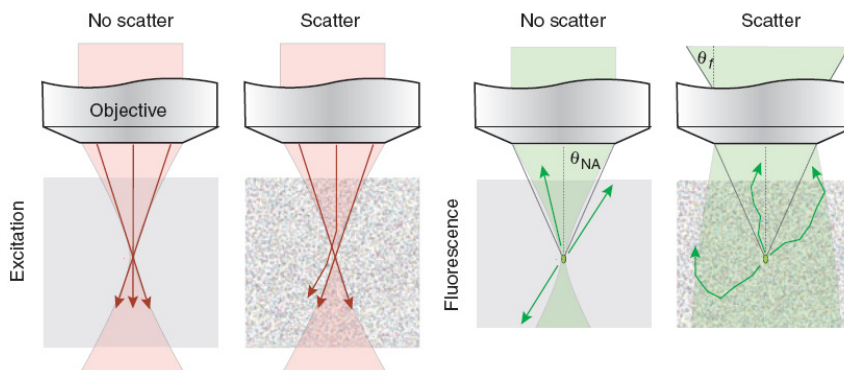
*Figure 10: **Signal generation and acquisition of fluorescence in scattering and non-scattering tissue.** The images show signal generation and fluorescence collection in clear tissue (left) and in scattering tissue (right). In non-scattering tissue all excitation light reaches the focus, while in scattering tissue some of light rays miss the focus. This leads to a roughly exponential decrease in excitation with depth. In clear tissue only fluorescence light rays initially emitted into the collection cone, determined by the objective's NA, can be detected, but in scattering tissue fluorescence light is (multiply) scattered and may even 'turn around'. Fluorescence light apparently originates from a large field of view but a larger fraction than in the non-scattering case is actually within the angular acceptance range ϑf of the objective. From Helmchen and Denk, 2005 [182].*

When excitation photons enter the tissue, their paths are altered by inhomogeneities of the refractive index of the sample (Figure 10). Compared to one-photon techniques, TPE provides three key advantages on scattering specimens [181]. First of all, the excitation

wavelengths used in TPE microscopy (deep red and near IR) penetrate tissue better than the visible wavelength used in one-photon microscopy. Second, due to the non-linear excitation, scattered excitation photons generate only a weak signal and are not capable of exciting fluorescence emission. Third, thanks to the fact that even in deep tissue the excitation is mostly limited to the focal volume, all fluorescence photons constitute useful signal. Compared to other techniques, TPE microscopy dramatically improves the detection of signal photons per excitation event, especially when imaging deep in highly scattering tissue. The fundamental consequence of a localized excitation is the achievement of three-dimensional contrast and resolution [180]. Depending on the properties of the tissue TPE microscopy can image up to 1 mm deep in tissue [182]. This depth is determined by scattering.

1.9.3 Application of fluorescence microscopy in neuroscience

The brain is a complex and heterogeneous system and therefore is characterized by different levels of complexity from synapses (1 µm) to neuronal circuits (centimetres). Furthermore, the timescales range from the flickering of channels (less than a millisecond) to long-term memory (years). The great advantage of fluorescence microscopy is the capability to revolutionize the investigation on all of these spatial and temporal scales, allowing to study neurons in their natural habitat, and intact brain tissue. On the one hand although wide-field microscopy allows to investigate neurobiological phenomena over a large area, the strong scattering that affects the measurements represents a significant detriment [181]. On the other hand, confocal microscopy, even though it overcomes some of the effects of scattering, since the detector pinhole rejects fluorescence from off-focus locations [183, 184] suffers of many disadvantages. Indeed, the excitation of a large volume

of specimen along the illumination path induces phenomena of photobleaching and phototoxicity throughout the sample even though the signal is collected from the focal plane only.

Furthermore, deep tissue confocal microscopy is affected by a huge waste in terms of signal photons [183, 185]. Increasing fluorescence excitation in order to compensate signal-loss enhances phototoxicity and photobleaching. While confocal microscopy is thus best applied to thin specimens [186] experiments deeper in tissue benefit from multi-photon excitation since it allows high-resolution and high-contrast fluorescence signal in brain tissue [187]. In particular, TPE allows measurements with high sensitivity and resolution in intact nervous system [181]. Furthermore, TPE microscopy combined with transgenic mouse lines expressing fluorescent protein allows measuring neuronal calcium dynamics, investigating structural plasticity over time and monitoring neurodegenerative processes both in live animals [162 164, 188] and brain slices [189, 190].

- ## Application of wide-field microscopy in neuroscience

Wide-field microscopy, combined with the use of transgenic mice expressing calcium indicators in neurons, allows revealing simultaneously the cortical activity within a large field of view. During the last decades, neuroscientists focused their attention on mapping mesoscopic functional cortical connectivity [191]. By exploiting a transgenic mouse line (Emx1-creXRosa26-GCaMP3) characterized by a widespread and stable cell-specific expression, coupled with the high acquisition frame rate of wide-field microscopy, Murphy and colleagues [191] longitudinally recorded spontaneous activity in resting state. By lightly anaesthetizing under isoflurane the animals they reconstructed through somatosensory stimulation a somatotopic map of brain cortex. Then they evaluated whether the connections between regions of the cortex, revealed with cortical and sensory stimulation, could be observed also during spontaneous calcium imaging.
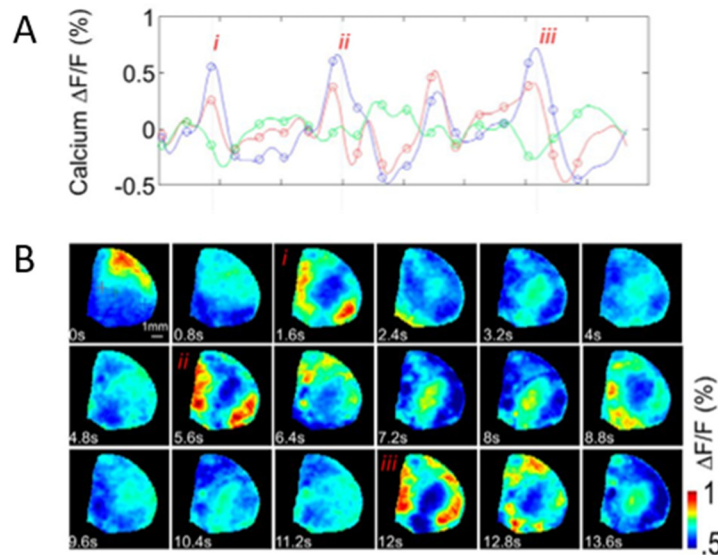
*Figure 11: **Region-specific spontaneous calcium activity.** (A) temporal pattern of activation during resting state in one location of primary sensory cortex (S1) corresponding to hind limb primary sensory area HLS1 (in red), secondary sensory area (in blue), and a reference region between these 2 areas (in green). (B) Calcium signals observed in each temporal location indicated in A. Modified from Vanni and Murphy, 2014 [191] .*

By analysing the temporal pattern of fluorescence signal (*Figure 11A*) they found a positive correlation between two regions of the cortex, such as hind limb primary sensory cortex (HLS1) and secondary sensory cortex (S2), compared to a reference region between these two areas. Then, the map of activation confirmed that HLS1 and S2 were coactivated (*Figure 11B*).

In a following study by Silasi and colleagues [192], owing to the capability of wide-field microscopy to reach a large field of view covering both hemispheres, the inter- and intrahemispheric connectivity in anaesthetized and awake conditions was evaluated. This work showed (*Figure 12*) a strongly correlated activity between homotopic region in the two hemispheres while the strongest intra-hemispheric correlation

was between the barrel and vibrissae motor cortex, both in awake and anesthetized conditions.
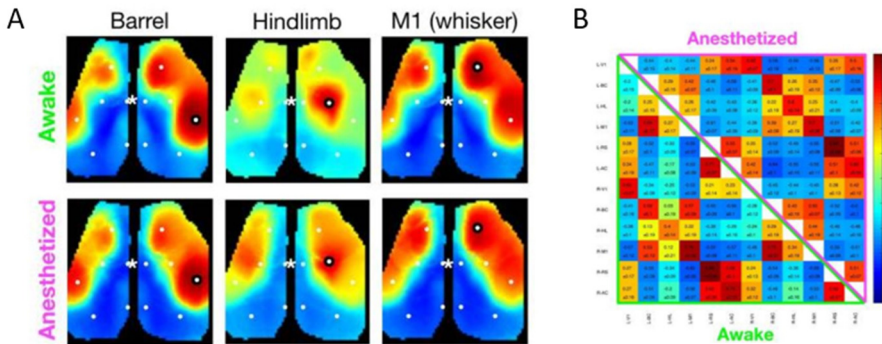
*Figure 12: **Seed-pixel correlation maps and matrixes in awake and anaesthetized mice.** (A) seed-pixel were placed in 3 different cortical regions (barrel cortex, hind-limb sensory-motor cortex, M1) (B) Correlation matrix of cortical activation reveals similar pattern of activation in the two states, with the homotopic cortex showing the most reliable correlated activity. Modified from Silasi et al., 2016 [192].*

Recently, other wide-field studies with bilateral preparation on GCaMP mice investigated connectivity mapping during resting state. Vanni and collaborators [193], for example, explored in a recent work mesoscale cortical activity in head-fixed, quiet awake GCaMP6 mice. By applying multiple approaches of parcellation, they discerned through spectral analysis two frequency modes: a low-frequency mode encompassing activity <1 Hz, associated with three main functional modules associated with major mouse behavioural functions (vision, locomotion and orofacial processing) and a higher frequency mode at 3 Hz, that segregated the cortex in two modules one lateral and one medial (described using fMRI both in humans and in rodents).

Finally, in Balbi et al. 2018 [194] mesoscopic functional connectivity was mapped longitudinally in awake GCaMP6 mice in a mouse model of microinfarcts. Longitudinal testing of neurodeficit and clasping scores revealed significant motor deficit during the first four weeks after

microinfarct induction. By recording spontaneous activity at different time point in both hemispheres the authors found no cortical dysfunction in terms of neuronal activity. On the contrary, they observed that focal photothrombotic stroke in the motor cortex caused a strong disruption to interhemispheric connectivity between bilateral motor cortices.

- ## Application of two-photon fluorescence microscopy in neuroscience

The first application of TPE microscopy to neurobiology imaged the structure and function of dendritic spines in brain slices [195].

Later long-term *in-vivo* imaging studies revealed the structural dynamics of neocortical neurons in healthy and injured brain. Here we reported some of the most relevant findings obtained through *in–vivo* longitudinal studies.

Changes in synaptic connectivity, through de novo growth or retraction of synaptic structures (such as axonal varicosities and dendritic spines), were investigated with two-photon imaging. These studies provided the evidence for synaptogenesis in the adult brain after behavioural enrichment [196]. In detail, it has been observed that the turnover of axonal varicosities is lower compared to dendritic spines [197-199].

In adult mice varicosities on thalamocortical axon show high level of stability [197]. On the contrary, a subpopulation of spines continues to turn over: some spines appear and disappear over days, whereas others persist for months, perhaps even for the entire life of the animals [200] (*Figure 13*).

Furthermore, longitudinal imaging studies of structural plasticity allow observing real-time changes in the structure of dendritic spines in vivo in pathological frameworks such as after ischemic stroke [40]. After a focal lesion of the cortex, dendritic spines become exceptionally malleable; this change in dendrites stability was manifested by a significant increase in spine formation, specific primarily in the peri-infarct area [201] (*Figure 14*).
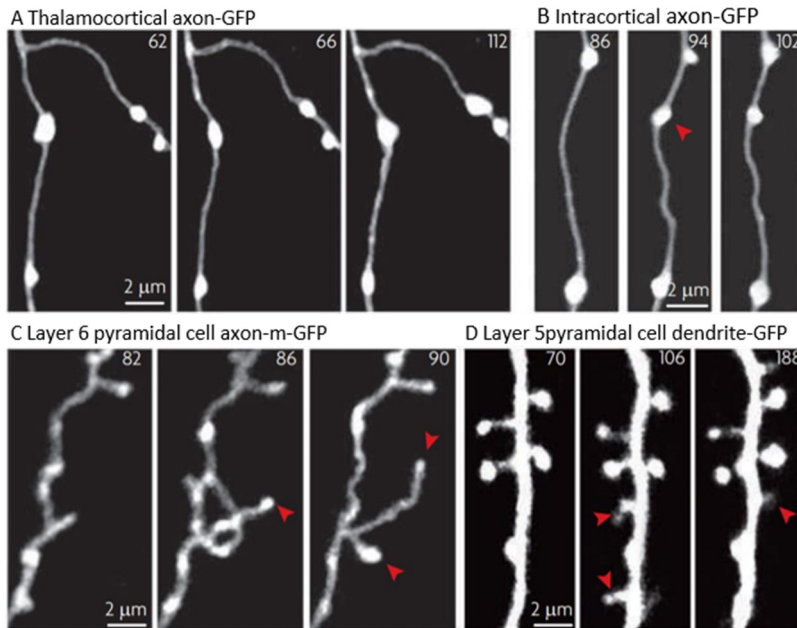
*Figure 13: **In vivo time-lapse imaging of axonal boutons and dendritic spines.** All panels show time-lapse images of axonal boutons (panels A-C) and dendritic spines (panels D) in adult mice. Images are from layer 1 or layer 2 in the barrel cortex under baseline conditions, except panel d (after chessboard whisker trimming). The numbers in the corners of the panels indicate the age (postnatal day) on which the image was taken. Neurons were labelled with GFP in Thy1 transgenic mice. (A)The panels show the hihgh stability of thalamocortical axons. (B) Intracortical axon with stable and new (arrowhead) en passant boutons. (C) Panels show axon from a layer 6 neuron labelled with membrane-bound green fluorescent protein (m-GFP), with dynamic terminaux boutons (arrow heads). (D)Panels show the spines turnover: some spines appear and disappear (arrowheads), whereas others are stable over long time periods. Modified from Holtmaat and Svoboda 2009 [200].*

The figure below shows an example of time-lapse imaging in the peri-infarct region of apical dendritic arbor. In particular, the left part of the figure depicts the formation of a spine during the first five hours after stroke. This study demonstrated that the rate of spine formation increased in peri-lesioned area during spontaneous recovery two

weeks after stroke, while in more distant regions was comparable with healthy animals (*Figure 14, right*).
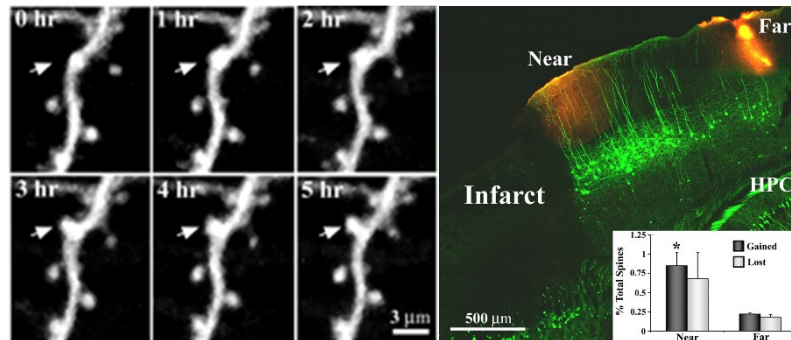
*Figure 14: **Two-photon imaging of apical dendrites**. On the left the time-laps imaging (taken 1h apart) of apical dendrites reveals the formation and retraction, respectively, of a dendritic spine. The image on the right shows a representative example of a fixed brain section from a YFP-transgenic mouse (sagittal plane, 2 weeks after stroke). Spine turnover was evaluated both in peri-infarct area and far from the infarct border (sites demarcated with DiI, red-orange color). The graph (inset) shows the increased levels of newly formed spines in proximal regions, but not distal to the infarct core (*p<0.05). Modified from Brown et al., 2007 [201].*

In other studies, structural plasticity of dendritic spines and axonal varicosities was shown to contribute to rewiring of damaged neuronal circuitry [40].
Recently Tennant and colleagues [110] using two-photon imaging showed that optogenetic stimulation promotes the formation of new and stable thalamocortical synaptic boutons. In particular, through longitudinal imaging session they observed that the increased turnover, significantly enhanced by optogenetic stimulation, is due to the formation of new varicosities 2-3 weeks after stroke.

Thesis outline

The review of literature indicates that in the last years many efforts have been made to develop forefront rehabilitative strategies allowing to improve post-stroke recovery. However, the complexity of mechanisms undergoing the functional and structural rearrangements during post-stroke recovery remain still unknown. After an ischemic event, extensive changes in cortical excitability affect both contralesional hemisphere and peri-infarct area. Based on the interhemispheric competition model neuromodulatory interventions act in order to re-establish the previous balance by inhibiting the contralesional side or by stimulating ipsilesional excitability.

During my PhD I worked on two complementary rehabilitative strategies exploiting two opposite neuromodulatory intervention such as the inhibition of the contralesional and the excitation of the ipsilesional hemisphere.

In a first set of experiment we combined a repetitive motor training on a robotic platform to a temporal inhibition of the contralesional M1. We evaluated the functional plasticity during rehabilitation by dissecting the calcium dynamic revealed with a wide-field microscope during the forelimb movement. Then, we applied an optogenetic approach to investigate the interhemispheric rewiring one month after stroke, and finally we evaluated the structural plasticity by analysing the synaptic turnover *in vivo* with a two-photon fluorescence microscope.

In a second set of experiment we evaluated the efficacy of optogenetic stimulation of the peri-infarct area coupled to an intensive motor training.

We tested the forelimb dexterity of mice during the rehabilitation month through Schallert test. We reconstructed the calcium dynamic during pulling movement of single treatments and combined rehabilitation.

Materials and Methods

3.1 Mice

All procedures involving mice were performed in accordance with the rules of the Italian Minister of Health. Mice were housed in clear plastic cages under a 12 h light/dark cycle and were given *ad libitum* access to water and food. We used two different mouse lines from Jackson Laboratories (Bar Harbor, Maine USA): Tg(Thy1-EGFP)MJrs/J (referred to as GFPM mice) for two-photon imaging experiments and C57BL/6J-Tg(Thy1GCaMP6f)GP5.17Dkim/J (referred to as GCaMP6f mice) for wide-field and optogenetics. Both lines express a genetically-encoded fluorescent indicator controlled by the Thy1 promoter. A subset of GFPM mice imaged for the structural plasticity experiment (dendrites and spines analysis) were used for blood vessels evaluation; a subset of GCaMP6f mice previously used for calcium imaging were analysed for inter-hemispheric connectivity. Each group contained comparable numbers of male and female mice, and the age of mice was consistent between the groups (4-12 months).

3.2 Photothrombotic stroke

A photosensitive dye, Rose Bengal, is injected systematically into animals through an intra peritoneal injection. The cortical blood vessel underlying the region of the damage are exposed to an epifluorescent light source, generating singlet oxygen species that lead to platelet activation and microvascular occlusion. This model can be used to produce small infarcts in any cortical region without invasive surgery.
In all experimental groups, except for CTRL animals, a photothrombotic damage in the M1 was performed. The animals were anaesthetized with Zoletil (50 mg/kg) and xylazine (9 mg/kg) anaesthesia. After checking by toe pinching that a deep level of sedation had been

reached, the animals were placed into a stereotaxic apparatus (Stoelting, Wheat Lane, Wood Dale, IL 60191). The eyes of the animal were protected from dehydration through application of eye gel (Lacrigel). After disinfecting the skin with betadine and applying the local anaesthetic lidocaine 2% (20 mg/mL), the skin over the skull was cut and the periosteum was removed by scraping the skull with a blade. The M1 was identified (stereotaxic coordinates +1,75 lateral, -0.5 rostral from bregma). Five minutes after intraperitoneal injection of Rose Bengal (0.2 ml, 10 mg/ml solution in Phosphate Buffer Saline (PBS); Sigma Aldrich, St. Louis, Missouri, USA), a white light from an LED lamp (CL 6000 LED, Carl Zeiss Microscopy, Oberkochen, Germany) was focused with a 20X objective (EC Plan Neofluar NA 0.5, Carl Zeiss Microscopy, Oberkochen, Germany) and used to illuminate the M1 for 15 min in order to induce unilateral stroke in the right hemisphere. Afterwards, based on the type of experiments mice are subjected to different type of procedures both to induce the expression of ChR2 in targeted regions, both to realize optical windows for wide field or two photon imaging.

3.3 Optical windows

For the experiments on GCaMP6f mice, we performed a thinned skull preparation on the right hemisphere between bregma and lambda to create an optical window. After applying the local anaesthetic lidocaine 2% (20 mg/mL), the skin over the skull and periosteum was removed. The skull over most of the right hemisphere was thinned using a dental drill. A cover glass and an aluminium head-post were attached to the skull using transparent dental cement (Super Bond, C&S). We waited at least four-five days after the surgery for the mice to recover before the first imaging session.

For the experiments on GFPM mice, we created a square (3x5 mm2) cranial window centred laterally on the right M1 (+1.75 mm from bregma) and extending rostro-caudally from 1 mm posterior to the

bregma to lambda. The protocol we followed for cranial window preparation was slightly modified from Holtmaat et al., 2009 [202] and Allegra Mascaro et al., 2014[203], *Figure 15*.
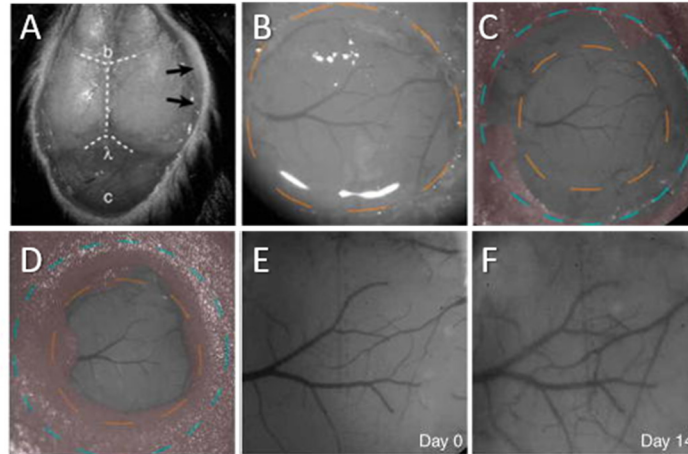
Figure 15: ***Surgical procedure for cranial window on the somato-sensory cortex of Thy1-GFP mice.*** *(A)The skin over the skull and the periosteum have been removed to expose the cranial bone. (B) A circular groove is drilled (dashed orange line) in the region of interest, when the island of bone is detached from the surrounding skull the bone is removed exposing the brain. (C) A cover glass is positioned (blue dashed circle) is positioned in order to cover the brain and part of the skull; (D) the cranial window is sealed with dental cement. (E) Bright field images show the superficial blood vessel through the glass window immediately after the surgery (F) and 24 days later. Modified from Holtmaat et al., 2009 [202].*

Briefly, we administered anesthetized mice a subcutaneous injection of dexamethasone (0.04 ml per 2 mg/ml). The animals were then placed into a stereotaxic apparatus; after applying the local anesthetic lidocaine 2% (20 mg/mL), the skin over the skull was removed. Using a dental drill (Silfradent, Forlì-Cesena Italia), the border of the area of interest was thinned and the central part of the bone was then gently removed. The exposed brain was covered with a circular cover glass; the optical window was sealed to the skull with a mixture of dental cement and acrylic glue. Finally, an aluminium head-post was attached

onto the skull using dental cement (Super Bond, C&S, Sun medical Moriyama City, Shiga, Japan). The surgery was followed by the first imaging session under the two-photon microscope. If the cranial windows were opaque on the second imaging session, the windows were removed and cleaned, and imaging was performed immediately afterwards. After the last imaging session, all animals were perfused with 150 mL of Paraformaldehyde 4% (PFA, Aldrich, St. Louis, Missouri, USA).

3.4 Intra-cortical injections

We used a dental drill to create a small craniotomy over M1, which was identified by stereotaxic coordinates (+0.5 rostrocaudal, -1.75 mediolateral). Botulinum Neurotoxin E (BoNT/E) injections were performed during the same surgical session in which the photothrombotic lesions were created. We injected with a glass capillary (Ø of the tip: 50 µm) 500 nl of BoNT/E (80 nM) divided in 2 separate injections of 250 nl at (i) +0.5 anteroposterior, +1.75 mediolateral and (ii) +0.4 rostrocaudal, +1.75 mediolateral at 700 µm cortical depth.

For virus injections, we delivered with a glass capillary (Ø of the tip: 50 µm) 1 µl of AAV9-CaMKII-ChR2-mCherry (2.48*1013 GC/mL) 700-900 µm deep inside the cortex. The skin over the skull was then sutured; the animals were placed in a heated cage (temperature 38°) until they fully recovered. For optogenetic rehabilitation an intracortical injection was performed in the peri-lesioned region (-0.75 rostrocaudal, +1.75 mediolateral) at 600 µm cortical depth. A volume of 0.5 µL was delivered with a glass capillary (Ø of the tip: 50 µm) with pression at 3 atm, 4 ms of duration and 7 Hz of frequency.

3.5 Motor training protocol on the M-Platform

Mice were allowed to become accustomed to the apparatus before the first imaging session so that they became acquainted with the new environment. The animals were trained by means of the M-Platform (*Figure 16*), which is a robotic system that allows mice to perform a retraction movement of their left forelimb [84]. The M-Platform is composed of a linear actuator, a 6-axis load cell, a precision linear slide with an adjustable friction system and a custom-designed handle that is fastened to the left wrist of the mouse. The handle is screwed onto the load cell, which permits a complete transfer of the forces applied by the animal to the sensor during the training session. Each training session was divided into "trials" that were repeated sequentially and consisted of 5 consecutive steps. First, the linear actuator moved the handle forward and extended the mouse left forelimb by 10 mm (full upper extremity extension). Next, the actuator quickly decoupled from the slide and a tone lasting 0.5 s informed the mouse that it should initiate the task. If the animal was able to overcome the static friction (approximately 0.2 N), it voluntarily pulled the handle back by retracting its forelimb (i.e. forelimb flexion back to the starting position). Upon successful completion of the task, a second tone that lasted 1 sec was emitted and the animal was given access to a liquid reward, i.e. 10 µl of sweetened condensed milk, before starting a new cycle.

To detect the movement of the wrist of the animal in the low-light condition of the experiment, an infrared (IR) emitter was placed on the linear slide, and rigidly connected to the load cell and thus to the animal's wrist. Slide displacement was recorded by an IR camera (EXIS WEBCAM #17003, Trust) that was placed perpendicular to the antero-posterior axis of the movement. Position and speed signals were subsequently extracted from the video recordings and synchronized with the force signals recorded by the load cell (sampling frequency = 100 Hz).

All groups performed at least one week (5 sessions) of daily training, starting 26 days after injury for STROKE mice, 5 days after stroke for the REHAB group and after the surgery for CTRL animal.
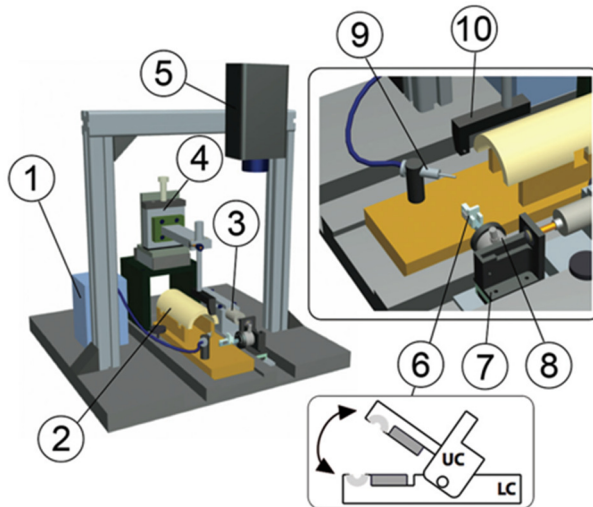
*Figure 16: **Representative scheme of M-Platform.** The robotic interface consists of a peristaltic pump for reward delivery (1), mouse restrainer (2), linear actuator (3), micromanipulator (4) for precise positioning of the mouse head, camera (5), handle (6), slide (7), load cell (8), gavage-feeding needle (9), and head fixation system (10). A schematic of the handle is also shown: the upper and lower components (respectively UC and LC), the 2 magnets (gray) and the semicircular groove (light grey).*

In the optogenetic rehabilitation experiment a new version of M-Platform was used. In order to permit a customized rehabilitation has been developed a robotic device characterized by a new actuated system to dynamically and precisely modulate the level of static friction, to provide a more adjustable rehabilitative approach, tailored on the spared capacity of the single animals. To realize the adjustment of the friction of the device during the calibration a rigid component connect the actuator with the slide. This component mimics the effect of the retraction movements performed by the animal, reproducing the applied forces in direction and point of application.

For the evaluation of the forces applied during the motor training we analysed the prominence of the force signal in the rostro-caudal direction.

All groups performed at least one week (5 sessions) of daily training, starting 26 days after injury for Sham and Optostim mice, 5 days after stroke for the Robot-F and Optostim+Robot group and after the surgery for Ctrl animal.

3.6 Behavioural evaluation of forelimb use asymmetry

Mice were put individually inside a clean cylinder (diameter, 8 cm; height, 20 cm) that was placed vertically above a transparent surface and were allowed to explore this enclosure for 5 minutes. Mice were video- taped with a camcorder (C270, Logitech) that was positioned underneath the transparent surface. The number of paw touches on the wall during rearing was recorded offline, and the percentage use of each paw relative to the total amount of touches was calculated.

$$\text{Ai} = \left(\frac{C_{ipsi}}{C_{ipsi} + C_{contra}}\right) \times 100 - \left(\frac{C_{contra}}{C_{ipsi} + C_{contra}}\right) \times 100$$

3.7 Optogenetic stimulation and simultaneous recording of GCaMP6f activity

After the last training session (i.e. 30 days after stroke and at least 2 weeks after the AAV injection in the CTRL group) mice were anesthetized under Zoletil (50 mg/kg) and xylazine (9 mg/kg) and placed into the stereotaxic holder. A small (2x2 mm2) craniotomy was performed over the injected area. After placing the mouse under the

wide field fluorescence microscope, we performed repeated laser (473 nm) stimulation (1-2 Hz, pulse duration 3-5 ms, pulse train duration 5 sec, laser power at the focal plane 5 mW) on the left M1, which was localized by mCherry fluorescence. Spurious activation of ChR2 from the green LED (used for GCaMP6f fluorescence excitation) was avoided by blocking half the illumination path with a shutter positioned after the collimator.

3.8 Optogenetic rehabilitation

Awake head fixed mice were place under the wide field microscope to perform daily session of optogenetic stimulation. A blue 473 nm laser is used to deliver 5 Hz, 10ms light pulses with a power range of 0.2-0.8 mW. The laser power is adjusted during the rehabilitation period according to the increment of the transfected area, and set at a value lower than the one necessary to elicit movements in the affected forelimb.

The system is provided with a random access scanning head, developed using two orthogonally-mounted acousto-optical deflectors (DTSXY400, AA Opto-Electronic). The acousto-optic deflectors rapidly scan lines with a commutation time ≈ 5 µs between a line and the next. After scanning the desired shape, in this case a cross, acousto-optic deflectors returned to the initial position and repeated the cycle for the total illumination time.

The stimulation protocol consists of 3 successive 30 s stimulation daily separated by 1 min rest intervals. All animals (Sham, Optostim and Optostim+Robot), except for Ctrl and Robot-F groups, were stimulated every day for four weeks, five days after photothrombosis.

3.9 Electrophysiology

Local field potential (LFP) were recorded in the peri-infarct cortex of anhestetized Thy1-GCaMP6f mice expressing ChR2 in excitatory neurons. After exposing the transfected region with a craniotomy (∅ 0.4 mm), a glass pipette was filled with artificial cerebral spinal fluid (ACSF) composed of (in mM) – NaCl, 130; KCl, 3.5; $NaHCO_3$, 25; glucose, 10; $CaCl_2$, 2; and $MgSO_4$,1. The electrode was advanced into the target area at an angle of 40˚ using a motorized micromanipulator (EXFO Burleigh PCS6000 Motorized Manipulator). Signals were amplified with the 3000 AC/DC differential amplifier, sampled at 10 kHz and lowpass filtered at 5 KHz. A reference electrode, teflon-coated, chlorided silver wire (0.125 mm) was placed on a metal screw placed on the parietal bone.

3.10 Wide-field fluorescence microscopy

The custom-made wide-field imaging setup (*Figure 17*) was equipped with two excitation sources for the simultaneous imaging of GCaMP6f fluorescence and light-stimulation of ChR2. For imaging of GCaMP6f fluorescence, a 505 nm LED (M505L3 Thorlabs, New Jersey, United States) light passed through a band pass filter (482/18 Semrock, Rochester, New York USA) was deflected by a dichroic filter (DC FF 495-DI02 Semrock, Rochester, New York USA) on the objective (2.5x EC Plan Neofluar, NA 0.085, Carl Zeiss Microscopy, Oberkochen, Germany). A 3D motorized platform (M-229 for xy plane, M-126 for z-axis movement; Physik Instrumente, Karlsruhe, Germany) allowed sample displacement.

The fluorescence signal was selected by a band pass filter (525/50 Semrock, Rochester, New York USA) and collected on the sensor of a high-speed complementary metal-oxide semiconductor (CMOS) camera (Orca Flash 4.0 Hamamatsu Photonics, NJ, USA).
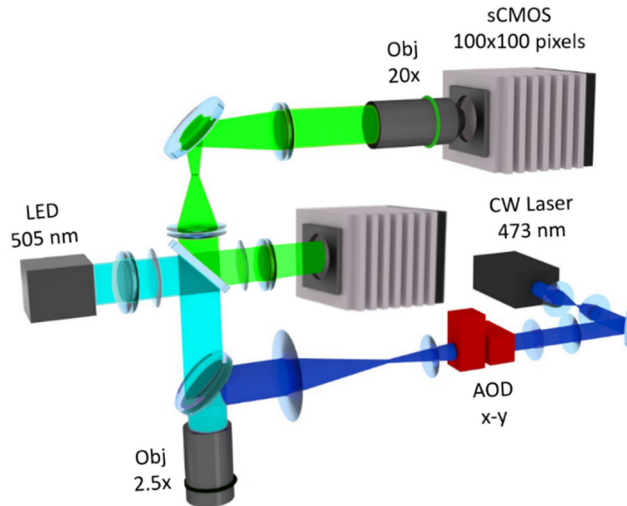
*Figure 17: **Wide field fluorescent microscope.** The scheme represents the setup used for calcium imaging (lower camera) and optogenetic stimulation (upper camera) on Thy1-GCaMP6f mice. A 505 nm LED, passed through a filter (482/18) and deflected by a dichroic filter (FF 495-DI02) is used to illuminate the sample through a 2.5X EC Plan Neofluar. The fluorescence signal passed through a band pass filter (525/50) and then is collected by a sCMOS camera. For optogenetic stimulation a 473 laser was scanned by acousto-optic deflector. The fluorescence signal is transmitted to the sensor through a 20X objective to demagnify the image onto a 100 x 100 pxl.*

To perform optogenetic stimulation of ChR2, a 473 nm continuous wavelength (CW) laser (OBIS 473nm LX 75mW, Coherent, Santa Clara, California, United States) was overlaid on the imaging path using a second dichroic beam splitter (FF484-Fdi01-25x36, Semrock, Rochester, New York USA). The system has a random-access scanning head with two orthogonally-mounted acousto-optical deflectors (DTSXY400, AA Opto-Electronic, Orsay France). A 20X objective (LD Plan Neofluar, 20x/0.4 M27, Carl Zeiss Microscopy, Oberkochen, Germany) was used to demagnify the image onto a 100 x 100 pxl^2 area of the sCMOS camera sensor (OrcaFLASH 4.0, Hamamatsu Photonics, NJ, USA). Images (512x512 pixels, pixel size 9 μm) were acquired at 25 Hz.

3.11 Two-photon fluorescence microscopy
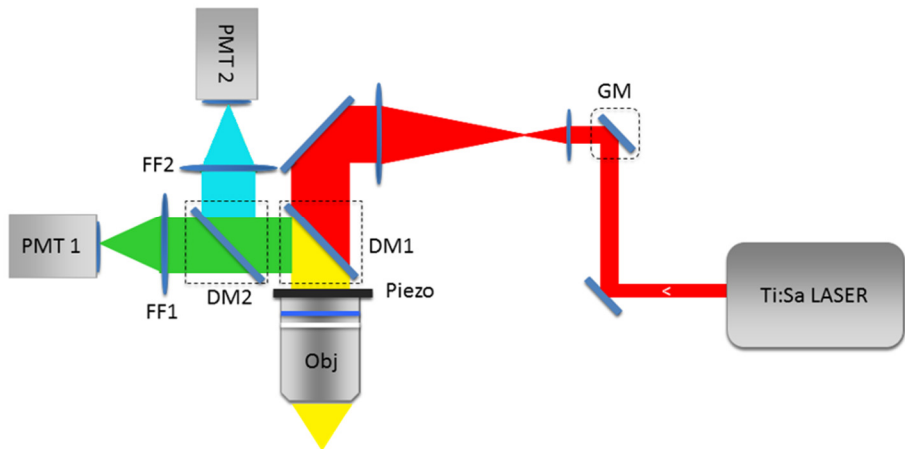
*Figure 18: **Wide two-photon fluorescent microscope.** The scheme represent the setup used for study of structural plasticity in vivo on Thy1-GFPM mice. The laser beam (in red) is scanned by two galvanometric mirrors (GM). A 20X Olimpus focused the beam onto the specimen. The fluorescent signal was collected by photomultiplier tube (PMT).*

The custom made apparatus for two-photon microscopy (*Figure 18*) included a mode-locked Ti: Sapphire laser (Chameleon, Coherent Inc.) that supplied the excitation light. The laser beam was scanned in the xy-plane by a galvo system (VM500, GSI Lumonics). An objective lens (XLUM 20X, NA 0.95, WD 2 mm, Olympus) focused the beam onto the specimen. A closed-loop piezoelectric stage (PIFOC ND72Z2LAQ, PhysikInstrumente, Karlsruhe Germany) allowed axial displacements of the objective up to 2 mm with micrometric precision. Finally, the fluorescence signal was collected by a photomultiplier tube (H7710-13, Hamamatsu Photonics). Custom-made software was developed in LabVIEW 2013 (National Instruments).

3.12 Image analysis

Wide-field calcium imaging: during each experimental session, the mouse's head was restrained and placed on the M-platform under the wide-field microscope. To avoid head movement artefacts, each frame of the fluorescence stack was offline registered by using two reference points (corresponding to bregma and lambda) that were previously marked on the glass window during the surgery procedure.

For each stack (*FluoSt*) a median time series of GCaMP6f fluorescence signal (*mF*) was extracted, where the value of mF at each *i-th* time point corresponded to the median value computed on all the pixels of the *i-th* frame of *FluoSt*. The *mF* was then oversampled and synchronized to the 100 Hz force and position signals.

The *mF* was used to define a GCaMP6f fluorescence signal baseline F_0, which was identified by the concomitant absence of fluorescence and force signal deflections. F_0 was selected within a 2.5 ± 0.7 s interval (*I*) of 62 frames where the fluorescence signal was below 1 standard deviation (STD) of the whole *mF* signal and the corresponding force signal showed a value below of 1 STD of the whole recorded force signal. The fluorescence signal interval was used to reconstruct a 512 x 512 matrix, i.e. baseline matrix, in which the value of each pixel *B* of the {*m*, coordinates of the matrix was computed as follows:

$$B_{\{m,n\}} = median(p_{\{m,n\},j}) \; with \; j = 1,...,N_{\{I\}}$$

where $p_{\{m,n\},j}$ is the value of the pixel *p* of the *{m,n}* coordinates at the *j-th* frame of the interval *I* and $N\{I\}$ is the length of Interval *I*. The baseline matrix was then used to normalize all the frames of the fluorescence stack *FluoSt*.

The noise-threshold of 1 STD of the whole recorded force signal was used as a measure of the force peaks exerted by the animal during the retraction task. According to Spalletti et al. 2014 [84], a force peak is defined as force values that transiently exceed the noise-threshold and result in a movement of the linear slide, as detected by variation of the

position signal. To maintain consistency in this analysis, peaks of force that did not result in a movement of the slide were not considered.

The onset of each force peak was used as reference time point to select a sequence of 60 frames (2.4 s, where 0.4 s preceded the force peak) from the *FluoSt*. All sequences were visually checked to exclude possible spurious activation (e.g. early activation or no activation) from the analysis. All the selected sequences (*Seq*s) of the animal *An* on day *d* were compiled, defining a *stack of Seqs*, to compute the *Summed Intensity Projection* for the *An* at *d* ($SIP_{An\ d}$). The SIP is a matrix of 512 x 512 pixels, in which the value *P* of the pixel of the *{m, n}* coordinates is computed as follows:

$$P_{\{m,n\}} = \sum_{k=1}^{Ns} p_{\{m,n\},k}$$

where $p_{\{m,n\},k}$ is the value of the pixel p of the *{m, n}* coordinates at the *k-th* frame of *stack of Seqs,* and Ns is the number of frames of the *stack of Seqs*.

The most active area of the $SIP_{An\ d}$ was then detected by thresholding the $SIP_{An\ d}$ with a *median* ($SIP_{An\ d}$) + *STD* ($SIP_{An\ d}$) threshold value. The threshold $SIP_{An\ d}$ (*th-* $SIP_{An\ d}$) computed for each week of training on the M-Platform (d=1,...,4 of week W) was superimposed and the common areas, activated at least for 3 daily sessions out of 5 (60%), were labelled as "regions of interest" (ROIs) of the SIP_{An}. We further refined the analysis by dividing the image into two areas, and identifying one anterior ROI [-0.25 - +1.95 mm from bregma (B), AP] and one posterior ROI [+1.95 - + 4.15 mm from B, AP].

We also used the ROIs defined for each individual animal to identify the average ROIs among mice from the same experimental group: ROI_g with g = "CTRL", "STROKE" and "REHAB" (see *Figure 22B*). Thus, the ROIs from animals of the same group were compiled and further

thresholded (60%) to define the ROI_g. The extent of the ROI_g was computed as follows:

$$Area_{ROIg} = Area_p \times N_{ROIg}$$

where $Area_p$ corresponds to the area of a single pixel of the image (0.0086 mm^2) and N_{ROIg} is the number of pixels composing the ROI_g. Moreover, the centroid of each ROI_g was identified and its Euclidean distance from bregma was computed (*Figure* 22A).

The ROIs defined for each individual animal were further used to extract the GCaMP6f fluorescence signal corresponding to the activity of those areas. Indeed, from each frame of the *FluoS*, only pixels belonging to the selected ROI were considered when calculating the representative median value. Thus, a median time series, F_{ROI}, was extracted from the whole *FluoS* and was representative of the ROI. The fluorescence signal was normalized ($\frac{\Delta F_{ROI}}{F_0}$ 100%) and low-pass filtered to clean the signal from the detected breathing artefacts (Chebyshev filter with cutting frequency = 9 Hz).

The previously detected force peaks were then used to select the GCamp6f fluorescence peaks from the $\frac{\Delta F_{ROI}}{F_0}$ signal. A time window that lasted 4 seconds, i.e. *wnd*, and was centred at the onset of the force peak, was used to delimit a part of the $\frac{\Delta F_{ROI}}{F_0}$ signal, i.e. F_{wnd}, to identify the corresponding fluorescence peak. A fluorescence peak was defined as the part of F_{wnd} that overcame the value of *median+3STD* calculated for the whole signal $\frac{\Delta F_{ROI}}{F_0}$. The onset of the peak was detected as:

$$t_{\{peak\ onset\}} = t_{\left\{min\left(\frac{dF_{wnd}}{dt}\right)\right\}}$$

calculated for the [$tst\ tmax$] time interval, where tst and $tmax$ are the time points corresponding to the start of the *wnd* and the maximum of F_{wnd}, respectively.

From the fluorescence and force peaks, different parameters were computed as follows:
- the maximum of the peak (*Peak amplitude*).

- the *Slope* of the peak was defined as follows:

$$Slope_{\{peak\}} = max\left(\frac{dS}{dt}\right)$$

between the $t_{\{S\ peak\ onset\}}$ and $t_{S\ max}$ where S = *fluo* or *force* signal.
- the time delay between the occurrence of the maximum of the fluorescence (*ΔT*).

The first movement time point was defined as the first variation of the position signal ($\frac{dx}{dt} > 0$) detected along the *wnd* interval.

Optogenetically-induced calcium activity: On every stack, we analysed the calcium activity averaged over a round ROI (2.3 mm of diameter) centred on the peri-infarct area. Changing in the variation of fluorescence signal (ΔF/F) triggered by light irradiation of the contralateral hemisphere that were below 1% were excluded from the analysis. A calcium response was considered optogenetically-triggered if it started within 120 ms of optogenetic stimulation. The activation delay refers to the average (± Standard Error of the Mean, SEM) delay of the calcium peak with respect to the onset of laser stimulation. The success rate reports the number of times the laser stimulation successfully triggered contralateral activation over the total number of stimulation trials.

Two-photon imaging:
For the structural plasticity analysis of dendrites and spines of pyramidal neurons, we compared stacks in a vertical mosaic acquired in the rostro-caudal direction. During the last week of training (1st and 4th day), we acquired a mosaic of 100 μm thick stacks (113 x 113 μm^2)

distanced 200 µm from each other along the rostro-caudal axis starting from the borders of the stroke core. We grouped stacks near (<500 µm) and far (from 1000 to 1500 µm) from the core, namely proximal and distal regions, respectively. Dendrite orientation was evaluated on 15 dendrites for each stack (on average) by measuring frame by frame the angle between each structure and the rostro-caudal axis. The stroke core was considered to be at 0°. For synaptic plasticity analysis, the fluorescence signal of a spine had to be at least 1 standard deviation higher than the dendritic shaft fluorescence to be included in the analysis. We quantified the plasticity of dendritic spines using two functions: surviving fraction (SF) and turnover ratio (TOR) [202]; the SF describes the fraction of persistent structures:

$$SF(t) = N(t2) / N(t1)$$

where N(t1) is the number of spines present during the first imaging session (26 days after injury for STROKE and REHAB mice), while N(t2) indicates those structures that present 4 days after the first imaging session. The TOR evaluates the fraction of newly appeared in the images and disappeared structures:

$$TOR (t1, t2) = (Nnew + Ndisappear) / (N(t1) + N (t2))$$

where Nnew is the number of structures that are reported for the first time at time t2, Ndisappear is the number of structures that were present at time t1 but which are no longer present at time t2; N (t1) and N (t2) are the total of spines present on t1 and t2, respectively. Unless otherwise stated, data are reported as mean ± SEM.

3.13 Statistical Analysis

Data were analysed using Origin Pro. The specific tests used are stated alongside all probability values reported.

Results

4.1 Combination of motor training and contralateral homotopic inhibition promotes the rewiring of functional and structural connectivity after stroke

In this thesis we applied a multi-level approach to investigate cortical remodelling induced by rehabilitation in a mouse model of photothrombotic stroke in the primary motor cortex. By combining different optical imaging techniques, we explored the cortical reshaping in the peri-infarct area at different scale, from the single synapses up to the entire hemisphere, induced by rehabilitation. The rehabilitative protocol combines pharmacological treatment and motor training. In detail, during the acute phase after stroke, through an intracortical injection of Botulinum Neurotoxin E (BoNT/E), the contralesional homotopic area in the healthy hemisphere is silenced. The mechanism of BoNT/E is based on the cleavage of membrane receptor SNAP-25, a main component of SNARE complex, resulting in the block of neurotransmitter release. Based on the interhemispheric competition model, which assess that loss of the mutual interhemispheric control leads to an excessive inhibition exerted by the undamaged hemisphere over the spared perilesional tissue, the temporary silencing of the healthy M1 could be a great target for rehabilitation therapy, especially in case of confined damaged. Indeed previous studies, showed that the inactivation of the healthy hemisphere via TMS or tDCS has yielded some positive yet variable effects in clinical trials [122-125, 204]. Neuronal modulation treatment is coupled to one month of motor training on a robotic platform. As previously observed by Spalletti et al. [100], the daily robotic training itself induced an improvement in the parameters related to the retraction task on the M-Platform only. As they asserted in their study, this improvement was not generalized to other forelimb tasks indicating that the daily training of the affected forelimb per se ameliorates

strength and motor control but only for those movements that are practiced.

We thus decided to combine the motor training with the contralateral inhibition of the homotopic area to generalize the recovery of the forelimb functionality.

In this thesis we set out to investigate how the rehabilitation protocol shapes functional and structural plasticity in the peri-infarct region.

To investigate functional plasticity, we performed calcium imaging of cortical activity at a meso-scale level with a wide-field microscope revealing the activation of cortical areas of GCaMP6f mice performing motor training during the rehabilitation month. Then, to evaluate the rewiring of interhemispheric remapping we applied an optogenetic approach to manipulate neuronal activity. By developing a wide-field system with a double illumination path and a split field of view, we simultaneously stimulated homotopic M1 in the healthy hemisphere and revealed the cortical activity in the peri-infarct area.

We finally investigated with a two photon fluorescence microscope the structural remodelling in the peri-infarct area of GFPM mice, at the synaptic level *in vivo*.

4.1.1 Experimental design

In my PhD project we used a photothrombotic model of ischemic stroke to realize a focal damage in the primary motor cortex (M1). We took advantage of a rehabilitation paradigm that combines motor training and pharmacological inhibition of the contralesional M1 with Botulinum Neurotoxin E (BoNT/E) [205]. The combined rehabilitation paradigm of the REHAB group consists in a combination of highly repeatable motor training of the mouse forelimb in a robotic platform (M-Platform [84]) and reversible pharmacological inactivation of the healthy, contralesional hemisphere via the synaptic blocker BoNT/E (*Figure 19A*). BoNT/E is a bacterial enzyme that enters synaptic terminals and reversibly blocks neurotransmission by cleaving SNAP-

25, a main component of the SNARE complex [99]. Spalletti et al. shown that BoNT/E injection reduced the excessive transcallosal inhibition exerted from the healthy to the stroke side [100]. Rehabilitation-associated training on the M-Platform consisted of repeated cycles of passively actuated contralesional forelimb extension followed by its active retraction triggered by an acoustic cue (*Figure 19B*). The combination of motor training and BoNT/E silencing was superior to either treatment alone in promoting recovery of motor skills in stroke mice [100]. Importantly, this combined therapy led to motor improvements that generalized to multiple motor tasks [100]. The induction of a generalized functional gain, i.e. the recovery of motor functions beyond the ones that are trained, is crucial when evaluating the efficacy of rehabilitative therapies.

In order to investigate how the combined treatment moulded functional and structural plasticity we used two different transgenic mouse line, Thy1-GCaMP6f and Thy1-GFP, expressing respectively in excitatory neurons the fast and sensitive calcium indicator GCaMP6f and the fluorescent protein GFP.

We splitted up our sample in three experimental groups, healthy mice (CTRL) preforming five days of motor training, mice impaired by photothrombosis performing five days of rehabilitation twentysix days after the damage (STROKE) and stroked mice undergoing the combined rehabilitative treatment (REHAB). REHAB mice were trained for four weeks starting five days after injury (*Figure 19C*), in line with the overall consensus that the initiation of rehabilitative training five or more days after stroke is mostly beneficial and has no adverse effects [206]. The motor task was rapidly learned and easily performed. Indeed, the amplitude and slope of the force peaks exerted during the voluntary forelimb-pulling task were not significantly different across groups, neither within a week nor across weeks of training (*Figure 19D*). The motor training does not require particular efforts, allowing the execution of the pulling task with the same application of force both in healthy and non-treated mice. Indeed, the force applied by animals of different experimental groups results comparable.
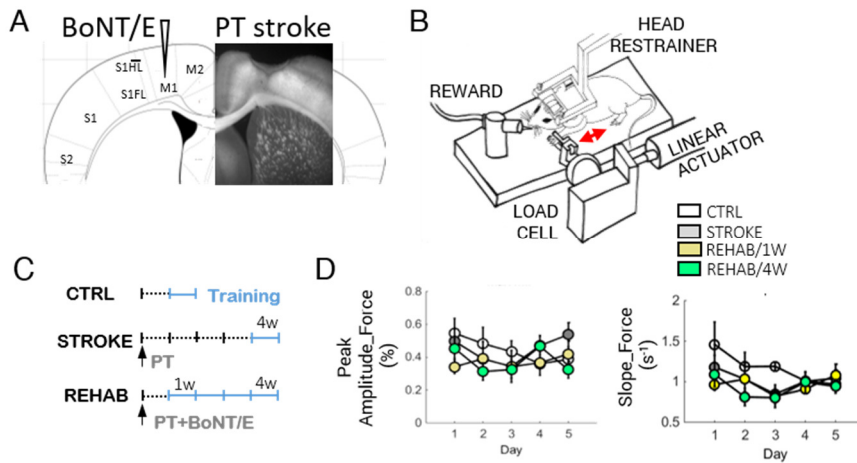
*Figure 19: **Experimental design.** (A) A schematic of the experimental protocol, which combines the photothrombotic stroke in the primary motor cortex (M1) with a contralesional injection of BoNT/E into the homotopic cortex. (B) A schematic representation of the M-Platform that was used for rehabilitative training. (C) The experimental timeline for the CTRL, STROKE and REHAB groups in the awake imaging experiment. Light blue lines refer to training weeks. W = week; PT = photothrombosis. (D) Graphs showing the Peak amplitude (left) and Slope (right) of the force signals recorded in the pulling phase during training on the M-Platform over 5 days (4 weeks after injury for STROKE mice, 1 and 4 weeks after injury for REHAB mice, during the week of training for CTRL mice). There is no significant difference between the groups and over the 5 days.*

4.1.2 Vascular reshaping after phothrombotic stroke

During imaging experiments, we longitudinally observed mouse cortices of all groups under both cranial window and thinned skull preparations for one month after stroke. We found that after stroke, the injured area consistently shrunk owing to the collapse of dead tissue in STROKE and REHAB mice (*Figure 20* and *25A*). More in details, in the cranial window preparation, we observed morphological modification of blood vessels and phenomena of neo angiogenesis that

took place four days after photothrombotic stroke (*Figure 20A*). At a glance new blood vessels were predominantly orientated towards the stroke core and characterized by a less regular structure. At the same time the morphological organization of the old ones was altered: some of them appear considerably larger, while others disappeared.
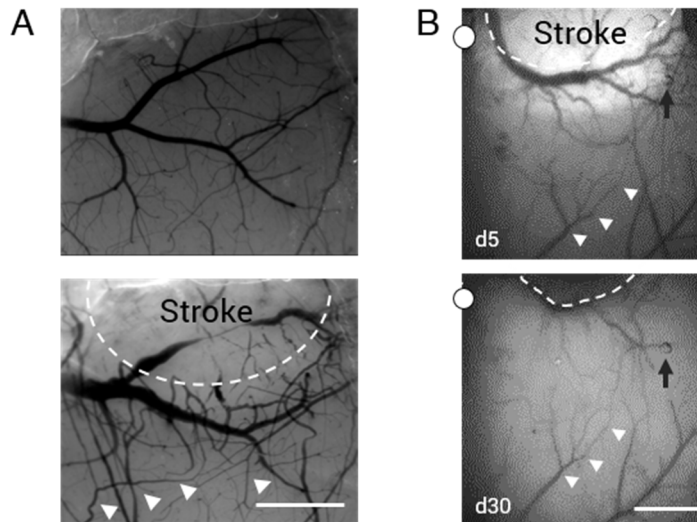
*Figure 20: **Vascular reshaping after stroke in two windows preparation.** (A) Imaging showing cranial window of the same animal before (top) and 4 days after (down) photothrombosis. Dotted line define the border of the stroke. White arrowheads point the changings of blood vessels morphology. Scale bar 1 mm. B) Brightfield images showing cortical vasculature after stroke under a thinned skull preparation. Dotted line emphasizes the profile of a large blood vessel shifting toward the stroke core from 5 days to 30 days after stroke; a similar shift is highlighted by the white arrowheads on a blood vessel distal to the injury site. Black arrow points to an internal reference on the image. White dots indicate bregma.*

In addition, a very bright area appeared in the peri-infarct region of STROKE and REHAB groups of GCaMP6 mice, possibly representing an excitotoxic response associated with calcium dysregulation [207] elicited by the photothrombotic stroke (see the left panel of *Figure 20B*; 13 out of 14 STROKE and REHAB mice). The enhanced brightness gradually

diminished and disappeared after the acute period (six-nineteen days after injury in STROKE and REHAB mice; see example in *Figure 20B*, right panel), and was accompanied by a large shrinkage of the necrotic tissue. The consequent displacement of the peri-infarct area was associated with a substantial remodelling of blood vessels (white arrowheads in *Figure 20*), in agreement with previous studies [201].

4.1.3 Combined rehabilitation treatment restores cortical activity patterns disrupted by stroke

In order to reveal cortical activation on awake mice during motor training, we implemented an integrated system for simultaneous imaging of the calcium indicator GCaMP6f over the injured hemisphere and recording of forces applied by the contralesional forelimb during the training sessions on the M-Platform (*Figure 21A-C*). Calcium imaging was used as a measure of cortical activity in the brains of GCaMP6f mice. We focalized on the analysis of cortical waves activated in the same time-window of the voluntary retraction movement (see example in *Figure 21C*, right panel). Wide-field calcium imaging showed that a small area located in the motor-sensory region reproducibly lit up in CTRL mice during the forelimb retraction movement on the M-platform (an example of cortical activation is reported in *Figure 21D*). On the contrary, a large area covering most of the cortical surface of the injured hemisphere was activated synchronously while performing the task in non-treated (STROKE) mice one month after stroke. Remarkably, calcium activation in REHAB mice was similar to healthy controls (CTRL) in terms of extension, location, timing and amplitude (*Figure 21D*, *Figure 22A-G*).

We analysed the extension and location of the motor representation by overlapping the movement-triggered activation maps obtained on every day of the training week (*ROIg*, see *Figure 22A-B* and Methods). Stroke expanded the motor representation from M1 toward more

caudal regions not specifically associated with motor control (STROKE group in *Figure 22B*, 2nd panel). Interestingly, the extension of motor representation in REHAB mice was reduced up to pre-stroke conditions (*Figure 22B* 3rd panel and *Figure 22C*). In terms of location, the motor representation was centred on the motor-associated region in the peri-infarct area. In most cases (5 out of 6 REHAB mice) we found a higher correlation (i.e. augmented functional connectivity) in the activity of spared motor-associated areas (*Figure 22H*) at the end of the training period (REHAB/4W) compared to the beginning (REHAB/1W).

We hypothesized that focalized versus spread motor representations could be associated with different patterns of propagation of calcium waves. To quantify the concurrent recruitment of motor-associated and other functional areas, we analysed the temporal profile of movement-triggered calcium waves over the injured hemisphere.

We assumed that an extended activation (as in STROKE mice) implied a synchronicity in the activation of the rostral peri-infarct and the caudal areas.

Indeed, we found that the delay between the maximum calcium peak of the rostral and caudal regions was slightly negative in STROKE mice, indicating that the activation of the caudal region somewhat preceded the activation of the rostral (peri-infarct) areas (*Figure 22E*). On the other hand, the delay was positive in CTRL and REHAB mice. Longitudinal imaging showed that the temporal pattern of rostro-caudal calcium activation in REHAB mice was gradually recovered towards pre-stroke conditions during four weeks of training (*Figure 22I*, left panel). To sum up, the combined rehabilitative treatment focalized the motor representation to the peri-infarct region. The motor representation of REHAB mice closely resembled CTRL animals in spatial and temporal terms.
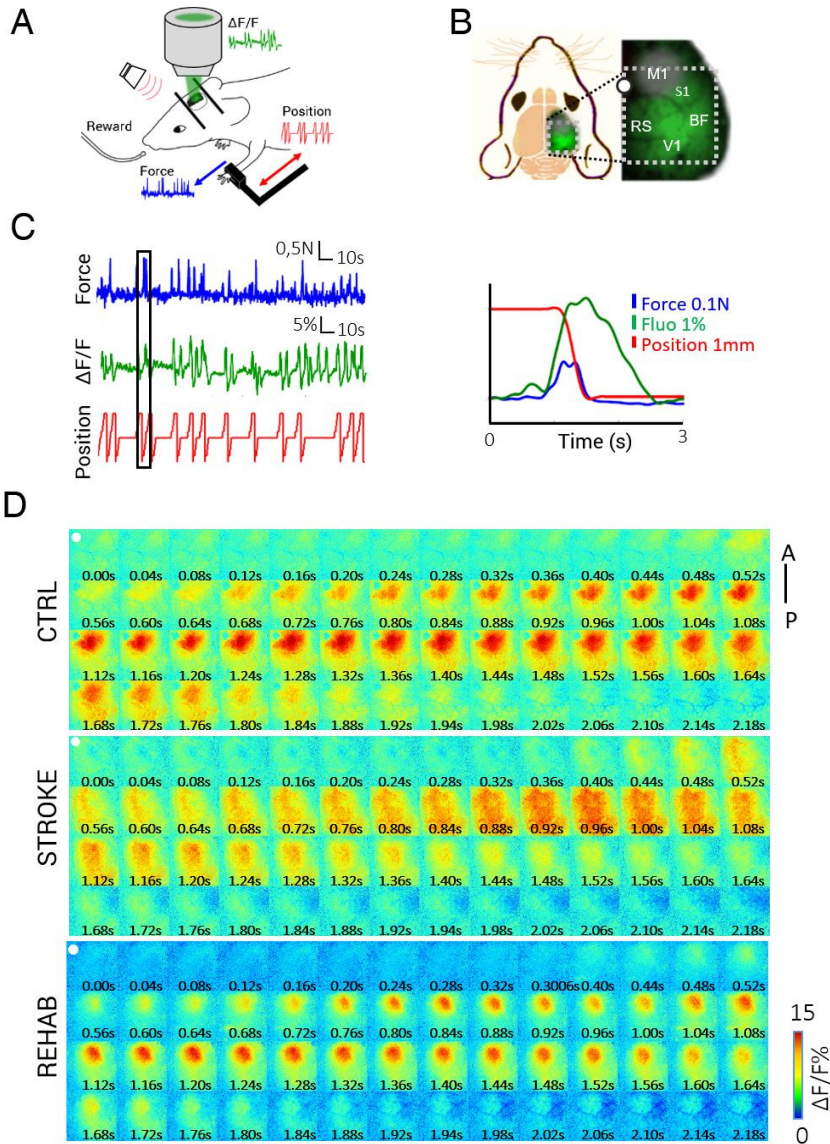
*Figure 21: **Combined rehabilitation counteracts cortical dedifferentiation and restores cortical activation profiles in the post stroke, peri-infarct region**. (A) Schematic representation of M-Platform: examples of simultaneously recorded force (blue), position (red) and ΔF/F traces (green) are reported. (B) Schematic representation of field of view (i.e. area within the dotted white square) used for wide-field calcium imaging in GCaMP6f mice. The gray circle on M1 region highlights the location and approximate extent of the lesion. M1, primary motor area; S1, primary somatosensory area; BF, barrel field; V1, primary visual cortex; RS, retrosplenial cortex. White dot indicates the bregma. (C) Example of force trace (blue), fluorescence trace (green) and handle position (red). The graph on the right shows an overlap of simultaneously recorded traces corresponding to the black box on the left. (D) Complete image sequences of cortical activation as assessed by calcium imaging during pulling of the handle by the contralateral forelimb of CTRL (top), STROKE (middle) and REHAB (bottom) GCaMP6f mice in the M-Platform. A-P, anterior-posterior. The white dot indicates bregma. Scale bar = 1 mm.*

We further analysed the calcium transients in peri-infarct area during contralateral forelimb retraction in CTRL, STROKE, and REHAB mice. At a glance, the average traces in *Figure 22D* show that stroke (in STROKE mice) and the combined treatment (REHAB mice) modified several features of the calcium transients. While a significant reduction in the amplitude of calcium transients during forelimb retraction was evident one month after stroke in the STROKE group, REHAB mice partially recovered to pre-stroke conditions (*Figure 22F*).

In detail, the combined treatment led to a progressive increase in the amplitude of the calcium response over the training period (*Figure 22I*, right upper panel). Moreover, REHAB animals showed progressively steeper slope of calcium activation along the weeks of training (*Figure 22I*, right lower panel). As compared to STROKE animals, a faster rise of calcium transient in the peri-infarct region was observed in REHAB mice at the end of the training period (*Figure 22G*).

In brief, our results showed that combined rehabilitative treatment promoted the formation of a new motor representation in the peri-infarct area where temporal and spatial features of cortical activation recovered towards pre-stroke condition.
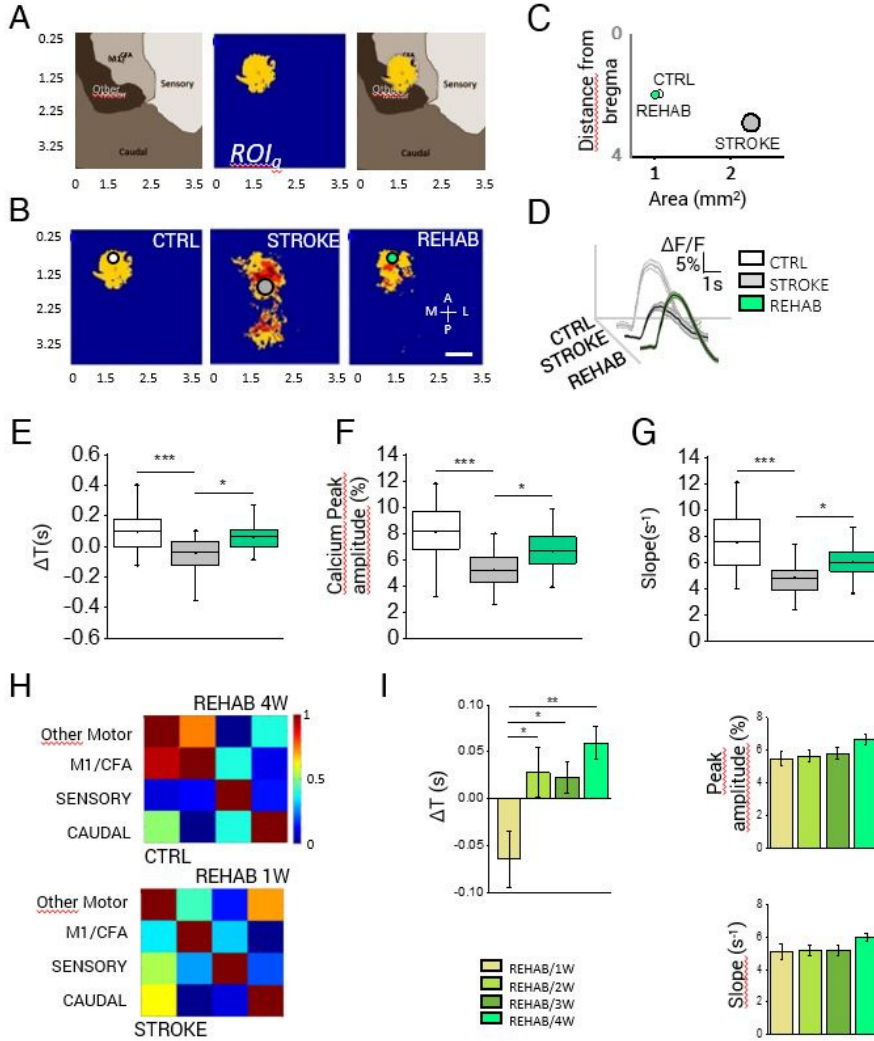
Figure 22. **Wide-field imaging of cortical activation profiles over 4 weeks of rehabilitation.** *(A) The image on the left shows a functional map based on the intracortical microstimulation (ICMS) studies of Tennant (2011, Cerebral Cortex) and Alia (2016, Sci Reports) that was used as a reference map. The middle panel shows the average thresholded ROI (ROIg) computed for CTRL animals during voluntary contralateral forelimb pulling in the M-Platform. The image on the right shows a merged image of the functional map and ROIg. CFA, caudal forelimb area. The caudal area includes visual and associative regions. (B) The panels show the average thresholded ROI (ROIg) computed for each experimental group. The circles represent the centroids of the ROIg for CTRL (white), STROKE (light gray), and REHAB (green) groups. Scale bar = 1 mm. (C) The areas of the ROIg and their distance from bregma are presented in the scatter plot. (D) Average calcium traces recorded in the region of maximal activation, ROI_g (see Methods), during contralateral forelimb retraction for the experimental groups; the shadows indicate the SEM values. (E) Delays in cortical activation in caudal regions in response to contralateral forelimb retraction are shown for the 3 groups (Nmice$_{CTRL}$= 4, Nmice$_{STROKE}$ = 6, Nmice$_{REHAB}$ = 6; ΔT_{CTRL} = 0.10 ± 0.03 s, ΔT_{STROKE} = -0.04 ± 0.02 s, ΔT_{REHAB}= 0.06 ± 0.02 s; Kruskal-Wallis One Way followed by Tukey's test: *** P = 0.006, * P = 0.016). (F) Graph shows the maximum of fluorescence peaks from the same calcium traces as in (D) (Peak amplitude$_{CTRL}$ = 8.1 ± 0.5 %; Peak amplitude$_{STROKE}$ = 5.2 ± 0.3%; Peak amplitude$_{REHAB}$ = 6.6 ± 0.3%; one-way ANOVA followed by Tukey's test: *** P = 0.000005, * P =0.017). (G) Graph shows the slope (average ± SEM) of the fluorescence in the rising phase of the trace (Slope$_{CTRL}$ = 7.5 ± 0.5 s^{-1}; Slope$_{STROKE}$ = 4.8 ± 0.2 s^{-1}, Slope$_{REHAB}$ = 6.0 ± 0.2 s^{-1}; Kruskal-Wallis One Way followed by Tukey's test: *** P = 0.00004, * P = 0.015). (H) Examples of partial correlation matrices of cortical activation during voluntary pulling. The correlation analysis on REHAB mice was performed based on two evaluation time points: one week (REHAB/1W) and four weeks (REHAB/4W) after stroke. (I) Longitudinal analysis of cortical activation profiles over the four rehabilitation weeks.. Left panel: Delays in cortical activation in caudal regions following the forelimb retraction task are reported for the 4 weeks of rehabilitative training (Nmice$_{REHAB}$= 6; $\Delta T_{REHAB/1W}$ = -0.06 ± 0.03 s, $\Delta T_{REHAB/2W}$ = -0.03 ± 0.03 s, $\Delta T_{REHAB/3W}$ = 0.02 ± 0.02 s, $\Delta T_{REHAB/4W}$ = 0.06 ± 0.02 s; one-way ANOVA followed by the Tukey test: ** P <0.01, *P <0.05; REHAB/4W here corresponds to the REHAB group in all the other panels). Upper right panel: the maximum of calcium imaging fluorescence peaks for the 4 weeks of rehabilitative training (Nmice$_{REHAB}$= 6; Peak amplitude$_{REHAB/1W}$= 5.4 ± 0.4%, Peak amplitude$_{REHAB/2W}$ = 5.6 ±0.4 %, Peak amplitude$_{REHAB/3W}$ = 5.8 ± 0.4%, Peak amplitude$_{REHAB/4W}$ = 6.6 ± 0.3 %; No significant changes were observed over the 4 weeks period).Lower right panel: The graph shows the slope (average ± SEM) of the calcium imaging fluorescence in the rising phase (Nmice$_{REHAB}$= 6; Slope$_{REHAB/1W}$= 5.1 ±0.5 s-1, Slope$_{REHAB/2W}$= 5.2 ±0.3 s-1, Slope$_{REHAB/3W}$= 5.2 ±0.3 s-1, Slope$_{REHAB/4W}$= 6.0 ±0.2 s-1; No significant changes were observed over the 4 weeks period).*

4.1.4 Inter-hemispheric functional connectivity is improved by combined rehabilitation

We then investigated on the same animals the long-distance effects of combined treatment, in particular how rehabilitation modified the functional connectivity of the new motor representation with the contralesional motor cortex. Several studies in mice and humans have shown that interhemispheric M1 connectivity is reduced after stroke [208-210]. Increased interhemispheric connectivity is hypothesized to positively correlate with the recovery of motor performance in the subacute stage after stroke in humans [211].

Based on this hypothesis, we tested whether transcallosal projections were modulated by rehabilitation by using an all-optical approach that combined optogenetic activation of the intact M1 with calcium imaging on the injured hemisphere. In these experiments, the spared (left) M1 of GCaMP6f mice was injected with AAV9-CaMKII-ChR2-mCherry to induce the expression of ChR2 in excitatory neurons (*Figure 23A*).

One month after stroke, we optogenetically stimulated the intact M1. To avoid ChR2 stimulation while exciting GCaMP6f fluorescence, we partially occluded the 505 nm LED in our custom-made wide-field microscope (*Figure 23B-C*). Optogenetic stimulation was achieved with a second excitation path in which a 473 nm laser was focused on the AAV-transfected region via acousto-optic deflectors (AODs) [212].

Laser stimulation of the contralesional M1 reproducibly triggered the activation of calcium waves in the injured hemisphere (*Figure 23D*) mainly spreading from the homotopic M1 of CTRL mice, or in the peri-infarct area of STROKE and REHAB animals (*Figure 24*). Calcium waves then propagated to functionally connected regions that were located either anterior or posterior to the primary source of activation in all 3 groups of animals. At a glance, the temporal dynamics of calcium waves were comparable between CTRL and STROKE mice (*Figure 24*). By quantifying the delay between the start of the optogenetic stimulation on the left hemisphere and the peak of calcium activity in the right

hemisphere, we found no significant difference between the STROKE and CTRL mice (*Figure 23E*).
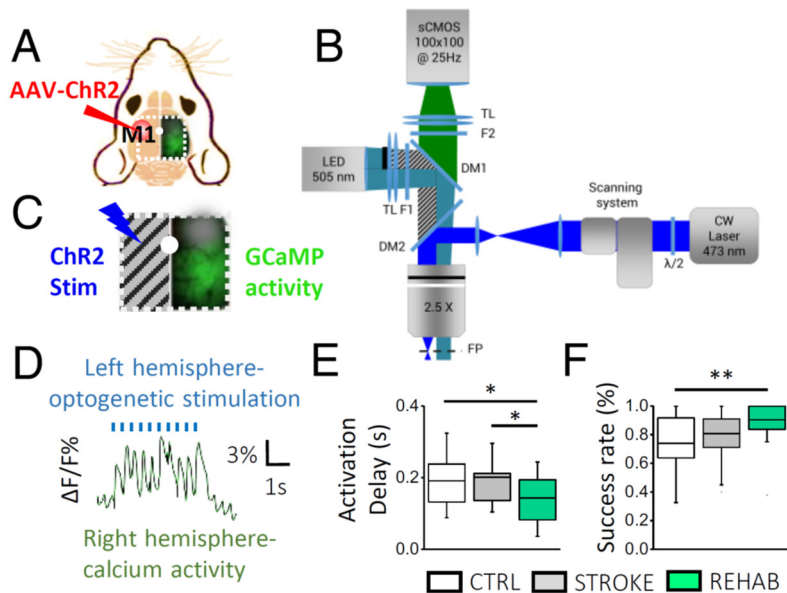
*Figure 23: **Combined rehabilitation strengthens interhemispheric connectivity after stroke.** (A) Schematic representation of field of view (i.e. area within the white dotted square) for all-optical investigation of inter-hemispheric functional connectivity in GCaMP6f mice. The red circle in the left hemisphere indicates M1 injected with AAV-ChR2-mCherry. White dot indicates bregma. (B) Schematic representation of wide-field microscope. (C) Panel shows simultaneous ChR2 laser stimulation on the left hemisphere (not illuminated by LED) and the detection of the evoked GCaMP6f fluorescence on the right side. (D) Trace of optogenetically elicited calcium activity in the right cortex. (E) Box and whiskers plot showing the delay between the onset of left hemisphere laser stimulation and the peak of the calcium responses in the right hemisphere (average ± SEM; Nmice$_{CTRL}$ = 4, Nmice$_{STROKE}$ = 3, Nmice$_{REHAB}$ = 3; Activation Delay$_{CTRL}$ = 0.19 ± 0.02 s, Activation Delay$_{STROKE}$ = 0.20 ± 0.02 s, Activation Delay$_{REHAB}$ = 0.14 ± 0.01 s; one-way ANOVA post hoc Fisher, P <0.05 for all comparisons;). (F) Success rate (SR) of laser stimulation, calculated as number of times laser stimulation successfully triggered contralateral activation over total number of stimulation trials (average ± SEM, same Nmice as in (E); SR$_{CTRL}$= 0.74 ± 0.04, SR$_{STROKE}$= 0.81 ± 0.03, SR$_{REAHAB}$= 0.90± 0.03; ANOVA with post hoc Bonferroni test: P < 0.01).*
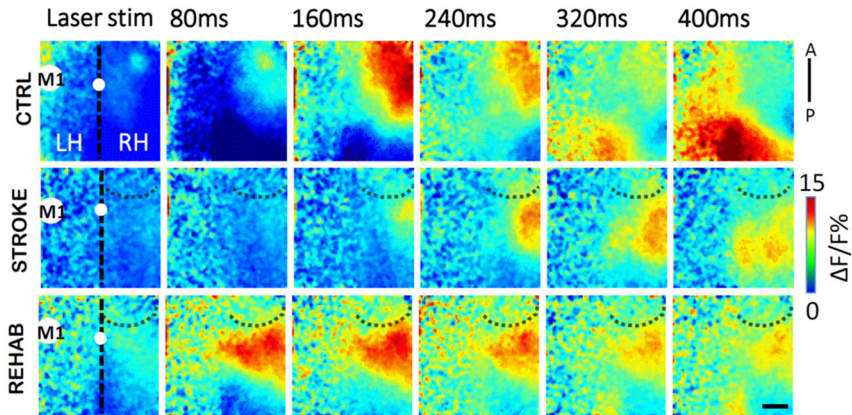
Figure 24: ***Optogenetic activation of contralateral hemisphere.*** *Representative image sequences from a single animal in each group showing ipsilesional cortical activation as assessed by calcium imaging following 473 nm laser stimulation (1 Hz, 5ms pulse duration) of the ChR2-expressing intact M1. The white spot on the vertical black dotted line (midline) indicates bregma. The dotted curve lines highlight the area injured by stroke. A,P: anterior, posterior. LH, left hemisphere; RH, right hemisphere. Scale bar = 1 mm.*

In contrast, this delay was significantly reduced in REHAB mice as compared to both CTRL and STROKE mice (*Figure 23E*). In addition, the success rate of contralateral activation in response to optogenetic stimulation was higher in REHAB mice than in CTRL and STROKE animals (*Figure 23F*). Therefore, this series of all-optical experiments suggests that combined rehabilitation strengthens the functional connectivity between the spared motor cortex and the perilesional cortex one month after stroke.

4.1.5 Combined motor rehabilitation and contralesional M1 inhibition preserves pyramidal neurons architecture and promotes the stabilization of synaptic contacts in the peri-infarct area

We further explored structural rewiring of dendrites and spines to define their contribution to functional recovery. Heightened spontaneous structural remodelling has been observed in animals in both presynaptic (axonal fibres and terminals) and postsynaptic (dendrites and dendritic spines) neuronal structures in the peri-infarct cortex in the weeks following stroke [213-217]. In the next set of *in vivo* experiments, we performed TPF microscopy of pyramidal apical dendrites and axons (up to 100 µm deep relative to the pial surface) at increasing distances (up to 4 mm) from stroke core in the cortex of GFPM mice. The imaging area overlapped with the region visualized in GCaMP6f mice (*Figure 26A*). Orientation of dendrites and axons was evaluated on the fourth week after injury in STROKE and REHAB mice. The reorganization of cortical tissue (*Figure 25A*, left panels) that led to a considerable alignment of blood vessels towards the stroke core produced an analogous re-orientation of dendrites and axons in peri-infarct area of STROKE mice (white arrow in *Figure 25A*, right panels). Reorientation was less pronounced at distal regions from the ischemic core (>1 mm; *Figure 26C*). In contrast, reorientation was not visible in REHAB animals (*Figure 25B* and *Figure 26B*) even though stroke profoundly altered the spatial distribution of blood vessels around the stroke core in the same mice. Indeed, the randomness in dendrite orientation in REHAB mice resembled healthy (CTRL) subjects (*Figure 25B*. Alterations induced by ischemic damage on neural circuitry are known to affect dendrites as well as synaptic contacts, producing a large increase in spine turnover in peri-infarct area [201, 218].
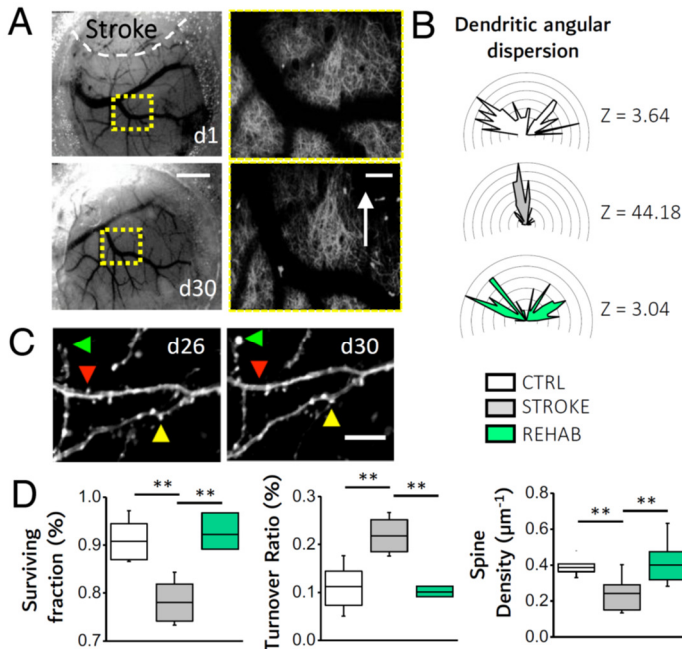
Figure 25: **Combined rehabilitation affects dendritic orientation and stabilizes spine turnover.** *(A) Brightfield images showing cranial window 1 day and 30 days after stroke (STROKE group). The rostral shift of cortical tissue due to the shrinkage of the stroke core is highlighted by the displacement of a reference point (i.e. blood vessel branching point) framed by the dotted yellow square. Scale bar = 1 mm. Panels on the right show the stitched two-photon images (4x4 Maximum Intensity Projections, MIPs of 130x130x50 μm^3) acquired within the region framed by the respective yellow squares in the left panels. White arrow highlights the alignment of dendrites and axons towards the stroke core. Scale bar = 100 µm. (B) Polar plots showing angular distribution of dendrites in peri-infarct area. Plots are oriented as in Figure 4A, where lesioned area is toward the uppermost center of the plot (for all panels, Nmice$_{CTRL}$ = 5, Nmice$_{STROKE}$ = 4, Nmice$_{REHAB}$ = 3). Z scores, calculated by Rayleigh Test for circular statistics, are reported for each experimental class on the right of the polar plot. (C) MIPs of two-photon stacks (z depth 8 µm) of dendritic branches at 26 and 30 days after stroke (STROKE group). Arrows point to a newly formed (green), lost (red), and stable (yellow) spine. Scale bar = 5 µm. (D) Box and whiskers plot showing surviving fraction (SF) ± SEM (left; SF$_{CTRL}$= 0.93 ± 0.03%; SF$_{STROKE}$= 0.80 ± 0.04%; SF$_{REHAB}$= 0.92 ± 0.02%; one-way ANOVA with post hoc Bonferroni test, P $_{CTRL/STROKE}$ = 0.003, P $_{REAHB/STROKE}$ = 0.005), turnover ratio (TOR) ± SEM (middle; TOR$_{CTRL}$= 0.11 ± 0.02%; TOR$_{STROKE}$ = 0.20*

± 0.04%; TOR$_{REHAB}$= 0.10 ± 0.01%; one-way ANOVA with post hoc Bonferroni test, P $_{CTRL/STROKE}$ = 0.007, P $_{REAHB/STROKE}$ = 0.01) and spine density (SD) ± SEM (right panel; SD$_{CTRL}$= 0.39 ± 0.01 μm^{-1}; SD$_{STROKE}$= 0.24 ± 0.03 μm^{-1}; SD$_{REHAB}$= 0.40 ± 0.04 μm^{-1}; one-way ANOVA with post hoc Fisher test, P $_{CTRL/STROKE}$ = 0.006, P $_{REAHB/STROKE}$ = 0.003) in the peri-infarct area.

We next asked whether rehabilitation modified synaptic turnover. We thus monitored the appearance and disappearance of apical dendritic spines (*Figure 25C*) by performing a frame-by-frame comparison of spines in the mosaic we acquired along the rostro-caudal axis with a TPF microscope.

Spines in the peri-infarct region of REHAB animals exhibited increased synaptic stability (*Figure 25D*, left panel) and a lower turnover (*Figure 25D*, middle panel) than STROKE mice, thereby recapturing features of pre-stroke conditions. The combined rehabilitative treatment also resulted in higher synaptic densities that were comparable to healthy CTRL values (*Figure 25D*, right panel). The stabilization of synaptic contacts induced by rehabilitation was stronger at the proximal level and weakened with increasing distance from ischemic core (*Figure 26D*, upper and middle panels). On the other hand, the change in density of spines extended beyond peri-infarct region (*Figure 26D*, lower panel).

In brief, longitudinal imaging of cortical neurons revealed that combined rehabilitative therapy helped preserving the organization of dendritic arbors in peri-infarct cortex and restored dendritic spine plasticity.
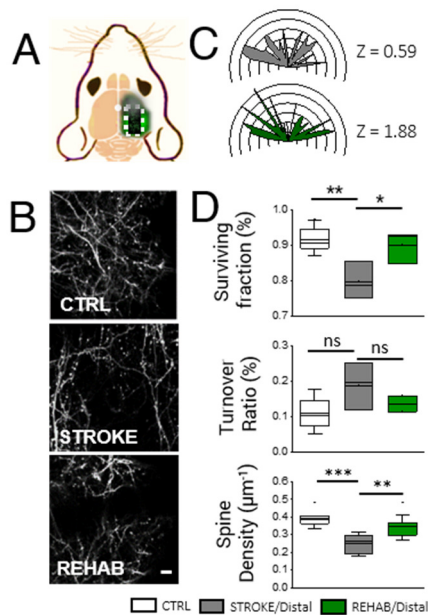
*Figure 26: **In vivo imaging of dendritic and spine plasticity in regions proximal and distal from stroke core.** (A) A schematic representation of the field of view (i.e. area within the white dotted square) of two-photon imaging of dendritic and spine plasticity in GFPM mice. The red spot indicates the site of the stroke lesion. (B) Representative examples of maximum intensity projection of two-photons stacks of dendritic branch orientation in the peri-infarct area in the CTRL, STROKE and REHAB groups. Scale bar = 10 µm. (C) Polar plots showing the angular distribution of dendrites in the distal area (Nmice$_{CTRL}$= 5, Nmice$_{STROKE}$ = 4, Nmice$_{REHAB}$= 3). Z scores, calculated by the Rayleigh Test for circular statistics, are reported for each experimental class on the right of the polar plot; ns, not significant). (D) Histograms showing the SF (upper panel; Nmice$_{CTRL}$= 6, Nmice$_{STROKE}$ = 4, Nmice$_{REHAB}$= 3; SF$_{CTRL}$= 0.92 ± 0.02%; SF$_{STROKE}$ Distal= 0.80 ± 0.03%; SF$_{REHAB}$ Distal= 0.90 ± 0.03%; one way ANOVA with post hoc Bonferroni: ** P =0.007, * P =0.023), TOR (lower panel; Nmice$_{CTRL}$= 6, Nmice$_{STROKE}$ = 4, Nmice$_{REHAB}$= 3; TOR$_{CTRL}$= 0.11 ± 0.02%; TOR$_{STROKE}$ Distal = 0.19 ± 0.04%; TOR$_{REHAB}$ Distal= 0.13 ± 0.01% t-test: one way ANOVA with post hoc Bonferroni: not significant for all comparisons) and spine density (SD) (right panel; Nmice$_{CTRL}$= 3, Nmice$_{STROKE}$= 3, Nmice$_{REHAB}$= 3; SD$_{CTRL}$ = 0.39 ± 0.01 µm-1; SD$_{STROKE}$ Distal = 0.25 ± 0.02 µm-1; SD$_{REHAB}$ Distal = 0.35 ± 0.02 µm-1; one-way ANOVA with post hoc Fisher test, P CTRL/STROKE = 0.0001, P REHAB/STROKE = 0.005) in the distal region (>1000 µm from the stroke core). Data are means ± SEM*

4.2 Combination of intense motor training and optogenetic stimulation of peri-infarct area promotes functional remapping and recovery of motor functionality after stroke

In the second set of experiments, we evaluated cortical changes in functional plasticity with a different rehabilitative therapy. As previously described, an ischemic event is followed by extensive changes in cortical excitability involving both peri-infarct area and contralesional hemisphere. In this framework, plasticity in the injured hemisphere plays a major role in post-stroke motor recovery and is a primary target for rehabilitation therapy. Indeed, stimulation of the ipsilesional motor cortex, especially when paired with motor training, facilitates plasticity and functional restoration [107, 108]. Here we coupled the optogenetic stimulation of the peri-infarct area, as neuro-plasticizing treatment, with a more intense motor training performed on the robotic platform. The optogenetic stimulation required the expression in peri-infarct area's excitatory neurons of a cation channel, ChR2, sensitive to blue light. When the laser stimulates the ChR2 expressing cells, induces the opening of the channel and the consequent neuronal excitation.

We then took advantage of a new robotic platform characterized by an automated system for friction regulation. This device allows to calibrate the friction of the slit making the motor training more intense for mice compared to the previous system.

In this set of experiment, we evaluated the effect of the combined rehabilitation and of single treatments on cortical reshaping of functional areas, during the execution of the motor task. The same animals were also tested through behavioural experiment, such as Schallert test, to evaluate the dexterity of the mouse forelimb during the rehabilitation month.

4.2.1 A new robotic system for adaptive training

In this set of experiments, the M-Platform was implemented with a device allowing to calibrate the friction of the handle. This new version of M-Platform significantly extends its possibility for mice experiment during motor task as the actuation system for friction adjustment allows modulating pulling difficulty [219].

By calibrating the friction for every animal, forelimb training proves to be more intense for mice; by analysing the peak prominence (see Methods) for every retraction movement during four weeks of motor rehabilitation, we observe an increment of peak force (*Figure 27*) in mice performing the intense motor training (Robot-F) compared with the previous setup (Robot).
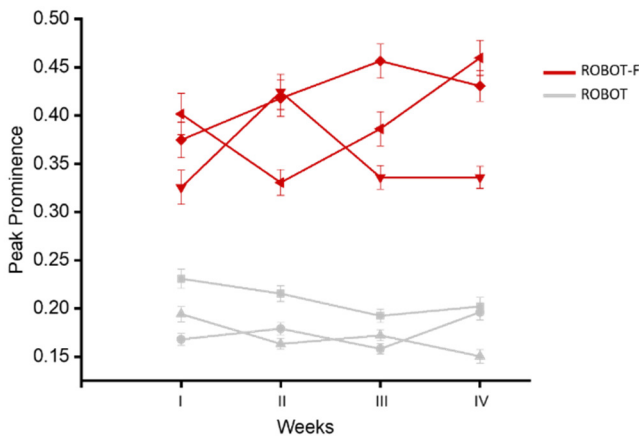
*Figure 27: **Characterization of forces exercised during the pulling task.** The scatter plot shows the Peak Prominence (average ± SEM) during 4 weeks of training of Robot mice (in grey) and Robot-F mice (in red). Nmice_Robot = 3; Nmice_Robot F = 3.*

In addition, by performing the calcium transient analysis we found that four weeks of training on this system improved the functionality of the affected forelimb one month after stroke compared to the previous system "without friction" (*Figure 28*).
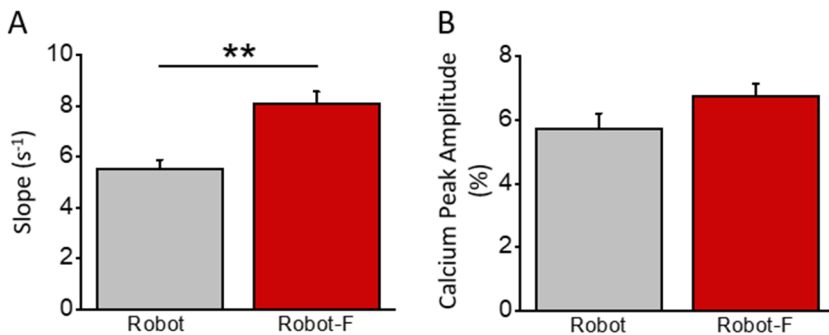
*Figure 28: **Characterization of cortical activation profiles.** (A) Graph shows the slope (average ± SEM) of the fluorescence in the rising phase of the trace (Slope$_{Robot}$ = 5.4 ± 0.5 s^{-1}; Slope$_{Robot-F}$ = 8.1 ± 0.5 s^{-1}; one-way ANOVA followed by Bonferroni's test *** P<0.001, ** P<0.01, * P <0.05t:) (B) Graph shows the maximum of fluorescence peaks from the same calcium traces (Peak amplitude$_{Robot}$ = 5.7 ± 0.5 %; Peak amplitude$_{Robot-F}$ = 6.7 ± 0.4%; one-way ANOVA followed by Bonferroni's test: *** P<0.001, ** P<0.01, * P <0.05) Nmice$_{Robot}$ = 3; Nmice$_{Robot-F}$ = 3.*

Given the positive results obtained with the intense rehabilitation, we decided to performed the following experiment with the new version of M-platform.

4.2.2 Experimental design

We tested if optogenetic stimulation of peri-infarct area of Thy1-GCaMP6f mice expressing ChR2 in excitatory neurons, coupled with repeated motor training, helps to achieve a good recovery of motor function after a photothrombotic stroke in the M1. Previous studies reported that repeated neuronal stimulation of the peri-lesioned area induces a significant improvement in cerebral blood flow and neurovascular coupling response [109]. Furthermore, it has been already demonstrated that the optogenetic stimulation of brain regions

neighbouring the infarct core enhances the remodelling at a structural, functional and behavioural level [109, 110].

In this set of experiments, in order to promote the functional recovery after stroke, we coupled an optogenetic strategy to stimulate targeted excitatory neurons in the peri-lesional region to motor training on the M-Platform. We revealed the cortical activity during motor training in order to evaluate the cortical reshaping induced by different rehab treatments, by using a wide field microscope that allow to perform simultaneous optogenetic stimulation (*Figure 29A*).

The stimulation protocol consisted of 3 successive 30 second trains separated by 1-minute rest (*Figure 29B*) performed with a 473nm blue laser (0.2-1.15 mW). In order to provide an adaptive rehabilitation, we decided to tune the power of the laser based on the mouse response to the stimulation. In detail, we set the laser power to a value lower than the one necessary to evocate the movement of the mouse forelimb.
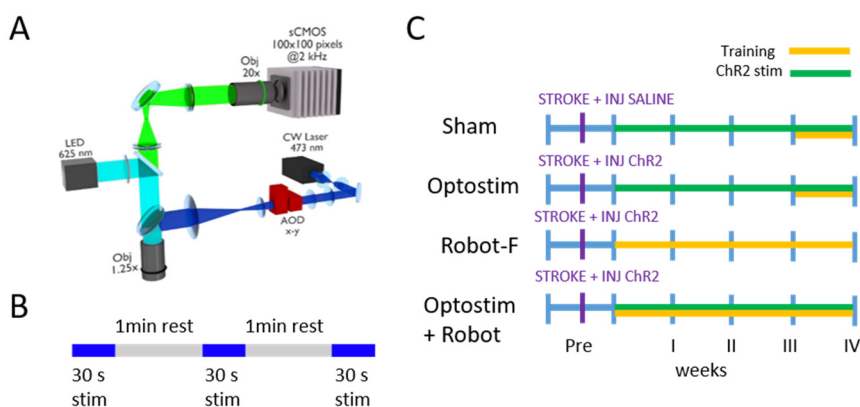
*Figure 29: **Experimental paradigm.** (A) A schematic representation of wide-field fluorescent microscope with a double illumination path allowing the imaging of GCaMP6f mouse cortex and the stimulation of ChR2 expressing neurons. (B) Laser stimulation protocol for optogenetic rehabilitation. (C) The experimental timeline for Sham, Optostim, Robot-F and Optositm+Robot groups in the awake imaging experiment.*

We divided our sample in four experimental groups (*Figure 29C*) to evaluate the consequences of enhanced motor training and optogenetic stimulation individually with respect to the combined treatment. In order to evaluate the effect of laser stimulation alone, we stimulated every day for four weeks the peri-infarct region of mice without ChR2 transfection (Sham). In the Optostim group, mice were stimulated in the peri-infarct area for four weeks, starting five days after stroke as in the previous experiments; during the last week mice were tested on the robotic platform. In Robot-F group mice were rehabilitated for four weeks on the new M-Platform starting five days after the damage; finally, in Optostim+Robot group mice performed one month of combined optogenetic and motor rehabilitation.

4.2.3 Electrophysiological characterization of ChR2 transfected neurons activation during GCaMP6f imaging.

In order to control for stimulation artefacts of the imaging LED on the activation of ChR2 transfected neurons, we evaluated the crosstalk between the two. To estimate if the 505 nm LED used for cortical imaging induced the activation of ChR2 expressing neurons in the peri-infarct area we performed an electrophysiological characterization. In order to reduce as much as possible the unwanted ChR2 excitation during the actual calcium imaging experiments we set the LED to very low power (0.2 mW after the objective). By recording the local field potential (LFP) of pyramidal neurons in the transfected region of anesthetized mice we evaluated if the double of the power used for imaging experiment was sufficient to elicit the activation of ChR2 transfected neurons. We observed that while the laser stimulation induced a strong local activation of neurons expressing ChR2, the LED illumination didn't affect spontaneous cortical activity (*Figure 30A*). We then analysed the power of frequency band from δ to γ with LED on

and off and observed that there are no significant differences between the two conditions (*Figure 30B*). To conclude, we showed that while the focalized light of the 473 nm blue laser, stimulating a region of 5 x 5 pixels, induced the activation of neuronal population expressing the light sensitive protein ChR2, the 505 nm LED mild illumination of an area of 100 x 100 pixel didn't induce any alteration in pyramidal neurons excitability.
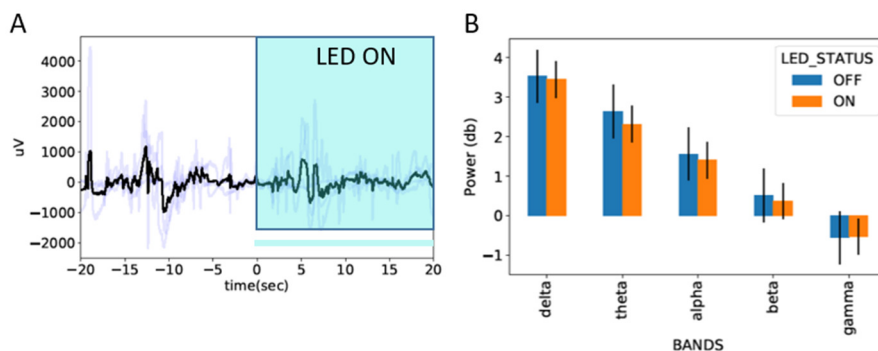
*Figure 30: **Electrophysiological characterization.** (A) Example of averaged LFP registration (dark trace) before and during LED illumination. (B) Power analysis of selected frequency bands while the 505 nm LED is on (orange) or off (blue) indicates that there is no significant alteration in pyramidal neurons excitability while the LED is on during calcium imaging.*

4.2.4 Behavioural evaluation of motor recovery during one month of combined optogenetic and motor rehabilitation

Since motor performances on M-Platform are not sufficient to assess if the recovery is generalized, we performed a behavioural analysis on dissimilar task. By using the Schallert cylinder test we evaluated changes of forelimb functionality during the month of rehabilitation compared to healthy condition. The information obtained with the M-

Platform on the forces applied by the animals in the pulling task didn't provide an effective evidence of forelimb recovery. To test the forelimb recovery during the rehabilitation period, we decided to test the motor functionality of mice forelimb in a different behavioural test. The Schallert test is widely used to verify the level of preference for use of the non-impaired forelimb after unilateral cortical injury [220]. Spontaneous forelimb use was assessed in mice via the Schallert cylinder test. This test has been developed in rats and adapted for mice [221]. As Spalletti et al. 2017 [100] observed, we confirmed that mice of every experimental group performed significantly worse in the first sessions after the lesion, using predominantly the healthy forelimb to lean (*Figure 31A-C*). More in detail, no significant recovery to baseline performance was observed in this task up to thirty days post-surgery in Sham group, indicating that the laser stimulation of neurons that didn't express ChR2 didn't imply any improvement of forelimb functionality.

At the same time motor training alone with the new platform (Robot-F group) was not sufficient to restore the pre-stroke performances. On the other hand, optogenetic stimulation induced the restoration of the Asymmetry index up to healthy condition both in the single treatment and in the combined group. In addition, while the Optostim alone recovered at the end of rehabilitative period, the Robot+Optostim animals indeed achieved a level of symmetry comparable with pre-stroke condition since the second week of rehabilitation.
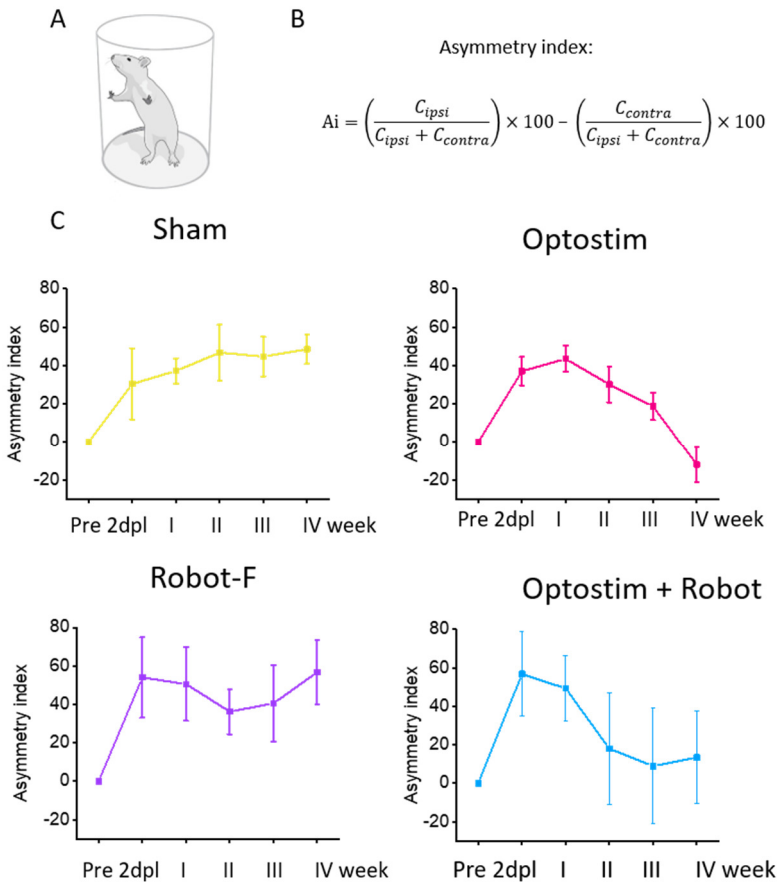
*Figure 31: **Behavioural experiment to evaluate through Schallert test forelimb impairment after stroke.** (A) A schematic representation of Schallert test experiment (B) Formula to calculate the Asymmetry index (Ai) to quantify the forelimb use asymmetry where the Cipsi and Ccontra refer, respectively, to the number of contacts performed with the limb ipsilateral and contralateral to the lesioned hemisphere (C) Pre- and post-lesion performances in the 4 different experimental groups measured as Asymmetry Index in the Schallert Cylinder test (Nmice_Sham = 4; Nmice_Optostim = 4; Nmice_Robot-F = 4; Nmice_Optostim+Robot = 4).*

4.2.5 Combined optogenetic cortical stimulation and intense motor training promotes the recovery of functional connectivity

As in the previous set of experiment we performed functional imaging with a wide field microscope while the awake animal performed the retraction task on the neuro robotic platform. By dissecting and aligning the signal derived from the M-Platform (forces and forelimb position) and the sCMOS camera (fluorescence signal from the imaging area, *Figure 32A*), we reconstructed the calcium dynamic during the forelimb movement. By comparing the peak amplitude in the different experimental groups we observed that individual treatments are not sufficient to induce full recovery of calcium transient in the peri-infarct area after stroke. On the other hand, the synergic effect of combined treatment promoted a functional restoration of the critical features of calcium activation (*Figure 32B, C*). More in detail, we observed a pronounced increment of Peak amplitude and Slope of calcium transient during the movement in the Optostim+Robot group, that became comparable with the parameters distinctive of healthy condition (Ctrl group, *Figure 32B-C*). Finally, we observed a trend in the reconstitution of a rostro-caudal pattern of activation during pulling, which can be used as a proxy for segregation of cortical activation areas during the movement, associated to the combined rehabilitative treatment (*Figure 32D*). Our preliminary results showed that the combination of an intense motor training and the optogenetic stimulation of excitatory neurons in the peri-infarct area produced a synergic effect improving the recovery of motor function and cortical calcium dynamic.
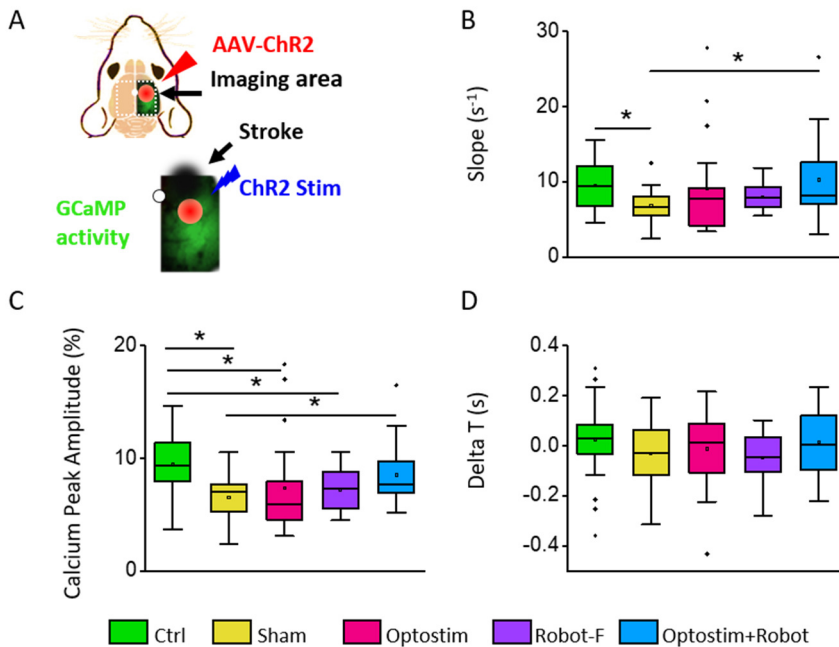
Figure 32: **In vivo calcium imaging of peri-infarct area during awake motor training.**
(A) A schematic representation of imaging field of view: the with dot indicated the
bregma, the red spot the ChR2 transfected area and the back cloud the extension of
the stroke. (B) Graph shows the slope (average ± SEM) of the fluorescence in the rising
phase of the trace (Slope$_{Ctrl}$ = 9.5 ± 0.5 s^{-1}; Slope$_{Sham}$ = 6.8 ± 0.5 s^{-1}, Slope$_{Optostim}$ = 9.0 ±
1.4 s^{-1}, Slope$_{Robot-F}$ = 8.0 ± 0.3 s^{-1}, Slope$_{Optostim+Robot}$ = 10.2± 1.1 s^{-1}; one-way ANOVA
followed by Fisher's test: * P <0.05). (C) Graph shows the maximum of fluorescence
peaks from the same calcium traces (Peak amplitude$_{Ctrl}$ = 9.4 ± 0.5 %; Peak
amplitude$_{Sham}$ = 6.5 ± 0.5%; Peak amplitude$_{Optostim}$ = 7.3 ± 0.9%, Peak amplitude$_{Robot-F}$
= 7.1 ±0.4%, Peak amplitude$_{Optostim+Robot}$= 8.5 ± 0.5; one-way ANOVA followed by
Fisher's test * P <0.05). (C) Graph shows the delays in cortical activation in caudal
regions in response to contralateral forelimb retraction (average± SEM) (ΔT$_{Ctrl}$ = 0.02
± 0.02 s, ΔT$_{Sham}$ = -0.03 ± 0.03 s, ΔT$_{Optostim}$ = -0.01 ± 0.03 s ΔT$_{Robot-F}$ = 0.05 ± 0.1 s,
ΔT$_{Optostim+Robot}$ = 0.01 ± 0.02 s). Nmice$_{Ctrl}$=4; Nmice$_{Sham}$ = 4; Nmice$_{Optostim}$ = 4; Nmice$_{Robot-F}$ = 4; Nmice$_{Optostim+Robot}$ = 4.

Discussion

During my PhD I tested two combined rehabilitative approaches in a mouse model of cortical photothrombotic stroke.

We combined motor training on a robotic platform designed for the rehabilitation of mouse left forelimb with two different neuromodulatory treatment, the first one aimed at silencing the contralesional hemisphere, the second one at stimulating the peri-infarct region.

In the first set of experiment by exploiting BoNT/E transient inhibition we observed a significant remodelling in the peri-infarct region both from a functional and structural point of view. More in detail our study highlights that the rehabilitation paradigm restores the features of neuronal dynamics proper to healthy mice. We then observed, through optogenetic investigation, a reinforcement of transcallosal projection from the peri-infarct area to the homotopic functional area in the healthy hemisphere. Furthermore, by analysing spines turnover in the peri-infarct area we found out that the combined rehabilitation promoted the re-orientation of dendrites and stabilized the synaptic contacts.

In the second set of experiment the robotic training is coupled to a plasticizing treatment consisting in a repeated stimulation of excitatory neurons in the peri-infarct area. The evaluation of mouse dexterity during one month of rehabilitation, through Schallert test, endorses that the combined approach induces a good recovery of the mouse forelimb. Furthermore, the synergic effect of motor training and ipsilesional stimulation provides the restoration of some crucial features of calcium transient during retraction movement.

In this study we reproduce a model of focal ischemia in the cerebral cortex on order to investigate with two different rehabilitative approaches, different features of structural and functional plasiticty.

The great advantage of the photothrombotic stroke model chosen is that it can be opportunely tuned to produce focal lesions in a specific area of brain cortex allowing a more reproducible infarct and thus a

sample population more homogeneous compared to studies on humans.

In a first set of experiments we showed that rehabilitative treatment combining physical training and BoNT/E inhibition of contralesional hemisphere restored features of cortical activation typical of pre-stroke conditions and stabilized perilesional synaptic contacts.

In a second set of experiment, by exploiting the pro-plasticizing effect of optogenetic stimulation combined with an intensive motor training, we observed, through behavioural test and calcium imaging, a generalized recovery of forelimb functionality associated with the restoration of some parameters of pre-stroke cortical functionality.

Both these combined treatments take advantage of a mechatronic device (M-Platform) for mouse forelimb training [84] that mimics a robot for upper limb rehabilitation in humans, the "Arm-Guide" [222].

In Spalletti et al., 2017, robotic rehabilitation *per se* was not able to induce in mice a generalized recovery to untrained motor tasks (i.e. Schallert Cylinder test). They also showed that BoNT/E silencing of the contra-lesioned homotopic cortex, active in the motor cortex for about 10 days after injection, produced a small and transient improvement in general forelimb motor tests (Gridwalk and Schallert Cylinder test).

Nevertheless, the guide of an appropriate motor rehabilitation regime was necessary to achieve a complete functional recovery. Given the incomplete rescue produced by the single treatments, here we focused on the combinatorial therapy that couples BoNT/E treatment with robotic training.

We first investigated the changes induced by the combined rehabilitation paradigm on cortical activity. It has been reported that motor-targeted focal stroke induces abnormally scattered cortical maps that persist for months after stroke (see [223]). In a recent study on humans, by analysing fMRI in resting state at different time points, Siegel et al.[18] observed a consistent decrease of brain modularity two weeks after stroke compared to controls. This indicates a reduction of integration within functional areas and segregation between brain systems in a subacute phase after stroke [17]. In our study, we showed

the persistence of a diffuse structure of motor representation in non-treated animals 4 weeks after stroke (STROKE group). On the contrary, the combined rehabilitation paradigm re-established a cluster of segregated movement-evoked neuronal activity in peri-infarct areas where location, timing, and amplitude parameters highly resembled those of healthy control animals.

By performing optogenetic stimulation on the same group of stroked-afflicted rehabilitated mice, we demonstrated that the progressive spatial and temporal segregation of motor control in the ipsilesional cortex is associated with increased interhemispheric connectivity. The functional coupling between homotopic motor cortices was restored four weeks after injury in STROKE mice, suggesting that some form of spontaneous recovery compensated for the loss of transcallosal projections from injured neurons after stroke. Our results are in accordance with a previous study in a rat model of MCAO by van Meer et al. [208] who using fMRI observed a reduction of interhemispheric functional connectivity during resting state, that was recovered three months after stroke. They suggest that this may reflect either the disappearance of temporary interruption of synchronization through corpus callosum, or the restoration of initial unilateral disruption of the cortico-thalamo-cortical circuit.

The interhemispheric connectivity is further enhanced after the rehabilitative therapy, suggesting a possible correlation between the recovery of activation patterns in the perilesional area and the reinforcement of connectivity with pyramidal neurons projecting from healthy M1. While there are no studies examining, on the same animals, cortical functionality and transcallosal connectivity to draw direct comparisons with, our results are consistent with the hypothesis that rehabilitative training of the paretic upper limb can, on one side, increase the functional activation of motor regions of the ipsilesional cortex [224, 225] and, on the other, decrease interhemispheric inhibition from the contralesional motor cortex [226]. We speculate that segregation of the motor representation could be supported by dendritic rewiring in the peri-lesional area (as shown by our *in vivo*

imaging structural plasticity results), as well as by the activity of contralesional pyramidal cells projecting to the peri-infarct area. Further analysis on targeted neuronal populations is needed to clarify how rehabilitation-induced changes in transcallosal connectivity are specifically linked to alterations in the excitatory/inhibitory balance in the ipsilesional spared tissue.

The mouse model of stroke used in this study provides several advantages over more traditional models. Recently, Lim and colleagues [227] used voltage-sensitive dyes combined with optogenetics to demonstrate a spontaneous partial recovery of cortical functional connectivity 8 weeks after stroke. The combination of AAV-induced ChR2 expression in the homotopic M1 of GCaMP6 transgenic mice has the advantage of enabling the reliable control and the stable monitoring of neuronal activity over weeks and months, respectively.

A commonly agreed hypothesis is that synaptogenesis and dendritic remodelling might be enhanced by the genesis of an enriched vascular milieu around the infarct area [12, 213, 228]. In parallel, a recent review by Wahl and colleagues [130] suggested that rehabilitative training might shape the spared and the new circuits by stabilizing the active contacts. Alongside with these hypotheses, we observe that our rehabilitative treatment, combining motor training and temporary inhibition of M1 in the healthy hemisphere, promotes the increase of synaptic contacts density and stabilization of synaptic turnover. Although there are no other *in vivo* studies examining rehabilitation-induced spine plasticity after stroke to make a comparison with, our results are also in agreement with recent post-mortem histological studies where rehabilitation was shown to determine significant increases in spine density of distal apical dendrites in corticospinal neurons [229].

In a previous human study of Siegel and colleagues [17] robust changes in network synchrony were identified during acute and subacute phase after stroke. Through R-fMRI investigation they observed alteration of inter- and intra-hemispheric functional connectivity. Accordingly to these results, we found an alteration of calcium transients in stroked mice during pulling task (*Figure 21, 22*) and during inter-hemispheric

optogenetic stimulation (*Figure* 23, 24). Both the combined rehabilitative treatments we tested proved to act towards restoring the temporal dynamic of activation profiles, and that recovery of activation transients goes along with the recovery of forelimb functionality.

In the second set of experiments we evaluated the effects of different rehabilitative approaches by analysing both the forelimb functionality with Schallert cylinder test and the cortical plasticity with wide-field calcium imaging. For this experiments we used as pro-plasticizing treatment the optogenetic stimulation to induce the excitation of peri-infarct ChR2 transfected neurons. As shown by previous works [109,110], the great advantage of optogenetic stimulation is the capability to manipulate targeted neuronal population. In this framework, our optogenetic approach, by allowing to calibrate the intensity and the spatial extension of the stimulation, provided an individualized tool to promote plasticity, to be calibrated in time based on the feedback of single mice.

We further took advantage of the new version of M-Platform, allowing an adaptive motor training [219]. By applying a calibrated friction during the pulling task we observed an increment of the force exerted by the animals during the rehabilitation month compared to previous experiments (*Figure 27*).

We first separately evaluated the effect of each rehabilitative treatment applied, i.e. four weeks of optogenetic stimulation in the peri-infarct area (*Optostim group*) and four weeks of intensive motor training on the robotic platform (*Robot-F group*), on forelimb functional recovery. Similarly to Spalletti et al. [100], we observed through behavioural experiment (*Figure 31*) that motor training alone, though intense, was not sufficient to promote generalized the recovery of the functionality of the affected forelimb. Indeed, the trend of Robot-F mice observed during the four weeks of training resembled those of untreated stroke mice (*Sham group*). At the same time the features of calcium transients evoked by the retraction movement appeared to become only partially restored (*Figure 32*).

Then, according to Tennant et al. [110] who observed that optogenetic stimulation of thalamocortical axons enhances the recovery of forepaw sensorimotor abilities, we found that the four weeks of optogenetic stimulation is sufficient to promote the recovery of forelimb functionality. Nevertheless, this treatment *per se* did not produce large-scale modifications of cortical functionality. As Balbi and colleagues [194] showed in a recent work, dissociations between behavioural and meso-scale cortical functionality can occur. In accordance with previous works [18, 110], in which modular network structure was recovered over a longer experimental time-window (months), we hypothesize that a complete recover of cortical circuitry may occur after a longer lasting stimulation.

Finally, by combining the two treatments we observed a synergic effect in mice performing four weeks of both optogenetic stimulation and motor training (*Optostim+Robot group*). Indeed, asymmetry index analysis indicated that the combination of this two strategies induces an early restoration of the forelimb functionality as measured in the Schallert test, towards healthy conditions (*Figure 29*). At the same time the features of calcium transient in the peri-infarct area well approximated those of healthy animals (*Ctrl group*). These results suggest that the combination of intensive motor training and optogenetic stimulation of the peri-infarct area acts in parallel by promoting the remodelling and of vicarious regions. In this thesis we have thus shown that different rehabilitative protocols combining motor training and neuronal modulation of specific cortical regions promote the recovery of functional and structural features of healthy neuronal networks.

In this thesis we performed different sets of experiment based on rehabilitative motor training on M-Platform, where we applied two complementary protocols to mould neuronal activity, i.e. the pharmacological inhibition of the contralesional homotopic region (in the first set), and the optogenetic activation of the peri-infarct area (in the second one). Our results pointed out the fundamental role of multi-level therapies: the combination of repetitive motor training and

plasticizing treatments, respectively aimed at rebalancing the interhemispheric neural activity and at stimulating regions of the cortex bordering the stroke, was shown to provide a synergic effect on functional recovery.

Although the first paradigm applied showed some disadvantages (such as the high mortality rate due to the BoNT/E injection) it had the great advantage to allow ChR2-mediated investigation of interhemispheric connectivity through optogenetic stimulation.

The second paradigm, less invasive with respect to the first one, though still far from being applied on humans, allowed to regulate the therapy according to the daily mouse response, during the rehabilitation month. However, owing to the crosstalk existing between the GCaMP6 and ChR2 excitation spectra we couldn't investigate the cortical activation during optogenetic stimulation.

The results presented in this thesis addressed, by using different optical imaging and manipulation techniques (i.e. wide-field calcium imaging, two-photon microscopy and optogenetic stimulation) could address previously unanswered questions like the longitudinal remapping underlying the cortical rearrangement in the peri-infarct cortex, the subcellular remodelling during rehabilitative treatment and large scale interhemispheric rewiring after stroke. In conclusion, our multi-scale investigation brought to light complementary aspects of the structural and functional plasticity induced by different rehabilitative approaches. Currently, the data produced in this thesis are shared within several theoretical groups (Prof. Jirsa, Prof. Destexhe and Prof. Deco) of the Human Brain Project (HBP) consortium to build and validate predictive brain models of recovery and rehabilitation, that eventually will be used as a prognostic tool in clinic settings.

We believe that a deeper understanding of the mechanisms underlying neural circuitry repair will lead to the development of more efficient therapies and improve post-stroke recovery in patient populations.

Bibliography

1. Hossmann, K.A. Pathophysiology and therapy of experimental stroke. *Cell Mol Neurobiol* **26**, 1057-1083 (2006).
2. Murphy, T.H., Li, P., Betts, K. & Liu, R. Two-photon imaging of stroke onset in vivo reveals that NMDA-receptor independent ischemic depolarization is the major cause of rapid reversible damage to dendrites and spines. *J Neurosci* **28**, 1756-1772 (2008).
3. Zhang, S. & Murphy, T.H. Imaging the impact of cortical microcirculation on synaptic structure and sensory-evoked hemodynamic responses in vivo. *PLoS Biol* **5**, e119 (2007).
4. Besancon, E., Guo, S., Lok, J., Tymianski, M. & Lo, E.H. Beyond NMDA and AMPA glutamate receptors: emerging mechanisms for ionic imbalance and cell death in stroke. *Trends Pharmacol Sci* **29**, 268-275 (2008).
5. Sist, B., Jesudasan, S.J.B. & Winship, I.R. *Acute Ischemic Stroke*, Vol. Diaschisis, Degeneration, and Adaptive Plasticity After Focal Ischemic Stroke (2012)
6. Adeoye, O., Hornung, R., Khatri, P. & Kleindorfer, D. Recombinant tissue-type plasminogen activator use for ischemic stroke in the United States: a doubling of treatment rates over the course of 5 years. *Stroke* **42**, 1952-1955 (2011).
7. Fang, M.C., Cutler, D.M. & Rosen, A.B. Trends in thrombolytic use for ischemic stroke in the United States. *J Hosp Med* **5**, 406-409 (2010).
8. Jones, T.A. & Adkins, D.L. Motor System Reorganization After Stroke: Stimulating and Training Toward Perfection. *Physiology (Bethesda)* **30**, 358-370 (2015).
9. Phillips, L.L., Chan, J.L., Doperalski, A.E. & Reeves, T.M. Time dependent integration of matrix metalloproteinases and their targeted substrates directs axonal sprouting and synaptogenesis following central nervous system injury. *Neural Regen Res* **9**, 362-376 (2014).
10. Zhang, Z.G. & Chopp, M. Neurorestorative therapies for stroke: underlying mechanisms and translation to the clinic. *Lancet Neurol* **8**, 491-500 (2009).
11. Mironova, Y.A. & Giger, R.J. Where no synapses go: gatekeepers of circuit remodeling and synaptic strength. *Trends Neurosci* **36**, 363-373 (2013).

12.   Carmichael, S.T. Cellular and molecular mechanisms of neural repair after stroke: making waves. *Ann Neurol* **59**, 735-742 (2006).
13.   Benowitz, L.I. & Carmichael, S.T. Promoting axonal rewiring to improve outcome after stroke. *Neurobiol Dis* **37**, 259-266 (2010).
14.   Perederiy, J.V. & Westbrook, G.L. Structural plasticity in the dentate gyrus- revisiting a classic injury model. *Front Neural Circuits* **7**, 17 (2013).
15.   Steward, O. Reorganization of neuronal connections following CNS trauma: principles and experimental paradigms. *J Neurotrauma* **6**, 99-152 (1989).
16.   Siegel, J.S. *et al.* Data Quality Influences Observed Links Between Functional Connectivity and Behavior. *Cereb Cortex* **27**, 4492-4502 (2017).
17.   Siegel, J.S. *et al.* Disruptions of network connectivity predict impairment in multiple behavioral domains after stroke. *Proc Natl Acad Sci U S A* **113**, E4367-4376 (2016).
18.   Siegel, J.S. *et al.* Re-emergence of modular brain networks in stroke recovery. *Cortex* **101**, 44-59 (2018).
19.   Adkins, D.L., Bury, S.D. & Jones, T.A. Laminar-dependent dendritic spine alterations in the motor cortex of adult rats following callosal transection and forced forelimb use. *Neurobiol Learn Mem* **78**, 35-52 (2002).
20.   Cheng, H.W. *et al.* Differential spine loss and regrowth of striatal neurons following multiple forms of deafferentation: a Golgi study. *Exp Neurol* **147**, 287-298 (1997).
21.   Vuksic, M. *et al.* Unilateral entorhinal denervation leads to long-lasting dendritic alterations of mouse hippocampal granule cells. *Exp Neurol* **230**, 176-185 (2011).
22.   Allegra Mascaro, A.L. *et al.* In vivo single branch axotomy induces GAP-43-dependent sprouting and synaptic remodeling in cerebellar cortex. *Proc Natl Acad Sci U S A* **110**, 10824-10829 (2013).
23.   Papadopoulos, C.M. *et al.* Dendritic plasticity in the adult rat following middle cerebral artery occlusion and Nogo-a neutralization. *Cereb Cortex* **16**, 529-536 (2006).
24.   Carmichael, S.T. Brain excitability in stroke: the yin and yang of stroke progression. *Arch Neurol* **69**, 161-167 (2012).

25. Witte, O.W., Bidmon, H.J., Schiene, K., Redecker, C. & Hagemann, G. Functional differentiation of multiple perilesional zones after focal cerebral ischemia. *J Cereb Blood Flow Metab* **20**, 1149-1165 (2000).

26. Brus-Ramer, M., Carmel, J.B., Chakrabarty, S. & Martin, J.H. Electrical stimulation of spared corticospinal axons augments connections with ipsilateral spinal motor circuits after injury. *J Neurosci* **27**, 13793-13801 (2007).

27. Carmichael, S.T. Plasticity of cortical projections after stroke. *Neuroscientist* **9**, 64-75 (2003).

28. Carmichael, S.T. & Chesselet, M.F. Synchronous neuronal activity is a signal for axonal sprouting after cortical lesions in the adult. *J Neurosci* **22**, 6062-6070 (2002).

29. Friel, K.M. & Martin, J.H. Bilateral activity-dependent interactions in the developing corticospinal system. *J Neurosci* **27**, 11083-11090 (2007).

30. Raisman, G. & Field, P.M. Synapse formation in the adult brain after lesions and after transplantation of embryonic tissue. *J Exp Biol* **153**, 277-287 (1990).

31. Salimi, I., Friel, K.M. & Martin, J.H. Pyramidal tract stimulation restores normal corticospinal tract connections and visuomotor skill after early postnatal motor cortex activity blockade. *J Neurosci* **28**, 7426-7434 (2008).

32. Corbetta, M. Functional connectivity and neurological recovery. *Dev Psychobiol* **54**, 239-253 (2012).

33. Nudo, R.J., Wise, B.M., SiFuentes, F. & Milliken, G.W. Neural substrates for the effects of rehabilitative training on motor recovery after ischemic infarct. *Science* **272**, 1791-1794 (1996).

34. Dijkhuizen, R.M. *et al.* Functional magnetic resonance imaging of reorganization in rat brain after stroke. *Proc Natl Acad Sci U S A* **98**, 12766-12771 (2001).

35. Jaillard, A., Martin, C.D., Garambois, K., Lebas, J.F. & Hommel, M. Vicarious function within the human primary motor cortex? A longitudinal fMRI stroke study. *Brain* **128**, 1122-1138 (2005).

36. Wei, L., Erinjeri, J.P., Rovainen, C.M. & Woolsey, T.A. Collateral growth and angiogenesis around cortical stroke. *Stroke* **32**, 2179-2184 (2001).

37.   Li, S. & Carmichael, S.T. Growth-associated gene and protein
       expression in the region of axonal sprouting in the aged brain after
       stroke. *Neurobiol Dis* **23**, 362-373 (2006).
38.   Carmichael, S.T. Gene expression changes after focal stroke,
       traumatic brain and spinal cord injuries. *Curr Opin Neurol* **16**, 699-704
       (2003).
39.   Zhao, B.Q. *et al.* Role of matrix metalloproteinases in delayed cortical
       responses after stroke. *Nat Med* **12**, 441-445 (2006).
40.   Murphy, T.H. & Corbett, D. Plasticity during stroke recovery: from
       synapse to behaviour. *Nat Rev Neurosci* **10**, 861-872 (2009).
41.   Liepert, J. *et al.* Motor cortex plasticity during constraint-induced
       movement therapy in stroke patients. *Neurosci Lett* **250**, 5-8 (1998).
42.   Xerri, C., Merzenich, M.M., Peterson, B.E. & Jenkins, W. Plasticity of
       primary somatosensory cortex paralleling sensorimotor skill recovery
       from stroke in adult monkeys. *J Neurophysiol* **79**, 2119-2148 (1998).
43.   Dancause, N. Vicarious function of remote cortex following stroke:
       recent evidence from human and animal studies. *Neuroscientist* **12**,
       489-499 (2006).
44.   Caleo, M. Rehabilitation and plasticity following stroke: Insights from
       rodent models. *Neuroscience* **311**, 180-194 (2015).
45.   Longa, E.Z., Weinstein, P.R., Carlson, S. & Cummins, R. Reversible
       middle cerebral artery occlusion without craniectomy in rats. *Stroke*
       20, 84-91 (1989).
46.   Carmichael, S.T. Rodent models of focal stroke: size, mechanism, and
       purpose. *NeuroRx* **2**, 396-409 (2005).
47.   McCabe, C. *et al.* Differences in the evolution of the ischemic
       penumbra in stroke-prone spontaneously hypertensive and Wistar-
       Kyoto rats. *Stroke* **40**, 3864-3868 (2009).
48.   Meng, X., Fisher, M., Shen, Q., Sotak, C.H. & Duong, T.Q.
       Characterizing the diffusion/perfusion mismatch in experimental
       focal cerebral ischemia. *Ann Neurol* **55**, 207-212 (2004).
49.   Shen, Q., Meng, X., Fisher, M., Sotak, C.H. & Duong, T.Q. Pixel-by-pixel
       spatiotemporal progression of focal ischemia derived using
       quantitative perfusion and diffusion imaging. *J Cereb Blood Flow
       Metab* **23**, 1479-1488 (2003).
50.   Henninger, N., Bouley, J., Nelligan, J.M., Sicard, K.M. & Fisher, M.
       Normobaric hyperoxia delays perfusion/diffusion mismatch

evolution, reduces infarct volume, and differentially affects neuronal cell death pathways after suture middle cerebral artery occlusion in rats. *J Cereb Blood Flow Metab* **27**, 1632-1642 (2007).

51.   Henninger, N. & Fisher, M. Stimulating circle of Willis nerve fibers preserves the diffusion-perfusion mismatch in experimental stroke. *Stroke* **38**, 2779-2786 (2007).

52.   Tarr, D. *et al.* Hyperglycemia accelerates apparent diffusion coefficient-defined lesion growth after focal cerebral ischemia in rats with and without features of metabolic syndrome. *J Cereb Blood Flow Metab* **33**, 1556-1563 (2013).

53.   Sharkey, J., Ritchie, I.M. & Kelly, P.A. Perivascular microapplication of endothelin-1: a new model of focal cerebral ischaemia in the rat. *J Cereb Blood Flow Metab* **13**, 865-871 (1993).

54.   Windle, V. *et al.* An analysis of four different methods of producing focal cerebral ischemia with endothelin-1 in the rat. *Exp Neurol* **201**, 324-334 (2006).

55.   Callaway, J.K. *et al.* Sodium channel blocking activity of AM-36 and sipatrigine (BW619C89): in vitro and in vivo evidence. *Neuropharmacology* **47**, 146-155 (2004).

56.   McCarthy, C.A., Vinh, A., Callaway, J.K. & Widdop, R.E. Angiotensin AT2 receptor stimulation causes neuroprotection in a conscious rat model of stroke. *Stroke* **40**, 1482-1489 (2009).

57.   Stoop, W. *et al.* Post-stroke treatment with 17beta-estradiol exerts neuroprotective effects in both normotensive and hypertensive rats. *Neuroscience* **348**, 335-345 (2017).

58.   Dietrich, W.D., Watson, B.D., Busto, R., Ginsberg, M.D. & Bethea, J.R. Photochemically induced cerebral infarction. I. Early microvascular alterations. *Acta Neuropathol* **72**, 315-325 (1987).

59.   Qian, C. *et al.* Precise Characterization of the Penumbra Revealed by MRI: A Modified Photothrombotic Stroke Model Study. *PLoS One* **11**, e0153756 (2016).

60.   McCabe, C., Arroja, M.M., Reid, E. & Macrae, I.M. Animal models of ischaemic stroke and characterisation of the ischaemic penumbra. *Neuropharmacology* **134**, 169-177 (2018).

61.   Schroeter, M., Jander, S. & Stoll, G. Non-invasive induction of focal cerebral ischemia in mice by photothrombosis of cortical

microvessels: characterization of inflammatory responses. *J Neurosci Methods* **117**, 43-49 (2002).

62. Kandel, E.R., Schwartz, J.H., Jessell, T.M., Siegelbaum, S.A. & Hudspeth, A.J. *Principles of Neural Science*, Edn. Fifth Edition. (2013).

63. Mohajerani, M.H., Aminoltejari, K. & Murphy, T.H. Targeted mini-strokes produce changes in interhemispheric sensory signal processing that are indicative of disinhibition within minutes. *Proc Natl Acad Sci U S A* **108**, E183-191 (2011).

64. Carmichael, S.T., Kathirvelu, B., Schweppe, C.A. & Nie, E.H. Molecular, cellular and functional events in axonal sprouting after stroke. *Exp Neurol* **287**, 384-394 (2017).

65. Schaechter, J.D. & Perdue, K.L. Enhanced cortical activation in the contralesional hemisphere of chronic stroke patients in response to motor skill challenge. *Cereb Cortex* **18**, 638-647 (2008).

66. Butefisch, C.M., Wessling, M., Netz, J., Seitz, R.J. & Homberg, V. Relationship between interhemispheric inhibition and motor cortex excitability in subacute stroke patients. *Neurorehabil Neural Repair* **22**, 4-21 (2008).

67. Domann, R., Hagemann, G., Kraemer, M., Freund, H.J. & Witte, O.W. Electrophysiological changes in the surrounding brain tissue of photochemically induced cortical infarcts in the rat. *Neurosci Lett* **155**, 69-72 (1993).

68. Harris-Love, M.L., Perez, M.A., Chen, R. & Cohen, L.G. Interhemispheric inhibition in distal and proximal arm representations in the primary motor cortex. *J Neurophysiol* **97**, 2511-2515 (2007).

69. Shimizu, T. *et al.* Motor cortical disinhibition in the unaffected hemisphere after unilateral cortical stroke. *Brain* **125**, 1896-1907 (2002).

70. Butefisch, C.M. Neurobiological bases of rehabilitation. *Neurol Sci* **27 Suppl 1**, S18-23 (2006).

71. Dong, Y., Winstein, C.J., Albistegui-DuBois, R. & Dobkin, B.H. Evolution of FMRI activation in the perilesional primary motor cortex and cerebellum with rehabilitation training-related motor gains after stroke: a pilot study. *Neurorehabil Neural Repair* **21**, 412-428 (2007).

72. Liepert, J., Graef, S., Uhde, I., Leidner, O. & Weiller, C. Training-induced changes of motor cortex representations in stroke patients. *Acta Neurol Scand* **101**, 321-326 (2000).

73. Sawaki, L. *et al.* Constraint-induced movement therapy results in increased motor map area in subjects 3 to 9 months after stroke. *Neurorehabil Neural Repair* **22**, 505-513 (2008).

74. Biernaskie, J. & Corbett, D. Enriched rehabilitative training promotes improved forelimb motor function and enhanced dendritic growth after focal ischemic injury. *J Neurosci* **21**, 5272-5280 (2001).

75. Jones, T.A., Chu, C.J., Grande, L.A. & Gregory, A.D. Motor skills training enhances lesion-induced structural plasticity in the motor cortex of adult rats. *J Neurosci* **19**, 10153-10163 (1999).

76. Castro-Alamancos, M.A. & Borrel, J. Functional recovery of forelimb response capacity after forelimb primary motor cortex damage in the rat is due to the reorganization of adjacent areas of cortex. *Neuroscience* **68**, 793-805 (1995).

77. Ramanathan, D., Conner, J.M. & Tuszynski, M.H. A form of motor cortical plasticity that correlates with recovery of function after brain injury. *Proc Natl Acad Sci U S A* **103**, 11370-11375 (2006).

78. Barbay, S., Guggenmos, D.J., Nishibe, M. & Nudo, R.J. Motor representations in the intact hemisphere of the rat are reduced after repetitive training of the impaired forelimb. *Neurorehabil Neural Repair* **27**, 381-384 (2013).

79. Barbay, S. *et al.* Behavioral and neurophysiological effects of delayed training following a small ischemic infarct in primary motor cortex of squirrel monkeys. *Exp Brain Res* **169**, 106-116 (2006).

80. Biernaskie, J., Chernenko, G. & Corbett, D. Efficacy of rehabilitative experience declines with time after focal ischemic brain injury. *J Neurosci* **24**, 1245-1254 (2004).

81. Park, J.W. *et al.* Early treadmill training promotes motor function after hemorrhagic stroke in rats. *Neurosci Lett* **471**, 104-108 (2010).

82. Lotze, M. *et al.* Contralesional motor cortex activation depends on ipsilesional corticospinal tract integrity in well-recovered subcortical stroke patients. *Neurorehabil Neural Repair* **26**, 594-603 (2012).

83. Reis, J. *et al.* Noninvasive cortical stimulation enhances motor skill acquisition over multiple days through an effect on consolidation. *Proc Natl Acad Sci U S A* **106**, 1590-1595 (2009).

84.   Spalletti, C. *et al.* A robotic system for quantitative assessment and poststroke training of forelimb retraction in mice. *Neurorehabil Neural Repair* **28**, 188-196 (2014).

85.   Schabitz, W.R. *et al.* Effect of brain-derived neurotrophic factor treatment and forced arm use on functional motor recovery after small cortical ischemia. *Stroke* **35**, 992-997 (2004).

86.   Schabitz, W.R., Schwab, S., Spranger, M. & Hacke, W. Intraventricular brain-derived neurotrophic factor reduces infarct size after focal cerebral ischemia in rats. *J Cereb Blood Flow Metab* **17**, 500-506 (1997).

87.   Schabitz, W.R. *et al.* Intravenous brain-derived neurotrophic factor reduces infarct size and counterregulates Bax and Bcl-2 expression after temporary focal cerebral ischemia. *Stroke* **31**, 2212-2217 (2000).

88.   Wu, D. & Pardridge, W.M. Neuroprotection with noninvasive neurotrophin delivery to the brain. *Proc Natl Acad Sci U S A* **96**, 254-259 (1999).

89.   Kiprianova, I., Sandkuhler, J., Schwab, S., Hoyer, S. & Spranger, M. Brain-derived neurotrophic factor improves long-term potentiation and cognitive functions after transient forebrain ischemia in the rat. *Exp Neurol* **159**, 511-519 (1999).

90.   Schiene, K. *et al.* Neuronal hyperexcitability and reduction of GABAA-receptor expression in the surround of cerebral photothrombosis. *J Cereb Blood Flow Metab* **16**, 906-914 (1996).

91.   Kawamata, T. *et al.* Intracisternal basic fibroblast growth factor enhances functional recovery and up-regulates the expression of a molecular marker of neuronal sprouting following focal cerebral infarction. *Proc Natl Acad Sci U S A* **94**, 8179-8184 (1997).

92.   Stroemer, R.P., Kent, T.A. & Hulsebosch, C.E. Enhanced neocortical neural sprouting, synaptogenesis, and behavioral recovery with D-amphetamine therapy after neocortical infarction in rats. *Stroke* **29**, 2381-2393; discussion 2393-2385 (1998).

93.   Soleman, S., Filippov, M.A., Dityatev, A. & Fawcett, J.W. Targeting the neural extracellular matrix in neurological disorders. *Neuroscience* **253**, 194-213 (2013).

94.   Soleman, S., Yip, P.K., Duricki, D.A. & Moon, L.D. Delayed treatment with chondroitinase ABC promotes sensorimotor recovery and plasticity after stroke in aged rats. *Brain* **135**, 1210-1223 (2012).

95. Overman, J.J. *et al.* A role for ephrin-A5 in axonal sprouting, recovery, and activity-dependent plasticity after stroke. *Proc Natl Acad Sci U S A* **109**, E2230-2239 (2012).

96. Schiavo, G., Matteoli, M. & Montecucco, C. Neurotoxins affecting neuroexocytosis. *Physiol Rev* **80**, 717-766 (2000).

97. Davletov, B., Bajohrs, M. & Binz, T. Beyond BOTOX: advantages and limitations of individual botulinum neurotoxins. *Trends Neurosci* **28**, 446-452 (2005).

98. Costantin, L. *et al.* Antiepileptic effects of botulinum neurotoxin E. *J Neurosci* **25**, 1943-1951 (2005).

99. Caleo, M. *et al.* Transient synaptic silencing of developing striate cortex has persistent effects on visual function and plasticity. *J Neurosci* **27**, 4530-4540 (2007).

100. Spalletti, C. *et al.* Combining robotic training and inactivation of the healthy hemisphere restores pre-stroke motor patterns in mice. *Elife* **6** (2017).

101. Floel, A. tDCS-enhanced motor and cognitive function in neurological diseases. *Neuroimage* **85 Pt 3**, 934-947 (2014).

102. Fregni, F. & Pascual-Leone, A. Technology insight: noninvasive brain stimulation in neurology-perspectives on the therapeutic potential of rTMS and tDCS. *Nat Clin Pract Neurol* **3**, 383-393 (2007).

103. Nitsche, M.A. *et al.* Transcranial direct current stimulation: State of the art 2008. *Brain Stimul* **1**, 206-223 (2008).

104. Fritsch, B. *et al.* Direct current stimulation promotes BDNF-dependent synaptic plasticity: potential implications for motor learning. *Neuron* **66**, 198-204 (2010).

105. Monte-Silva, K. *et al.* Induction of late LTP-like plasticity in the human motor cortex by repeated non-invasive brain stimulation. *Brain Stimul* **6**, 424-432 (2013).

106. Nitsche, M.A. *et al.* Modulation of cortical excitability by weak direct current stimulation--technical, safety and functional aspects. *Suppl Clin Neurophysiol* **56**, 255-276 (2003).

107. Allman, C. *et al.* Ipsilesional anodal tDCS enhances the functional benefits of rehabilitation in patients after stroke. *Sci Transl Med* **8**, 330re331 (2016).

108. Dodd, K.C., Nair, V.A. & Prabhakaran, V. Role of the Contralesional vs. Ipsilesional Hemisphere in Stroke Recovery. *Front Hum Neurosci* **11**, 469 (2017).

109. Cheng, M.Y. *et al.* Optogenetic neuronal stimulation promotes functional recovery after stroke. *Proc Natl Acad Sci U S A* **111**, 12913-12918 (2014).

110. Tennant, K.A., Taylor, S.L., White, E.R. & Brown, C.E. Optogenetic rewiring of thalamocortical circuits to restore function in the stroke injured brain. *Nat Commun* **8**, 15879 (2017).

111. Dancause, N., Touvykine, B. & Mansoori, B.K. Inhibition of the contralesional hemisphere after stroke: reviewing a few of the building blocks with a focus on animal models. *Prog Brain Res* **218**, 361-387 (2015).

112. Talelli, P. *et al.* Theta burst stimulation in the rehabilitation of the upper limb: a semirandomized, placebo-controlled trial in chronic stroke patients. *Neurorehabil Neural Repair* **26**, 976-987 (2012).

113. Buetefisch, C.M. Role of the Contralesional Hemisphere in Post-Stroke Recovery of Upper Extremity Motor Function. *Front Neurol* **6**, 214 (2015).

114. Murase, N., Duque, J., Mazzocchio, R. & Cohen, L.G. Influence of interhemispheric interactions on motor function in chronic stroke. *Ann Neurol* **55**, 400-409 (2004).

115. Silasi, G. & Murphy, T.H. Removing the brakes on post-stroke plasticity drives recovery from the intact hemisphere and spinal cord. *Brain* **137**, 648-650 (2014).

116. Boddington, L.J. & Reynolds, J.N. Targeting interhemispheric inhibition with neuromodulation to enhance stroke rehabilitation. *Brain Stimul* **10**, 214-222 (2017).

117. Mansoori, B.K. *et al.* Acute inactivation of the contralesional hemisphere for longer durations improves recovery after cortical injury. *Exp Neurol* **254**, 18-28 (2014).

118. Di Lazzaro, V. *et al.* Modulating cortical excitability in acute stroke: a repetitive TMS study. *Clin Neurophysiol* **119**, 715-723 (2008).

119. Fregni, F. *et al.* Transcranial direct current stimulation of the unaffected hemisphere in stroke patients. *Neuroreport* **16**, 1551-1555 (2005).

120. Hummel, F. *et al.* Effects of non-invasive cortical stimulation on skilled motor function in chronic stroke. *Brain* **128**, 490-499 (2005).

121. Hummel, F.C. & Cohen, L.G. Non-invasive brain stimulation: a new strategy to improve neurorehabilitation after stroke? *Lancet Neurol* **5**, 708-712 (2006).

122. Kim, D.Y. *et al.* Effect of transcranial direct current stimulation on motor recovery in patients with subacute stroke. *Am J Phys Med Rehabil* **89**, 879-886 (2010).

123. Lefaucheur, J.P. *et al.* Evidence-based guidelines on the therapeutic use of repetitive transcranial magnetic stimulation (rTMS). *Clin Neurophysiol* **125**, 2150-2206 (2014).

124. Plow, E.B. *et al.* Models to Tailor Brain Stimulation Therapies in Stroke. *Neural Plast* **2016**, 4071620 (2016).

125. Di Pino, G. *et al.* Modulation of brain plasticity in stroke: a novel model for neurorehabilitation. *Nat Rev Neurol* **10**, 597-608 (2014).

126. Bradnam, L.V., Stinear, C.M., Barber, P.A. & Byblow, W.D. Contralesional hemisphere control of the proximal paretic upper limb following stroke. *Cereb Cortex* **22**, 2662-2671 (2012).

127. Zeiler, S.R. & Krakauer, J.W. The interaction between training and plasticity in the poststroke brain. *Curr Opin Neurol* **26**, 609-616 (2013).

128. Straudi, S. *et al.* Monitoring Step Activity During Task-Oriented Circuit Training in High-Functioning Chronic Stroke Survivors: A Proof-of-Concept Feasibility Study. *Ann Rehabil Med* **40**, 989-997 (2016).

129. Alia, C. *et al.* Neuroplastic Changes Following Brain Ischemia and their Contribution to Stroke Recovery: Novel Approaches in Neurorehabilitation. *Front Cell Neurosci* **11**, 76 (2017).

130. Wahl, A.S. *et al.* Neuronal repair. Asynchronous therapy restores motor control by rewiring of the rat corticospinal tract after stroke. *Science* **344**, 1250-1255 (2014).

131. Khodaparast, N. *et al.* Vagus nerve stimulation during rehabilitative training improves forelimb strength following ischemic stroke. *Neurobiol Dis* **60**, 80-88 (2013).

132. Sineshchekov, O.A., Jung, K.H. & Spudich, J.L. Two rhodopsins mediate phototaxis to low- and high-intensity light in Chlamydomonas reinhardtii. *Proc Natl Acad Sci U S A* **99**, 8689-8694 (2002).

133. Nagel, G. *et al.* Channelrhodopsin-1: a light-gated proton channel in green algae. *Science* **296**, 2395-2398 (2002).
134. Nagel, G. *et al.* Channelrhodopsin-2, a directly light-gated cation-selective membrane channel. *Proc Natl Acad Sci U S A* **100**, 13940-13945 (2003).
135. Suzuki, T. *et al.* Archaeal-type rhodopsins in Chlamydomonas: model structure and intracellular localization. *Biochem Biophys Res Commun* **301**, 711-717 (2003).
136. Hegemann, P. Algal sensory photoreceptors. *Annu Rev Plant Biol* **59**, 167-189 (2008).
137. Ernst, O.P. *et al.* Photoactivation of channelrhodopsin. *J Biol Chem* **283**, 1637-1643 (2008).
138. Zhang, F. *et al.* Red-shifted optogenetic excitation: a tool for fast neural control derived from Volvox carteri. *Nat Neurosci* **11**, 631-633 (2008).
139. Kianianmomeni, A., Stehfest, K., Nematollahi, G., Hegemann, P. & Hallmann, A. Channelrhodopsins of Volvox carteri are photochromic proteins that are specifically expressed in somatic cells under control of light, temperature, and the sex inducer. *Plant Physiol* **151**, 347-366 (2009).
140. Zhang, F. *et al.* The microbial opsin family of optogenetic tools. *Cell* **147**, 1446-1457 (2011).
141. Govorunova, E.G., Spudich, E.N., Lane, C.E., Sineshchekov, O.A. & Spudich, J.L. New channelrhodopsin with a red-shifted spectrum and rapid kinetics from Mesostigma viride. *MBio* **2**, e00115-00111 (2011).
142. Ritter, E., Stehfest, K., Berndt, A., Hegemann, P. & Bartl, F.J. Monitoring light-induced structural changes of Channelrhodopsin-2 by UV-visible and Fourier transform infrared spectroscopy. *J Biol Chem* **283**, 35033-35041 (2008).
143. Stehfest, K. & Hegemann, P. Evolution of the channelrhodopsin photocycle model. *Chemphyschem* **11**, 1120-1126 (2010).
144. Volkov, O. *et al.* Structural insights into ion conduction by channelrhodopsin 2. *Science* **358** (2017).
145. Lorenz-Fonfria, V.A. & Heberle, J. Channelrhodopsin unchained: structure and mechanism of a light-gated cation channel. *Biochim Biophys Acta* **1837**, 626-642 (2014).

146. Melchior, J.R., Ferris, M.J., Stuber, G.D., Riddle, D.R. & Jones, S.R. Optogenetic versus electrical stimulation of dopamine terminals in the nucleus accumbens reveals local modulation of presynaptic release. *J Neurochem* **134**, 833-844 (2015).

147. Asrican, B. *et al.* Next-generation transgenic mice for optogenetic analysis of neural circuits. *Front Neural Circuits* **7**, 160 (2013).

148. Kim, T.K. & Eberwine, J.H. Mammalian cell transfection: the present and the future. *Anal Bioanal Chem* **397**, 3173-3178 (2010).

149. Pfeifer, A. & Verma, I.M. Gene therapy: Promises and problems. *Annu Rev Genom Hum G* **2**, 177-211 (2001).

150. Schenborn, E.T. & Goiffon, V. DEAE-Dextran Transfection of Mammalian Cultured Cells. *Methods in Molecular Biology* **130**, 147-153 (2000).

151. Mehier-Humbert, S. & Guy, R.H. Physical methods for gene transfer: Improving the kinetics of gene delivery into cells. *Adv Drug Deliver Rev* **57**, 733-753 (2005).

152. Inoue, T. & Krumlauf, R. An impulse to the brain - using in vivo electroporation. *Nature Neuroscience* **4**, 1156-1158 (2001).

153. Fenno, L.E., Gunaydin, L.A. & Deisseroth, K. Mapping Anatomy to Behavior in Thy1:18 ChR2-YFP Transgenic Mice Using Optogenetics. *Cold Spring Harb Protoc* **2015**, 537-548 (2015).

154. Madisen, L. *et al.* A toolbox of Cre-dependent optogenetic transgenic mice for light-induced activation and silencing. *Nat Neurosci* **15**, 793-802 (2012).

155. Grienberger, C. & Konnerth, A. Imaging calcium in neurons. *Neuron* **73**, 862-885 (2012).

156. Higley, M.J. & Sabatini, B.L. Calcium signaling in dendritic spines. *Cold Spring Harb Perspect Biol* **4**, a005686 (2012).

157. Stuart, G.J. & Spruston, N. Dendritic integration: 60 years of progress. *Nat Neurosci* **18**, 1713-1721 (2015).

158. Helmchen, F., Borst, J.G. & Sakmann, B. Calcium dynamics associated with a single action potential in a CNS presynaptic terminal. *Biophys J* **72**, 1458-1471 (1997).

159. Koester, H.J. & Sakmann, B. Calcium dynamics associated with action potentials in single nerve terminals of pyramidal cells in layer 2/3 of the young rat neocortex. *J Physiol* **529 Pt 3**, 625-646 (2000).

160. Helmchen, F., Imoto, K. & Sakmann, B. Ca2+ buffering and action potential-evoked Ca2+ signaling in dendrites of pyramidal neurons. *Biophys J* **70**, 1069-1081 (1996).

161. Yuste, R., Peinado, A. & Katz, L.C. Neuronal domains in developing neocortex. *Science* **257**, 665-669 (1992).

162. Svoboda, K., Denk, W., Kleinfeld, D. & Tank, D.W. In vivo dendritic calcium dynamics in neocortical pyramidal neurons. *Nature* **385**, 161-165 (1997).

163. Fetcho, J.R., Cox, K.J. & O'Malley, D.M. Monitoring activity in neuronal populations with single-cell resolution in a behaving vertebrate. *Histochem J* **30**, 153-167 (1998).

164. Stosiek, C., Garaschuk, O., Holthoff, K. & Konnerth, A. In vivo two-photon calcium imaging of neuronal networks. *Proc Natl Acad Sci U S A* **100**, 7319-7324 (2003).

165. Tour, O. *et al.* Calcium Green FlAsH as a genetically targeted small-molecule calcium indicator. *Nat Chem Biol* **3**, 423-431 (2007).

166. Palmer, A.E. & Tsien, R.Y. Measuring calcium signaling using genetically targetable fluorescent indicators. *Nat Protoc* **1**, 1057-1065 (2006).

167. Sabatini, B.L., Oertner, T.G. & Svoboda, K. The life cycle of Ca(2+) ions in dendritic spines. *Neuron* **33**, 439-452 (2002).

168. Tian, L. *et al.* Imaging neural activity in worms, flies and mice with improved GCaMP calcium indicators. *Nat Methods* **6**, 875-881 (2009).

169. Mao, T., O'Connor, D.H., Scheuss, V., Nakai, J. & Svoboda, K. Characterization and subcellular targeting of GCaMP-type genetically-encoded calcium indicators. *PLoS One* **3**, e1796 (2008).

170. Pologruto, T.A., Yasuda, R. & Svoboda, K. Monitoring neural activity and [Ca2+] with genetically encoded Ca2+ indicators. *J Neurosci* **24**, 9572-9579 (2004).

171. Reiff, D.F. *et al.* In vivo performance of genetically encoded indicators of neural activity in flies. *J Neurosci* **25**, 4766-4778 (2005).

172. Tian, L., Hires, S.A. & Looger, L.L. Imaging neuronal activity with genetically encoded calcium indicators. *Cold Spring Harb Protoc* **2012**, 647-656 (2012).

173. Baird, G.S., Zacharias, D.A. & Tsien, R.Y. Circular permutation and receptor insertion within green fluorescent proteins. *Proc Natl Acad Sci U S A* **96**, 11241-11246 (1999).

174. Palmer, A.E. *et al.* Ca2+ indicators based on computationally redesigned calmodulin-peptide pairs. *Chem Biol* **13**, 521-530 (2006).

175. Frommer, W.B., Davidson, M.W. & Campbell, R.E. Genetically encoded biosensors based on engineered fluorescent proteins. *Chem Soc Rev* **38**, 2833-2841 (2009).

176. Miyawaki, A. *et al.* Fluorescent indicators for Ca2+ based on green fluorescent proteins and calmodulin. *Nature* **388**, 882-887 (1997).

177. Chen, T.W. *et al.* Ultrasensitive fluorescent proteins for imaging neuronal activity. *Nature* **499**, 295-300 (2013).

178. Podor, B. *et al.* Comparison of genetically encoded calcium indicators for monitoring action potentials in mammalian brain by two-photon excitation fluorescence microscopy. *Neurophotonics* **2**, 021014 (2015).

179. Lakowicz, J.R. *Principles of fluorescence spectroscopy*, Edn. Third. (Springer, 2006).

180. Zipfel, W.R., Williams, R.M. & Webb, W.W. Nonlinear magic: multiphoton microscopy in the biosciences. *Nat Biotechnol* **21**, 1369-1377 (2003).

181. Svoboda, K. & Yasuda, R. Principles of two-photon excitation microscopy and its applications to neuroscience. *Neuron* **50**, 823-839 (2006).

182. Helmchen, F. & Denk, W. Deep tissue two-photon microscopy. *Nat Methods* **2**, 932-940 (2005).

183. Conchello, J.A. & Lichtman, J.W. Optical sectioning microscopy. *Nat Methods* **2**, 920-931 (2005).

184. Denk, W. & Svoboda, K. Photon upmanship: why multiphoton imaging is more than a gimmick. *Neuron* **18**, 351-357 (1997).

185. Centonze, V.E. & White, J.G. Multiphoton excitation provides optical sections from deeper within scattering specimens than confocal imaging. *Biophys J* **75**, 2015-2024 (1998).

186. Lichtman, J.W., Magrassi, L. & Purves, D. Visualization of neuromuscular junctions over periods of several months in living mice. *J Neurosci* **7**, 1215-1222 (1987).

187. Denk, W. *et al.* Anatomical and functional imaging of neurons using 2-photon laser scanning microscopy. *J Neurosci Methods* **54**, 151-162 (1994).

188. Helmchen, F., Svoboda, K., Denk, W. & Tank, D.W. In vivo dendritic calcium dynamics in deep-layer cortical pyramidal neurons. *Nat Neurosci* **2**, 989-996 (1999).

189. Yuste, R. & Denk, W. Dendritic spines as basic functional units of neuronal integration. *Nature* **375**, 682-684 (1995).

190. Mainen, Z.F., Malinow, R. & Svoboda, K. Synaptic calcium transients in single spines indicate that NMDA receptors are not saturated. *Nature* **399**, 151-155 (1999).

191. Vanni, M.P. & Murphy, T.H. Mesoscale transcranial spontaneous activity mapping in GCaMP3 transgenic mice reveals extensive reciprocal connections between areas of somatomotor cortex. *J Neurosci* **34**, 15931-15946 (2014).

192. Silasi, G., Xiao, D., Vanni, M.P., Chen, A.C. & Murphy, T.H. Intact skull chronic windows for mesoscopic wide-field imaging in awake mice. *J Neurosci Methods* **267**, 141-149 (2016).

193. Vanni, M.P., Chan, A.W., Balbi, M., Silasi, G. & Murphy, T.H. Mesoscale Mapping of Mouse Cortex Reveals Frequency-Dependent Cycling between Distinct Macroscale Functional Modules. *J Neurosci* **37**, 7513-7533 (2017).

194. Balbi, M. *et al.* Longitudinal monitoring of mesoscopic cortical activity in a mouse model of microinfarcts reveals dissociations with behavioral and motor function. *J Cereb Blood Flow Metab*, 271678X18763428 (2018).

195. Mainen, Z.F. *et al.* Two-photon imaging in living brain slices. *Methods* **18**, 231-239, 181 (1999).

196. Turner, A.M. & Greenough, W.T. Differential rearing effects on rat visual cortex synapses. I. Synaptic and neuronal density and synapses per neuron. *Brain Res* **329**, 195-203 (1985).

197. De Paola, V. *et al.* Cell type-specific structural plasticity of axonal branches and boutons in the adult neocortex. *Neuron* **49**, 861-875 (2006).

198. Nishiyama, H., Fukaya, M., Watanabe, M. & Linden, D.J. Axonal motility and its modulation by activity are branch-type specific in the intact adult cerebellum. *Neuron* **56**, 472-487 (2007).

199. Majewska, A.K., Newton, J.R. & Sur, M. Remodeling of synaptic structure in sensory cortical areas in vivo. *J Neurosci* **26**, 3021-3029 (2006).

200. Holtmaat, A. & Svoboda, K. Experience-dependent structural synaptic plasticity in the mammalian brain. *Nat Rev Neurosci* **10**, 647-658 (2009).

201. Brown, C.E., Li, P., Boyd, J.D., Delaney, K.R. & Murphy, T.H. Extensive turnover of dendritic spines and vascular remodeling in cortical tissues recovering from stroke. *J Neurosci* **27**, 4101-4109 (2007).

202. Holtmaat, A. *et al.* Long-term, high-resolution imaging in the mouse neocortex through a chronic cranial window. *Nat Protoc* **4**, 1128-1144 (2009).

203. Allegra Mascaro, A.L., Sacconi, L. & Pavone, F.S. Laser nanosurgery of cerebellar axons in vivo. *J Vis Exp*, e51371 (2014).

204. Volz, L.J. *et al.* Time-dependent functional role of the contralesional motor cortex after stroke. *Neuroimage Clin* **16**, 165-174 (2017).

205. Spalletti, C. *et al.* Combining robotic training and inactivation of the healthy hemisphere restores pre-stroke motor patterns in mice. *Elife* **6**, e28662 (2017).

206. Krakauer, J.W., Carmichael, S.T., Corbett, D. & Wittenberg, G.F. Getting neurorehabilitation right: what can be learned from animal models? *Neurorehabil Neural Repair* **26**, 923-931 (2012).

207. Ankarcrona, M. *et al.* Glutamate-induced neuronal death: a succession of necrosis or apoptosis depending on mitochondrial function. *Neuron* **15**, 961-973 (1995).

208. van Meer, M.P. *et al.* Recovery of sensorimotor function after experimental stroke correlates with restoration of resting-state interhemispheric functional connectivity. *J Neurosci* **30**, 3964-3972 (2010).

209. van Meer, M.P., van der Marel, K., Otte, W.M., Berkelbach van der Sprenkel, J.W. & Dijkhuizen, R.M. Correspondence between altered functional and structural connectivity in the contralesional sensorimotor cortex after unilateral stroke in rats: a combined resting-state functional MRI and manganese-enhanced MRI study. *Journal of cerebral blood flow and metabolism : official journal of the International Society of Cerebral Blood Flow and Metabolism* **30**, 1707-1711 (2010).

210. Bauer, A.Q. *et al.* Optical imaging of disrupted functional connectivity following ischemic stroke in mice. *NeuroImage* **99**, 388-401 (2014).

211. Carter, A.R. *et al.* Resting interhemispheric functional magnetic resonance imaging connectivity predicts performance after stroke. *Annals of neurology* **67**, 365-375 (2010).

212. Crocini, C. *et al.* Optogenetics design of mechanistically-based stimulation patterns for cardiac defibrillation. *Scientific reports* **6**, 35628 (2016).

213. Brown, C.E., Boyd, J.D. & Murphy, T.H. Longitudinal in vivo imaging reveals balanced and branch-specific remodeling of mature cortical pyramidal dendritic arbors after stroke. *Journal of cerebral blood flow and metabolism : official journal of the International Society of Cerebral Blood Flow and Metabolism* **30**, 783-791 (2010).

214. Carmichael, S.T., Wei, L., Rovainen, C.M. & Woolsey, T.A. New patterns of intracortical projections after focal cortical stroke. *Neurobiology of disease* **8**, 910-922 (2001).

215. Hsu, J.E. & Jones, T.A. Contralesional neural plasticity and functional changes in the less-affected forelimb after large and small cortical infarcts in rats. *Exp Neurol* **201**, 479-494 (2006).

216. Ueno, Y. *et al.* Axonal outgrowth and dendritic plasticity in the cortical peri-infarct area after experimental stroke. *Stroke* **43**, 2221-2228 (2012).

217. Dancause, N. *et al.* Extensive cortical rewiring after brain injury. *The Journal of neuroscience : the official journal of the Society for Neuroscience* **25**, 10167-10179 (2005).

218. Mostany, R. *et al.* Local hemodynamics dictate long-term dendritic plasticity in peri-infarct cortex. *The Journal of neuroscience : the official journal of the Society for Neuroscience* **30**, 14116-14126 (2010).

219. Pasquini, M. *et al.* A Robotic System for Adaptive Training and Function Assessment of Forelimb Retraction in Mice. *IEEE Trans Neural Syst Rehabil Eng* **26**, 1803-1812 (2018).

220. Schallert, T., Fleming, S.M., Leasure, J.L., Tillerson, J.L. & Bland, S.T. CNS plasticity and assessment of forelimb sensorimotor outcome in unilateral rat models of stroke, cortical ablation, parkinsonism and spinal cord injury. *Neuropharmacology* **39**, 777-787 (2000).

221. Baskin, Y.K., Dietrich, W.D. & Green, E.J. Two effective behavioral tasks for evaluating sensorimotor dysfunction following traumatic brain injury in mice. *J Neurosci Methods* **129**, 87-93 (2003).

222. Reinkensmeyer, D.J., Takahashi, C.D., Timoszyk, W.K., Reinkensmeyer, A.N. & Kahn, L.E. Design of robot assistance for arm movement therapy following stroke. *Advanced Robotics* **14**, 625-637 (2001).
223. Harrison, T.C., Silasi, G., Boyd, J.D. & Murphy, T.H. Displacement of sensory maps and disorganization of motor cortex after targeted stroke in mice. *Stroke* **44**, 2300-2306 (2013).
224. Hodics, T., Cohen, L.G. & Cramer, S.C. Functional imaging of intervention effects in stroke motor rehabilitation. *Archives of physical medicine and rehabilitation* **87**, S36-42 (2006).
225. Hubbard, I.J. *et al.* A Randomized Controlled Trial of the Effect of Early Upper-Limb Training on Stroke Recovery and Brain Activation. *Neurorehabilitation and neural repair* **29**, 703-713 (2015).
226. Harris-Love, M.L., Morton, S.M., Perez, M.A. & Cohen, L.G. Mechanisms of short-term training-induced reaching improvement in severely hemiparetic stroke patients: a TMS study. *Neurorehabilitation and neural repair* **25**, 398-411 (2011).
227. Lim, D.H., LeDue, J.M., Mohajerani, M.H. & Murphy, T.H. Optogenetic mapping after stroke reveals network-wide scaling of functional connections and heterogeneous recovery of the peri-infarct. *The Journal of neuroscience : the official journal of the Society for Neuroscience* **34**, 16455-16466 (2014).
228. Kelley, M.S. & Steward, O. Injury-induced physiological events that may modulate gene expression in neurons and glia. *Reviews in the neurosciences* **8**, 147-177 (1997).
229. Wang, L., Conner, J.M., Nagahara, A.H. & Tuszynski, M.H. Rehabilitation drives enhancement of neuronal structure in functionally relevant neuronal subsets. *Proceedings of the National Academy of Sciences of the United States of America* **113**, 2750-2755 (2016).

In primo luogo vorrei ringraziare Francesco S. Pavone per avermi motivato in questi anni a superare i miei limiti.

Vorrei ringraziare Leti per avermi seguito in questo percorso, spronandomi e incoraggiandomi; grazie per avermi trasmesso la tua passione nello studio tra una craniotomia e una "vendetta del fantasma formaggino".

Un grazie speciale va al grande Leo, che tutto può con la sola imposizione delle mani sul setup disallineato, e al mitico Ludo che col suo mantra "Hakuna matata" mi ha aiutato a districarmi tra le mille insidie dei paduli.

Grazie al pollaio, all'istituzione che rappresenta e ha rappresentato durante questi anni, e alle splendide che persone che lo hanno animato durante la mia permanenza; grazie a Claudia e alle ricettine scambiate nelle numerose serate passate a fare analisi, a Niccolò, a Irene C., ad Antonino e i babà di Napoli, a Lorenzo e ai nostri duetti canori, ad Erica e alle sue lezioni di botanica, a Tiziano, e infine grazie ad Elena e a tutte le ore passate insieme in laboratorio, alla Vale che mi ha fatto scoprire la bontà della crosta della porchetta e all'Ale che ha condiviso con me intense lezioni di pilates della Dorothy!

Grazie a Francesco R. e ad Eros per la bellissima crociera che abbiamo fatto a Miami.

Grazie a Caroline, alle alette di pollo, alla *nave di caxxo*, al cheesecake al peanut butter di San Diego e al sostegno che pur da oltremanica non mi ha mai fatto mancare.

Grazie alla Mari con la quale ho condiviso avventure scientifiche e non solo delle più disparate, dai topi blu alla guida di furgoni blu pronti per la rottamazione, a… forse elencarle tutte sarebbe troppo compromettente!

Grazie ad Ire e la sua calma rassicurante per essermi stata vicina in ogni momento di bisogno.

Vorrei ringraziare la mia amica Auro che continua ad essere la mia preziosa confidente sin dai banchi di scuola.

Grazie ai miei genitori che mi sono stati sempre vicino nei momenti di soddisfazione e di sconforto, grazie alla mia sorellina adorata e al mio nipotino Arturo che con una sua risata è in grado di sconvolgere i massimi sistemi.

Infine voglio ringraziare con tutto il mio cuore la mia Isottina che in questi anni mi ha sempre aspettato a casa e Lapo che da sempre è la mia forza in tutte le sfide che ho affrontato.